Masaryk University

Faculty of Science

Department Of Theoretical Physics And Astrophysics

Ph.D. Dissertation

Dynamical Evolution Of Be stars Disks

Klára Šejnová

Supervisor: Mgr. Viktor Votruba PhD.

Brno 2015

Bibliografický záznam

❧ ❧ ❧ ❧

Autor Klára Šejnová
Přírodovědecká fakulta, Masarykova univerzita
Ústav Teoretické fyziky a Astrofyziky

Název práce Dynamický vývoj obálek kolem Be hvězd

Studijní program Teoretická fyzika a Astrofyzika

Studijní obor Astrofyzika

Vedoucí práce Mgr. Viktor Votruba PhD.

Akademický rok 2020/2021

Počet stran xvi + 100

Klíčová slova Hvězdy: emisní čáry, Be – hvězdy: individuální, 60 Cyg, TT Hya,
κ Dra – hvězdy: okolohvězdná hmota

Bibliographic entry

❧ ❧ ❧ ❧

Abstrakt

Horké hvězdy spektrálního typu B patří díky svým fyzikálním vlastnostem mezi intenzivně studované hvězdné objekty u nichž stále zůstává velmi mnoho otevřených otázek.

Hlavní část této práce je zaměřena na vývoj parametrického kódu, schopného namodelovat syntetické spektrum a srovnat ho s pozorovaným. Náš cíl byl využít efektivní metodu, v našem případě genetické algoritmy, která by prohledávala okolí parametrů, a která nám pomůže najít dobré odhady fyzikálních parametrů disků Be hvězd.

Abychom potrvdili správnost kódu, použili jsme kód na hvězdy TT Hya a κ Dra. Porovnali jsme naše výsledné hodnoty s hodnotami, které byly dříve publikované. Naše výsledky dobře souhlasí s hodnotami dříve publikovanými. Tyto výsledky také potvrzují, že náš modifikovaný kód je dobrým nástrojem na modelování disků Be hvězd.

Nakonec jsme kód použili na Be hvězdu 60 Cygni, kde jsme ze sbírky 38 pozorovaných spekter z let 2003–2011 objevili vývoj průměru disku, jeho hustoty a inklinaci hvězdy. Toto jsou první výsledky časového vývoje parametrů disku pro hvězdu 60 Cygni.

Abstract

Be stars are still very unknown in the respect of origin and geometry of circumstellar disk around a star. Furthermore many of the disk properties change in time for example radius of the disk etc. To describe evolution of the disk it is very important to understand the involved physical processes.

The main part of this work is focused on development of parametric code capable to model synthetic spectrum and compare it with the observed one. Our goal was to include an effective method, namely the genetic algorithms, to search in parameter space which can allow us to find a good estimation of physical parameters of a disk of a Be star.

We apply our code to stars TT Hya and κ Dra to verify the modified code works correctly. We compared estimated quantities with the previous published results about these two stars. Our results for stars are in a good agreement with previously published results. These results also verified that our modified code is a good tool to model Be stars disks.

Finally we apply our code on the Be star 60 Cygni where from collection of 38 observed spectra from years between 2003 and 2011 we found evolution of radius, density, opening angle of the disk in time and inclination of the star. These are the first results for time evolution of the disk parameters of the star 60 Cyg.

Poděkování

Díky Viktore, Péťo, Terezko, Barunko, maminko, tatínku, holky z Brna, a pane profesore Bureši, bez vás by to nešlo!

Contents

Introduction

In general Be stars are rapidly rotating non-super giant B type stars that produces a disk in its equatorial plane and whose spectrum have or had at some time, one or more Balmer lines in emission (Collins 1987) though their intensities are scattered and often variable (Kogure & Leung 2007). The latest two reviews for the Be stars were written by Porter & Rivinius (2003) and Rivinius et al. (2013).

The first viable model was proposed by Struve (1931), who suggested that Be stars were rapid rotators forming an equatorial mass-loss disk. However, the formation process of the disk seems not to be as straightforward as Struve suggested. There is now a consensus that a classical Be star is a rapidly rotating B-type star that produces a disk in its equatorial plane. This disk is not related to the natal disk the star had during its accretion phases. Although Be stars do rotate rapidly, it is widely quoted that they do so only at about 70%–80% of their critical limit. Thus, a significant part of the research is focused on the mechanism producing the disk, in addition to rotation.

There exist several hypothesis which are trying to explain the Be phenomenon (origin of a disk). Several models were written. But none of the hypothesis or model fits for all the Be stars and works in general. In this work we focus only on the dynamical evolution of properties of the disk around Be star. We do not try to explain the nature of the disk's origin, we would like to rather explore the evolution of the disk in the sense of the size of the disk etc.

The geometry of the envelope is now generally accepted to be a relatively thin disk. From several studies it is known that the opening angle should be smaller than 20°. For example studies of Porter (1996) and Hanuschik (1996) obtained value of the opening angle 5° and 13°, respectively. But not until the combining interferometry with polarimetry the upper limit for opening angle was confirmed. Quirrenbach et al. (1997) derived an upper limit of 20° for the disk opening angle of ζ Tau and other Be stars.

There exist several models calculating circumstellar matter around the Be stars. The most known and used codes are HDUST (see Carciofi & Bjorkman 2006), BE-DISK (see Sigut & Jones 2007), and Shellspec (Budaj & Richards 2004) on which this work is focused. The code is not as detailed in the physical problem as previous codes but for our need to study dynamical evolution of the disk it is sufficient.

In this work we present the modification of the Shellspec code. The code solves simple radiative transfer along the line of sight in moving media. This code is parametric which means that user must define and describe own model. For example we can choose STAR + DISK and set parameters describing geometry of the problem, radius of a star or a disk and also other characteristics like temperature, density and so on (more details about it can be found on page 19). After the setting up of the parameters the code is run and as a result we get synthetic spectrum. This spectrum can be compared with a observed spectrum. But the input of the free parameters is manual and finding the best value of the parameters can take a lot of time. There can be more then 10 free parameters and finding the best combination can be tricky.

Due to that reason we decided to modify the code and put algorithm which seeks in the field of free parameters and finds the best combination describing the observed spectrum in the best way. We used genetic algorithms for this problem namely PIKAIA library module which is based on the genetic algorithms. The whole descriptionof the modification can be found on page 31.

The main goal of this work was to study Be star 60 Cygni. But before we have made the model of this star we used the modified code to study TT Hydrae and κ Draconis stars. This was done to verify the correctness of the modified code. These two examples are well studied stars. First star TT Hydrae was studied by Budaj & Richards (2004) using original Shellspec. The second one κ Draconis is well studied Be star and was studied by Gies et al. (2007), Touhami et al. (2013) who estimated size of the disk radius and Jones et al. (2008), Silaj et al. (2010) who estimated values for the disk density and the inclination of the system. For both stars parameters of the circumstellar disks were known from works cited before. Since we knew these values we were able to compare our results with results by other authors. We discuss this problem in Chapter 6 on page 39.

The next Chapter is focusing on the modeling of the Be star 60 Cygni. In our study we have analyzed disk around Be star 60 Cygni applying the modified version of Shellspec code. This star was studied in several works, for example Koubský et al. (2000), Wisniewski et al. (2010), Draper et al. (2011) or Draper et al. (2014). For a long time, 60 Cyg (V1931 Cyg, HD 200 310, HR 8 053, MWC 360; B1 Ve, $V = 5^{\mathrm{m}}37$ (var.), $v \sin i = 320\,\mathrm{km\,s^{-1}}$, according to Hoffleit & Jaschek (1982)) has been known as an emission-line star.

Although this is the star when we did not know much about the dynamical evolution and geometry of the disk, Koubský et al. (2000) found that long-term variations, both spectroscopic and photometric, are indicative of a gradual formation and dispersal of the Be envelope around 60 Cyg. Medium and rapid time-scales changes were found as well. Periodical radial velocity variations of spectral lines Hα and He I 6678 suggest that the star might be a spectroscopic binary having a period of 146.6 ± 0.6 days, while 1.064 day line profile variations and 0.2997 day photometric variations may be caused by non-radial pulsations.

Article by Wisniewski et al. (2010) presented one of the most comprehensive spectropolarimetric view of transition from Be phase to normal B-star phase to date. They presented 35 spectropolarimetric and 65 Hα spectroscopic observations of Be star 60 Cyg spanning 14 years. They found that the timescale of the disk-loss events in 60 Cyg corresponds to almost 6 complete orbits of star's binary companion. This suggest that star's binary companion does not influence the primary star (or its disk). From Wisniewski et al. (2010) we also know that the position angle of intrinsic polarization arising from 60 Cyg's disk is $\theta_* = 107.7 \pm 0.4$ indicating that the disk situated in the equatorial plane is oriented on the sky at a position angle of $\theta_{disk} = 17.7$ (measured North to East). Our goal was to find properties of the disk.

The star was also studied by Draper et al. (2011) who analyzed the intrinsic polarization in the process of losing its circumstellar disk via Be to normal B star transition.

In the last chapter we present our results for dynamical evolution of parameters of the disk of the Be star 60 Cygni. We had 38 observed spectra which were taken at the Ondřejov Observatory in the period 2003-2011. Spectra were studied applying modified version of the Shellspec code. We present time evolution for each parameter (outer radius of the disk, disk density, the opening angle of the disk and microturbulent velocity) of the disk.

We also made spectral analysis of all the Hα profiles we had in disposal, we determined equivalent width (EW) and V/R variation for each profile. We plotted equivalent widths of the profiles depending on time of the observation. We also present results for the correlation between EW and disk parameters for each profile.

Be Stars

According to Collins' definition (Collins 1987), a Be star is *"a non-supergiant B star whose spectrum has or had at some time, one or more Balmer lines in emission"*. In general Be stars are rapidly rotating B type stars[1] that produce a disk in its equatorial plane and whose spectrum have or had at some time, one or more Balmer lines in emission though their intensities are scattered and often variable (Kogure & Leung 2007).

To date there exist two main reviews about Be stars: Porter & Rivinius (2003), Rivinius et al. (2013).

2.1 Discovery

On 1866 August 23, father Angelo Secchi wrote a letter (Secchi 1866) where he is describing his discovery in γ Cassiopei. He detected one of the first emission-line stars. This was also the first report of the Be star.

Another big milestone in understanding Be stars was done by Struve in the year 1931. He not only hypothesized that the doubly peaked Hα recombination emission lines observed towards bright Be stars originated from a rotating disk, he also backed this up with the model simulations, see Fig. 2.1, he suggested that the emission profile changes dependently on the angle of the line of sight of the observer. Struve's hypothesis suffered from the fact that spectroscopy can not provide direct evidence for a disk. Nowadays we know that his model does not explain the problem properly but his discovery was very helpfull for next studies of the Be stars.

2.2 Spectra of the Be stars

The most of the knowledge about the Be stars comes from the spectroscopic studies. The spectral lines of the Be stars comes from three regions, the star itself, disk and circumstellar environment above the disk. The observed spectral energy distribution[2] (SED) of Be stars results from a photospheric emission, disk emission of reprocessed radiation and disk absorption. Thomson scattering[3] by free electrons can also change the SED.

Recently, Collins' definition has had to be refined to exclude emission-line stars whose disk formation mechanisms were accretion, e.g. Herbig AeBe stars. Consequently, a new subgroup of these emission-line stars, termed "classical Be stars" was created (Porter & Rivinius 2003). Martayan et al. (2011) proposed a revision of the definition for the classical Be star: *"This is a star with innate or acquired very fast*

---

[1] B type stars are stars with effective temperature greater than $11\,000\,\mathrm{K}$ but lower than $30\,000\,\mathrm{K}$

[2] A spectral energy distribution (SED) is a plot of brightness or flux density versus frequency or wavelength of light

[3] Thomson scattering is the elastic scattering of electromagnetic radiation by a free charged particle
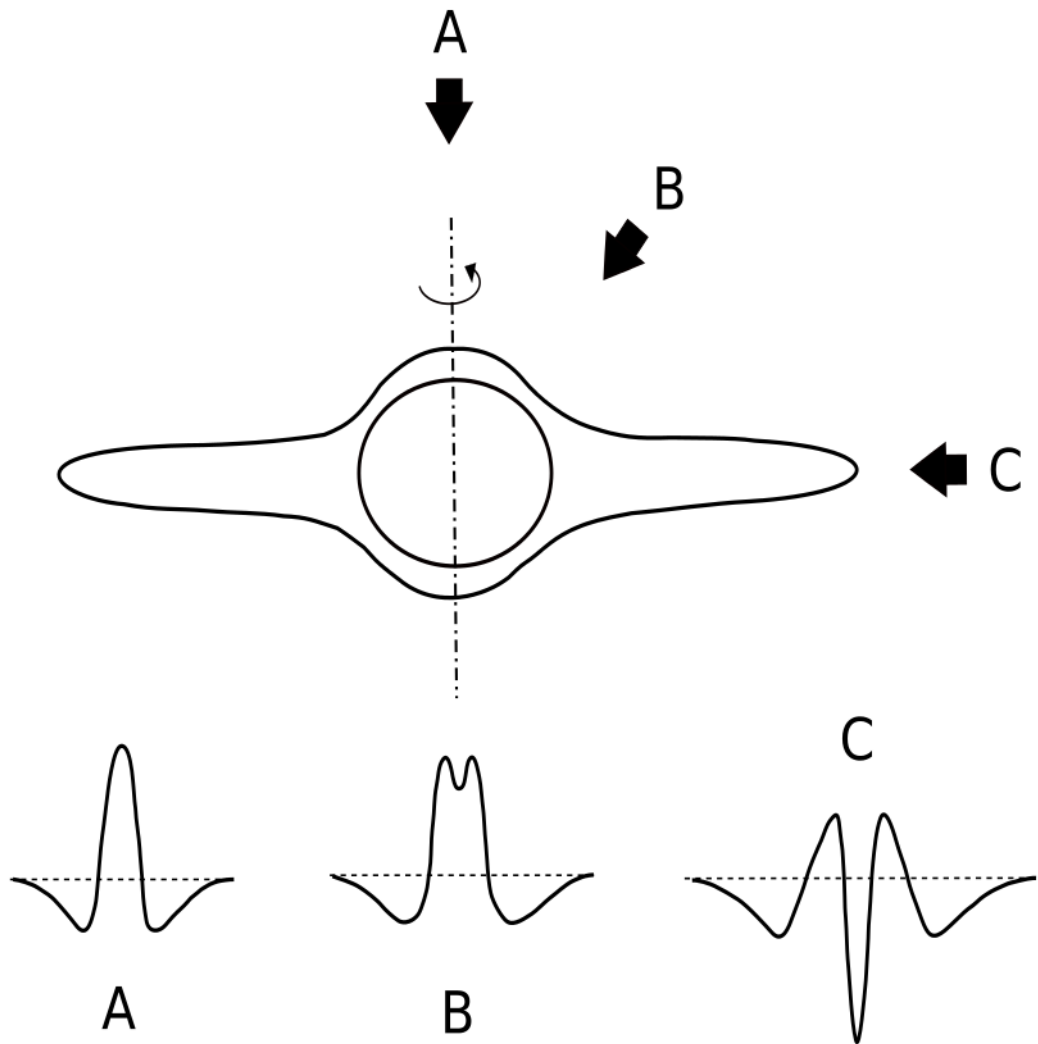
Figure 2.1: *Struve's model of the Be stars and its envelope. He suggested that the emission profile changes dependently on the angle of the line of sight of the observer. A ... pole on, B ... an inclination angle, C ... equator on*

rotation, which combined to other mechanism such as non-radial pulsations beating leads to episodic matter ejections creating a circumstellar decretion disk or envelope."

As was mentioned before Be stars are characterized by the presence of the emission lines in their spectra. Emission lines can have different shape.

They can be double peaked, with the peak separation correlated to the observed line width. Stars with these shapes of the lines are called *shell-line Be stars* (Porter & Rivinius 2003). These stars are also characterized by narrow absorption cores in addition to the broad photospheric absorption lines. Shell stars have the highest measured photospheric line widths among Be stars, and their emission peaks, when present, also have the largest separation. See row C in Fig. 2.1 for the shape of the line profile. Be-shell stars are thought to be the stars with the highest inclination angles, observed nearly from equatorial plane.

Other type is *Pole-on stars* which are characterized by single-peaked narrow emission lines superimposed on the photospheric absorption lines. See row A in Fig. 2.1. There are two types of pole-on stars. One is the intrinsic pole-on stars which exhibit always single-peaked emission lines without changing to double-peaks, whereas the other is the temporary pole-on stars which sometimes show exchange to double- and single-peaked emission in long-term variations. It is usually supposed that pole-on stars are observed almost from their rotational axes.

The last type is *Ordinary Be star*, star showing double-peaked emission-line profiles. Since this type is most prevalent among Be stars, they are often called the ordinary Be stars. See row B in Fig. 2.1. Double-peaked emission lines are formed when the inclination angle i is sufficiently large.

The most common lines in emission are those of H I, He I, Fe II and sometimes also Si II and Mg II.

The hydrogen lines are optically thick and the dominant formation process is recombination, while many metal lines are optically thin. While hydrogen lines form in a large part of the disk, from the kinematic properties of the line emission one can tell that the helium emission forms very close to the star only, as do doubly ionized metals, while singly ionized metal emission forms relatively far from the star. For optically thick lines, non-coherent scattering broadening shifts the peaks at polar inclinations and creates a "wine bottle" profile, see Fig. 2.1 row A. At equator-on inclinations, the disk is not only self-absorbing, but veils the star, and narrow and deep absorption lines are formed, see Fig. 2.1 row C.

2.3   Be phenomenon

But how does the disk originate? There exist several hypothesis which are trying to explain the Be phenomenon (origin of a disk). Several models were written. But none of the hypothesis or model fits for all the Be stars. None of them works in general.

Examples of some of the hypothesis which are discussed at most

Rapidly rotating stars

Be stars are the most rapidly rotating class of non-degenerate stars, certainly so in terms of $v \sin i$. As soon as this was recognized, it was hypothesized that the equatorial rotation velocities, v_e, may be sufficiently close to the critical velocity, v_c, for material to easily escape from the star. The results of studies were that Be stars do not rotate at their critical rotation rates. Instead, the distribution peaks at values of $70\% - 80\%$ of the critical rate with a rather small intrinsic width of the distribution.

Be stars as a binaries

Kříž & Harmanec (1975) proposed the idea that the Be phenomenon in B stars is a consequence of the binary nature of such objects. The mass exchange between components of binary stars with relatively longer periods can well serve as the desired mechanism of formation of Be envelopes. Since further observation discovered that not all Be stars are binaries we cannot take this hypothesis for Be stars as general.

Wind-compressed disk (WCD)

Bjorkman & Cassinelli (1993) introduced a model of the supersonic portion of the stellar wind from a rotating star. In the supersonic limit, the fluid equations are Newton's equations of motion for free particles. The orbital plane of each streamline is inclined with respect to the equatorial plane by the initial latitude of the streamline, thus the orbital dynamics inevitably leads to an equatorial concentration of the wind. If the rotation rate is large enough, the orbits attempt to cross the equator, and a standing shock must develop to turn the flow. The ram pressure of the wind compresses and confines the equatorial material, and creates a dense equatorial disk.

Figure 2.2: *Diagram of dense disk produced by the standing shock in wind. The shock turns the flow parallel to the equator, thereby preventing the streamlines from crossing at equator. Fig. adopted from Bjorkman & Cassinelli (1993)*

Initial dynamical simulations did in fact confirm much of the basic WCD paradigm, but subsequent work showed that non-radial components of the driving can effectively inhibit the formation of any disk.
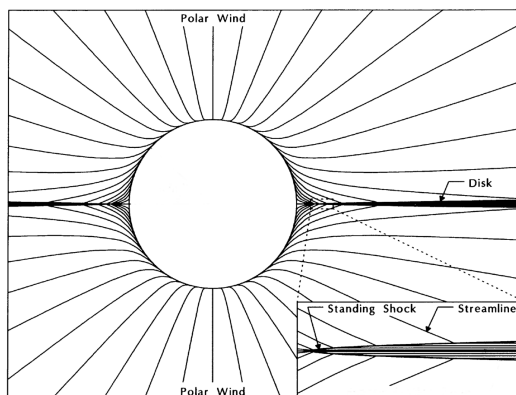
Magnetically torqued disk (MTD)

The WCD model has been revived with the addition of magnetic fields. By Cassinelli et al. (2002) for regions where the magnetic energy dominates over the kinetic energy density (sub-Alfvenic velocities), the flow streamlines follow the magnetic field lines. For the closed magnetic loops near the equator, this forces the gas to flow toward the equatorial plane from both hemispheres, and the resultant shocked region makes up the disk.

However magnetohydrodynamic simulations including stellar rotation by Owocki & Ud-Doula (2003) do not produce such a disk which would fit the observations.

There is also no firm observational evidence for large-scale, i.e., dipolar

Figure 2.3: *Overall structure assumed in the MTD model. Figure adopted from Cassinelli et al. (2002)*

magnetic fields at any strength. Small scale magnetic fields, such a localized loops, remain a possibility and have some indirect observational support, although a direct confirmation is lacking.

Viscous disk

An alternative to compression disks are viscous disks (Lee et al. (1991), Okazaki (2001)). The dynamics of these disks operate in a similar fashion to accretion disks, except that gas and angular momentum are added to the inner regions and then are diffused outward under the action of turbulent (presumably) magnetohydrodynamic viscosity. In its simplest form, the equatorial regions of the stellar atmosphere are spun up to slightly super-Keplerian rotation speeds, for example, by pulsation. If this gas is continually supplied with angular momentum, then it will be lifted from the stellar surface and continue to move farther away from star. For all its successes in describing Be star observations, the viscous disk model still lacks a good description of the vital angular momentum input.

Models by Lee et al. (1991), Okazaki (2001) and Lee (2013) were developed in last years and were compared by several observations by different science groups. Disks around Be stars are now believed to be viscous Keplerian decretion disks, although their formation mechanism has not been revealed yet.

2.4 Variability

The definition of the Be stars indicates that the variability is very important in understanding the Be stars. Be stars show several variabilities, long-term variations
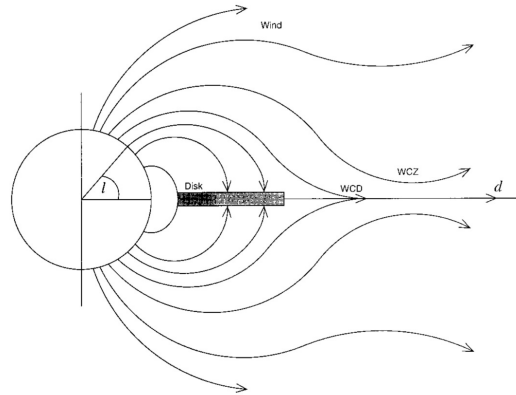
which take several years to short-term variations which can take only a few days or even minutes.

We know, according to Keplerian third law, that the Keplerian orbital period increases with radius as $r^{3/2}$. In Rivinius et al. (2013) they made simple time scale consideration: if at the stellar equator the disk material has an orbital period of typically one day this increases to about $30\,\mathrm{d}$ at $r = 10\,\mathrm{R_*}$ and $1000\,\mathrm{d}$ at $r = 100\,\mathrm{R_*}$, we can associate short-term variations to the photosphere proper or the immediate vicinity of the star, and variations with longer periods to the disk as a whole.

Long-term variations

Already the emission itself in Be stars is transient. These variations are the most remarkable in the Be stars phenomena. *Long-term variations* are connected with an appearance and disappearance of the disk that means presence of the emission lines - phase changes of stellar types: $\mathrm{B \rightleftharpoons Be}$, $\mathrm{Be \rightleftharpoons Be\text{-}shell}$, and $\mathrm{B \rightleftharpoons Be\text{-}shell}$ in time scales from a few years up to several decades. These variations are common for all the Be stars (Kogure & Leung 2007).

The phase change between normal B stars and Be stars are understandable by the formation or destruction of the disks, whereas the transformation between Be and Be-shell stars should be related to the structural changes of the stellar disks. In the classical view, the difference of Be and shell stars is the difference of the inclination angle. However, this picture can not be applied to the transformation between Be and shell stars, since the inclination angle should be fixed for any particular stars.

V/R variations

When the Be stars have double-peaked emission lines we also usually observe V/R (violet/red) variations. V/R variation is usually expressed as the ratio of respective emission-peak heights above the underlaying photospheric absorption profile. Long-term cyclic changes in the ratio V/R are observed in many stars, taking from a few years up to decades to complete the cycle. On Fig. 2.4 we can see the example of the line where $V = R$. But double-peak emission structure is not always symmetrical.

Figure 2.4: *Schematic picture of a double-peaked emission line marking V and R peaks*

Okazaki (1991) model suggested that the long-term V/R variations are phenomena caused by global one-armed oscillations of cool equatorial disks. This one-armed oscillation model was based on a theory of global oscillations of non-self-gravitating, geometrically thin disks.

Another possibility for explaining the V/R variation is in a binary system with an unseen less massive companion star, and that the decretion disk around the Be
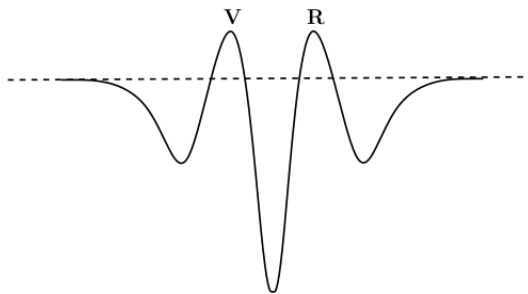
star suffers a tidal instability. Because of the tidal instability, the decretion disk is deformed to be elliptical and the semi-major axis of the eccentric disk is seen to do precession in the same direction of the orbital motion when observed in an inertial frame.

Short-term variations

Walker (1953) was the first one who discovered short-term variation. It was discovered by photoelectric observations while he observed Be star EW Lac. The variability was shorter than 1 day. In general short-term variations are in range of 0.3 to 2 days and usually have amplitudes among $0.01 - 0.1$ magnitude.

These timescales, and the spectral lines in which such variations are observed, favor either the photosphere proper or the immediate circumstellar environment as their formation region. Since rotation alone may not be sufficient to produce the disk, the short-term variations became a prime candidate to identify the additional mechanism required for a rapidly rotating B star to become a Be star.

The short-term variations of Be stars have been interpreted mainly by two different points of view: nonradial pulsation and the corotating circumstellar material. To be noted all Be stars, regardless of spectral type, that were analyzed with high-cadence, long duration space based photometry data have been reported to multiperiodic and to pulsate.

2.5 Dynamics and Kinematics of the Be stars

As was mentioned in introduction there is now a consensus that a classical Be star is a rapidly rotating B-type star that produces a disk in its equatorial plane. The disk is not related to the natal disk the star had during its accretion phases. The mechanisms that feed the disk are different from the mechanism that makes the disk grow. In other words, once the material is ejected and orbits the star, its fate is governed by an entirely different physics, and all memory on the process that brought it there is lost. Although Be stars do rotate rapidly, it is widely quoted that they do so only at about $70\,\%$–$80\,\%$ of their critical limit. Even though the rotating velocity is still matter of discussion.

In order to be closer to the physical core of the problem of forming a disk and as well not to limit the statistics by the validity of the Roche approximation for critical rotation Rivinius et al. (2013) proposed to abandon the notation

$$\Upsilon = v_{\mathrm{rot}}/v_{\mathrm{crit}} \quad \text{where} \quad v_{\mathrm{crit}} = \sqrt{\frac{2}{3}\frac{GM_*}{R_{\mathrm{pole}}}}$$

and

$$\omega = \Omega_{\mathrm{rot}}/\Omega_{\mathrm{crit}} \quad \text{where} \quad \Omega_{\mathrm{crit}} = \sqrt{\frac{8}{27}\frac{GM_*}{R_{\mathrm{pole}}^3}}$$

and use instead

$$W = \frac{v_{\text{rot}}}{v_{\text{orb}}} \quad \text{where} \quad v_{\text{orb}}(R_{\text{eq}}) = \sqrt{\frac{GM_*}{R_{\text{eq}}}} \tag{2.1}$$

which by them is the physically most meaningful and as it defines what velocity boost is required for a given star to launch material into the closest possible orbit, i.e., just above the photosphere at the equator.

In particular, Be disks share exactly the same physics with the well-studied accretion disks (Pringle 1981) around protostars but are called instead *decretion disks* in reference to the fact that in Be disks mass is usually flowing away from the star whereas in protostars disk matter flows forward it. Basic equations of decretion disk are basically the same as those of accretion disks and that only difference is due to the boundary conditions imposed.

Geometry of the disk

The geometry of the envelope is now generally accepted to be a relatively thin disk. To learn how thin the disk is it is necessary to know the opening angle of the disk.

From several studies it is known that the opening angle should be smaller then $20°$. For example studies of Porter (1996) and Hanuschik (1996) obtained value of the opening angle $5°$ and $13°$, respectively. But not until the combining interferometry with polarimetry the upper limit for opening angle was confirmed. Quirrenbach et al. (1997) derived an upper limit of $20°$ for the disk opening angle of ζ Tau and other Be stars.

The size of the disk is another challenging property of the disk to be determine. It should be distinguish between the disk physical extent and the size of the emitting region of a given line or continuum band. Observation can only probe the latter one. To date the physical extent has not yet been determine for any Be star.

We mentioned before that double-peaked emission lines shows V/R variation. The violet and red components of the profile are formed in the approaching and receding parts of the rotating envelope, respectively. If the rotational velocity is decreasing monotonously with the radius, the peak separation enables us to estimate the outer radius (Kogure & Leung 2007).

A simple formula which can estimate radius of the emitting region follows.

$$\Delta v = V \sin i (r_1/r_*)^{-j} \tag{2.2}$$

$2\Delta v$ is the V, R peak separation measured by velocity and Δv is expressed here as a function of the outer radius r_1 and rotational velocity $V \sin i$, given by (Huang (1972), Hirata & Kogure (1984)), r_* is a stellar radius. j is a parameter expressing the velocity law inside the envelope, i.e., the case of the angular momentum conservation ($j = 1$) and the Keplerian motion of the envelope ($j = 1/2$).

Fig. 2 in (Rivinius et al. 2013) illustrates the formation region of the continuum disk emission for several bands. They showed that different band has different formation loci. For instance, 80% of the V-band flux comes from inside $1.8 - 2.5\,R_*$, depending on the disk density. They also mentioned that the size of the emitting

region reflects the physical conditions in the disk. Currently Optical Long Baseline Interferometry (OLBI) is the only technique that provides a direct measurement of this for optical wavelengths.

Rivinius et al. (1998) revived the idea of a ring, suggesting that in some cases the disk might at some times be detached from the star, instead of starting right at its photosphere, and be separated from it by a relative minimum in density. The disk would, then, look more nearly like a ring.

Rivinius et al. (2001) present database of a emission line profiles with features indicating the simultaneous presence of two separate structures, namely inner disk and an outer disk. Instead of a stationary disk structure with constant, moderate outflow, several observed cases show indications for varying radius of the inner disk edge. The appearance of a disk in contact with stellar surface seems limited to the immediate times of outbursts. While some Be stars have never shown any strong variability of the emission, on most the disks are replenished, at least partly, by outbursts events, in which the disk emission and polarization rises steeply, signifying a density increase in the innermost parts. The evolution from a disk into a ring is closely correlated with circumstellar outbursts, which are common for early-type Be stars (includes cases described in paper by Rivinius et al. (2001)). Rivinius et al. (2001) also assume that the mechanisms at work to form a ring are also effective in other, if not all, early type Be stars.

Rivinius et al. (2001) observed, mainly in the optically thin metal and helium lines, graduate disappearance of the high velocity components of the line, which indicates that the high velocity material close to the star has been partially depleted. However Rivinius et al. (2013) mentioned that the suggestion that this was due to the formation of an inner ringlike void is inadequate, as this would be dynamically unstable in a viscous disk.

Temperature and Density of the disk

The main articles applying disk temperature and disk density are by Millar & Marlborough (1998), Pringle (1981) and Shakura & Sunyaev (1973). The last two cover mainly physics of accretion disks which is include in most of the articles we refer to. A brief history of studying disk temperature can be found in (Carciofi & Bjorkman 2006).

Density

To define density of a disk we need to know formula for hydrostatic equilibrium. Formula for hydrostatic equilibrium is

$$\nabla p = -\rho \nabla \Phi. \tag{2.3}$$

If we assume spherical symmetry, we have that $\nabla p = dp/dr$ and $\nabla \Phi = d\Phi/dr = GM(r)/r^2$. This formula represents one of the fundamental equations of stellar structure of spherically symmetric objects under the assumption that accelerations are negligible.

If we apply the equations of hydrostatic equilibrium and $r = \sqrt{R^2 + z^2}$ and $\partial r = (R^2 + z^2)^{-1/2} z \, \partial z$ we get

$$\frac{1}{\rho}\frac{\partial p}{\partial z} = \frac{\partial}{\partial z}\left[\frac{GM}{(R^2 + z^2)^{1/2}}\right], \tag{2.4}$$

which for small disk thickness becomes approximately

$$\frac{1}{\rho}\frac{\partial p}{\partial z} = -\frac{GMz}{R^3}. \tag{2.5}$$

If the disk is isothermal in the z-direction at given radius, then Eq. 2.5 integrates to give

$$\rho(z, R) = \rho_0(0, R)\exp\left(\frac{-z^2}{2H^2}\right), \tag{2.6}$$

where $H^2 = c_s^2 R^3 / GM$ is scale height, c_s is speed of sound ($p = c_s^2\rho$) and ρ_0 is density in the inner part of a disk.

Waters (1986) introduced a simple cone-shaped, pure hydrogen disk model to describe the disk-like, equatorially concentrated wind. Assuming that the density in the equatorial plane $\rho(0, R)$ is a power law, the density field is

$$\rho(R) = \rho_0\left(\frac{r}{R_*}\right)^{-n}. \tag{2.7}$$

where r is a radial distance, R_* is a stellar radius, ρ_0 is the density at $r = R_*$ and n is an index.

Waters et al. (1987) adopted the same simplified disk model, in which the disk has a constant opening angle and the density depends only on radius, to 101 Be stars observed by Coté & Waters (1987), and obtained the value of $n = 2.0 - 3.5$.

In a outflowing viscous disk model for Be stars by Porter (1999) density field for a steady, Keplerian and vertically isothermal disk, and with the assumption that the density in the equatorial plane $\rho(R, 0)$ is a power law, is defined as

$$\rho(R, z) = \rho_0\left(\frac{r}{R_*}\right)^{-n}\exp\left(-\frac{z^2}{2H^2}\right), \tag{2.8}$$

where quantities in this equation are similar to that in Eq. (2.6): ρ_0 is the density at the inner boundary, $\rho(R, 0)$ is the density in the equatorial plane at radius R, $H = r\, c_s / v_\phi$ is the density scale height (c_s is the sound speed) and v_ϕ is orbital speed of the outflowing viscous disk, $v_\phi \approx \sqrt{GM_*/R}$, M_* is the mass of the star, and G is the gravitational constant.

Temperature

To define the temperature of the disk it is convenient to present gradual studies of a disk.

Be star disk has often been assumed to be isothermal at $0.5 - 0.8\, T_{\text{eff}}$, where T_{eff} is effective temperature[4] of the central star. Millar & Marlborough (1998) were the first who tried to calculate disk temperature. They found that the isothermal assumption is a good first approximation except in a region close to the star, where the disk midplane temperature is lower than the temperature of the disk upper layers.

Porter (1999) presented on outflowing viscous disk models for Be stars. To ensure the disk is as general as possible, the temperature of the disk is assumed to follow a power law

$$T_{\text{d}} = 0.8\, T_{\text{eff}} \left(\frac{r}{R_*} \right)^{-m} . \tag{2.9}$$

The disk is outflowing if $2n + 3m > 7$. This value differs for the type of disk. To study non-radiation driven outflowing viscous disk, $2n + 3m > 7$, for Be star disk it should be larger than 6. Index n is the same index as in Eq. 2.7.

Since then, several other studies, with progressively more detailed calculations showed that the disk is indeed strongly nonisothermal (unlike a stellar wind), at least in the dense part close to the star.

It is important to understand what determines its temperature structure explain Carciofi & Bjorkman (2006).

In accretion disks around young stellar objects, the temperature typically falls as a power law with radius, $T \propto r^{-m}$, with an exponent m in the range $[\frac{1}{2}, \frac{3}{4}]$, depending on the disk flaring. This is because the surface of a very optically thick disk acts very much like a blackbody that processes the incident starlight. Since the star illuminates the surface at an increasingly oblique angle with radius, the temperature falls faster than usual $r^{-1/2}$ geometrical dilution star. For an infinitesimally thin flat (i.e. not flared) blackbody disk, the temperature falls as $r^{-3/4}$, but close to the star a detailed integration gives

$$T_{\text{d}} = \frac{T_*}{\pi^{1/4}} \left[\sin^{-1} \left(\frac{R_*}{r} \right) - \frac{R_*}{r} \sqrt{1 - \frac{R_*^2}{r^2}} \right]^{1/4} , \tag{2.10}$$

where T_* is the temperature of the radiation that illuminates the disk, Adams et al. (1987).

To summarize what the current look on the temperature of the midplane is: close to the star the temperature initially falls quickly and is described by Eq. (2.10), reaching a minimum whose position depends on the density (the temperature stops falling because the disk becomes vertically optically thin), and then returns back to the optically thin radiative equilibrium temperature with a value of about $60\,\%$ of T_{eff} (which is cooler than the value $80\,\%$ frequently quoted in the literature before (Waters 1986)). Carciofi & Bjorkman (2006) showed that the initial decline is well represented by an infinitesimally thin, flat re-processing disk by Eq. (2.10), see Fig. 2.5, adopted from study by Carciofi & Bjorkman (2006).

Currently there are two models that are used the most to study, not only, thermal properties of a disk.

---

[4] Effective temperature of a star is the temperature of a black body that would emit the same total amount of electromagnetic radiation.

The first one is HDUST (Carcioﬁ
& Bjorkman 2006) - three-dimensional
non-LTE Monte Carlo radiative trans-
fer code that is used to study the tem-
perature and ionization structure of Ke-
plerian disks around classical Be stars.
Carcioﬁ & Bjorkman (2008) build on
their previous work and solve the full
problem of the steady state nonisother-
mal viscous diffusion and vertical hy-
drostatic equilibrium. They found that
the self-consistent solution departs sig-
niﬁcantly from the analytic isothermal
density, with potentially large effects on
the emergent spectrum. This implies
that nonisothermal disk models must be
used for a detailed modeling of Be star
disks.

The second one is BEDISK (Sigut &
Jones 2007) - non-LTE radiative trans-
fer code which calculates the level pop-
ulations and temperature distribution
self-consistently on a specified computa-
tional grid throughout the circumstellar
disk.

Both of the code incorporate a num-
ber of improvements over previous treat-
ments of the disk's thermal structure by
Millar & Marlborough (1998). Both of
them are being improved by their au-
thors. User can use it for example to
study effect of density on the thermal
structure of a disk (McGill et al. 2013)
or thermal structure of gravitationally-darkened classical Be star disks (McGill et al.
2011).

Figure 2.5: *Midplane temperature. The radial dependence of the equatorial temperature is shown for models 1, 2, 3, and 4 (increasing density, respectively). We see that Eq. (2.10) reproduces the initial temperature decrease quite well (thick lines).*

2.6 Résumé

There are several possibilities how to study Be stars and their disks, we would like
to pointed out only the most important:

- We can study disk characteristics (radius, temperature, density, opening angle
  of a disk and other)

- We can study variations of the stars and changes in their line profiles (long-term
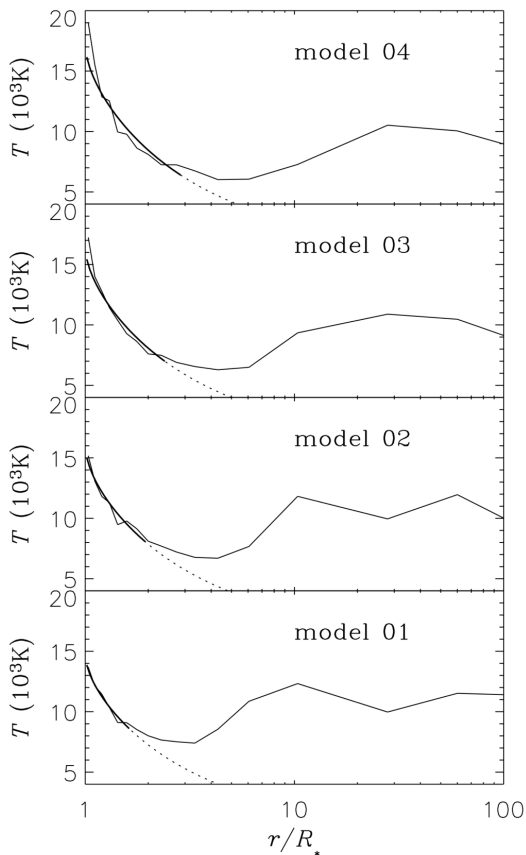 and short-term variations or study V/R ratio)

- We can look at these stars from different point of view (as a single star, binary, as a star beyond the Milky Way)

- We can use different techniques to study them (optically, interferometrically, using X-rays spectroscopy, polarimetry, etc.)

- There are also several works focusing on a survey of a group of stars with some similar features, for example stars that are situated in the same star cluster, for example in double cluster h and χ Persei (Bragg & Kenyon 2002), or belong to the brightest Be stars (Meilland et al. 2012), their sample was composed of eight bright classical Be stars, and trying to find the same pattern that could be general for such a group.

In my thesis we are using spectral line Hα of different stars. We are modeling observed optical spectra from a star taken at Ondřejov observatory. We chosen single star to be studied. In our work we are searching for the characteristics of the circumstellar disks of the Be stars. Even though we are using some assumptions and simplifications in the model, as a result we got first values of some parameters for several Be stars. At the end we present spectral analysis of all the line profiles (change of the equivalent width or V/R ratio).

Shellspec code

Shellspec code developed by Budaj & Richards (2004) is a parametric program designed to calculate lightcurves, spectra and images of interacting binaries immersed in a moving circumstellar environment which is optically thin. As Budaj & Richards (2004) say the main application are probably in the field of interacting binaries, cataclysmic variable stars, and Algol-type eclipsing binaries, extrasolar planets but the code is a flexible tool which can be used to study a large variety of objects and effects. It solves simple radiative transfer along the line of sight in moving media. The assumptions include LTE and optional known state quantities and velocity fields in 3D. Optional (non)transparent objects such as a spot, disk, stream, jet, shell or stars as well as an empty space may be defined in 3D and their composite synthetic spectrum calculated.

3.1   Introduction

As was mentioned before there exist several models calculating circumstellar matter around the Be stars. The most known and used codes are HDUST (see Carciofi & Bjorkman 2006) and BEDISK (see Sigut & Jones 2007). But it is not possible to use these two codes for the estimation of the disk properties directly, because disk properties are input parameters for the code. Both codes also includes NLTE effects which means that calculation are computationally very expensive, thus it is not possible to use those codes for large number of iteration. Also because codes are not free to use it is not possible to modified them for our purpose. We have decided to use Shellspec code (Budaj & Richards 2004) because it is free to use and the computational time is really cheap (single run goes only a few seconds). The code is not as detailed in the physical problem as previous codes but for our need to study dynamics of the disk it is sufficient.

3.2   Definition of a star and a disk

Since we study Be stars (in general a star with a disk) we describe our model as a star with a disk. Model is possible to define in the main input file called *shellspec.in*. Below example of the setting of model shows that we use model star (`istar`) with a disk (`idisc`).

```
#*ISTAR* *ICOMP* *ISPOT* *IDISC* *ISM* *IJET* *ISHELL*
1        0       0       1       0     0      0
```

To set different model for example star with a companion it is sufficient to set `istar=1`, `icomp=1` and other parameters set to zero and so on. For a binary stars there is also option to include Roche geometry in modeling by simply putting number 2 instead of number 1 for `istar` and `icomp`.

Star is defined as a central nontransparent object which can rotate as a solid body with an optional inclination of the rotational axis and have a net space velocity. It
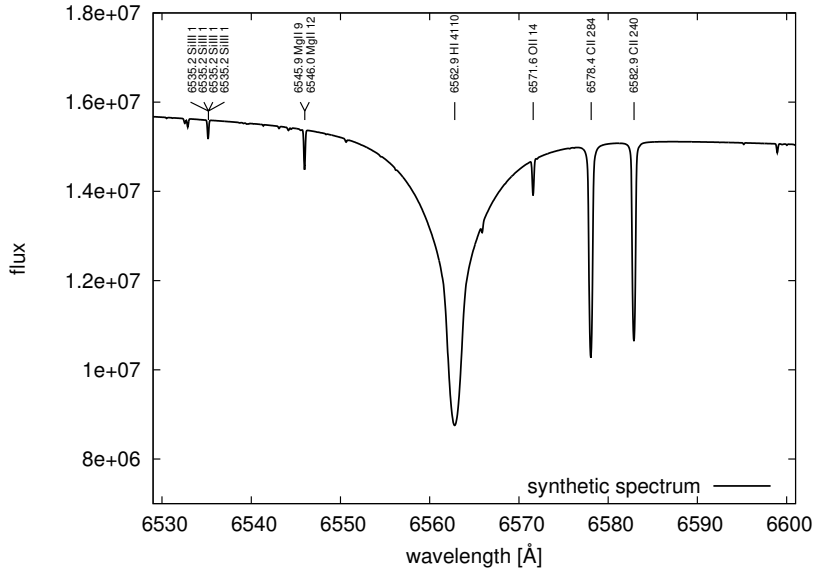
Figure 3.1: *Synthetic spectrum for the star with $T = 27\,000\,\mathrm{K}$ and $\log g = 4$ from program Synspec, some of the strong spectral lines are also marked*

can be treated as a blackbody or have its own spectrum. In our study the star 60 Cyg has its own spectrum (more about the star in Chapter 7). This spectrum was gained from Synspec (Hubeny & Lanz 1995). Spectrum for a star with $T = 27\,000\,\mathrm{K}$, $\log g = 4$ can be seen in Fig 3.1. Star can be surrounded by a Keplerian disk which is specified separately. User can define value for several parameters: radius, mass or effective temperature of a star and other. All of the parameters is possible to see in the file *shellspec.in* where description of them can be found as well.

Disk has either the shape of a rotating wedge or of a slab, or of a rotational ellipsoid surrounding the central object. It is farther constrained by two surfaces: its inner spherical surface with radius r_{in} and outer spherical or elliptical surface with radius r_{out}. In our work we decided to use wedge as the shape of disk. Again values for several free parameters describing a disk can be defined by user: inner and outer radius of a disk, temperature, density or opening angle.

Density of a disk in Shellspec code is defined as

$$\rho(r) = \rho(r_{\mathrm{in}}) \left(\frac{r}{r_{\mathrm{in}}} \right)^{-n} \tag{3.1}$$

where n is a density dependence exponent and it is a free parameter, value of this parameter is defined by user. Since determination of the density slope n from Silaj et al. (2010) showed that it is in the range of $1.5 - 4$ with a statistically significant peak at 3.5 we defined n as $n = 3.5$.

Disk can be defined as an isothermal or the temperature of a disk can change dependently on the radial distance r. In original Shellspec code the temperature of
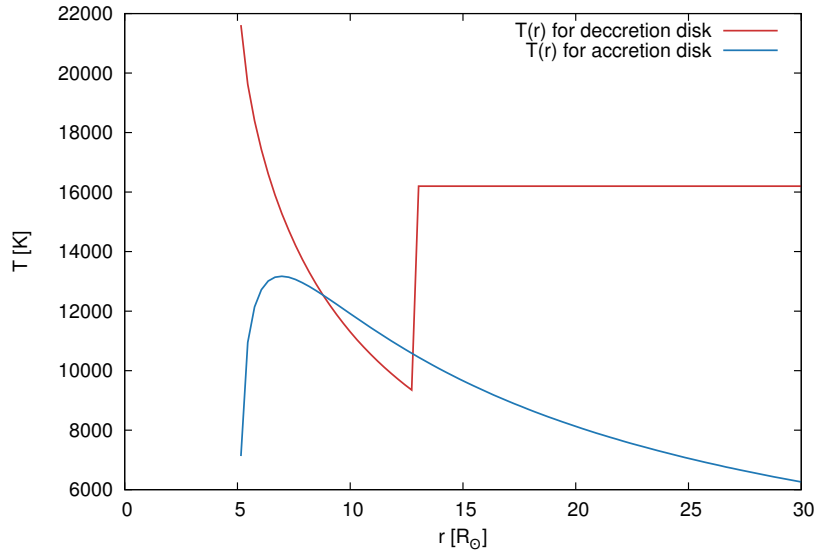
Figure 3.2: *Shape of curve for the temperature distribution Eq. (3.3): the red line, where $T_* = 27\,000\,\mathrm{K}$, $R_* = 5.1\,\mathrm{R_\odot}$ and $r_c = 2.5\,R_*$ and for temperature distribution Eq. (3.2): the blue line where $T_\mathrm{d} = 27\,000\,\mathrm{K}$*

a disk (non-isothermal) is defined as

$$T(r) = T_{dc} \left(\frac{R_*}{r}\right)^{\frac{3}{4}} \left(1 - \sqrt{\frac{R_*}{r}}\right)^{\frac{1}{4}} \tag{3.2}$$

where T_{dc} is the characteristic temperature (Pringle 1981). Parameter `itdc`, from *shellspec.in* file, controls whether user want use isothermal or non-isothermal disk. Both of these quantities (density and temperature) can be redefined, user can find the definition in the main program *shellspec17.f* [1].

Disk in our model is non-isothermal. We kept the density as it was defined in Budaj & Richards (2004). Temperature of the disk was redefined since the shape of the temperature distribution does not respond to the concept of the temperature distribution for Be stars, see Fig. 13 in Rivinius et al. (2013) or Fig. 7 in Carciofi & Bjorkman (2006). We used the current look on the temperature distribution which was discussed before (subsection 2.5) and simplified it. We drew a comparison between distribution of a temperature for accretion disk and deccretion disk in Fig. 3.2.

We knew the precise description of the initial fall (Eq. 2.10). At some point r_c the temperature stops falling, from Fig 13 in Rivinius et al. (2013) we can see that this point is approximately at $2.5\,R_*$. Behind this point temperature starts to rise back to a value of about $60\,\%$ of T_eff. Shape of the temperature in the interval between the r_c point and the point where the value of temperature occurs $60\,\%$ of T_eff is not described at any article. For that reason we used Heaviside step function

---

[1]code line 2934 - `ftemp(i,j,k)=tempdc*ratio**0.75d0*dsqrt(dsqrt(1.d0-dsqrt(ratio)))`
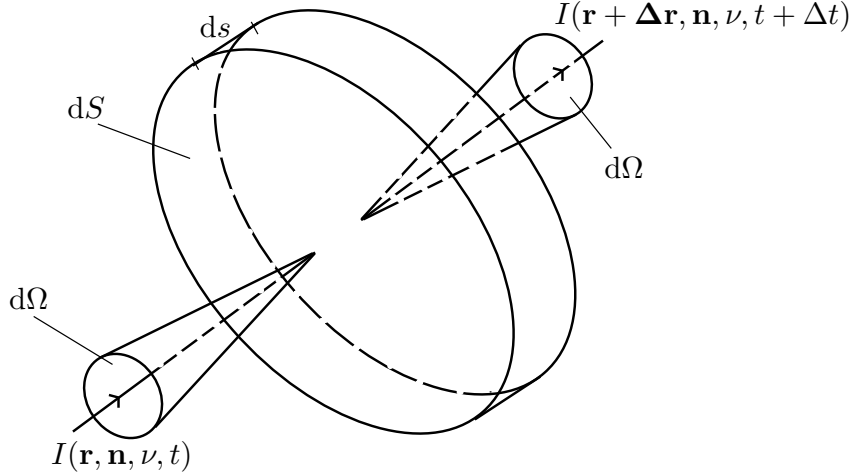
Figure 3.3: *Element of absorbing and emitting material considered in derivation of radiative transfer equation*

to simplified this problem. The precise definition of the temperature we used in our model follows, the shape can be seen in Fig. 3.2, visualized by red line.

$$T_{\mathrm{d}} = \frac{T_*}{\pi^{1/4}} \left[\sin^{-1} \left(\frac{R_*}{r} \right) - \frac{R_*}{r} \sqrt{1 - \frac{R_*^2}{r^2}} \right]^{1/4} H(x) + 0.6\, T_*\, H(-x) \qquad (3.3)$$

where $x = r_c - r$ and $H(x)$ is Heaviside step function

$$H(x) = \begin{cases} 1 & x > 0 \\ \frac{1}{2} & x = 0 \\ 0 & x < 0 \end{cases} \qquad (3.4)$$

3.3 Local Thermodynamic Equilibrium

The aim of the original Shellspec code was to provide a tool which would solve in Local Thermodynamic Equilibrium (LTE) the simple radiative transfer along the line of sight in an optional optically thin 3D moving medium with the possible nontransparent objects embedded in. On next few pages we would like to briefly summarize radiative transfer physics used by Budaj & Richards (2004).

In LTE all material energy partitioning, i.e., all atomic, ionic, molecular level populations, is given by Saha-Boltzmann statistics defined by the local temperature, just as if that location sits within TE (thermodynamic equilibrium). The definition of LTE is to assume the validity of all TE material distribution laws at the local temperature (Rutten 2003).

The energy in a frequency interval $\mathrm{d}\nu$, passing in a time $\mathrm{d}t$ through a volume element of length $\mathrm{d}s$ and cross-section $\mathrm{d}S$ oriented normal to a ray travelling in a direction $\boldsymbol{n}$ into solid angle $\mathrm{d}\Omega$, see Fig. 3.3. The difference between the amount of

energy that emerges (at position $\boldsymbol{r} + \boldsymbol{\Delta r}$ at time $t + \Delta t$) and the incident (at $\boldsymbol{r}$ and t) must equal the amount created by emission from material in the volume minus the amount absorbed. That is

$$
\begin{aligned}
[I(\boldsymbol{r} + \boldsymbol{\Delta r}, \boldsymbol{n}, \nu, t + \Delta t) &- I(\boldsymbol{r}, \boldsymbol{n}, \nu, t)] \, \mathrm{d}S \, \mathrm{d}\omega \, \mathrm{d}\nu \, t \\
&= [\epsilon(\boldsymbol{r}, \boldsymbol{n}, \nu, t) - \chi(\boldsymbol{r}, \boldsymbol{n}, \nu, t) \, I(\boldsymbol{r}, \boldsymbol{n}, \nu, t)] \mathrm{d}s \, \mathrm{d}S \, \mathrm{d}\omega \, \mathrm{d}\nu \, t
\end{aligned}
\tag{3.5}
$$

The radiation transfer equation in work by Budaj & Richards (2004) (their calculations were carried out in the observer's Cartesian frame with z pointing towards the observer) was defined in simplified shape

$$
\mathrm{d}I_\nu = I_\nu(z + \mathrm{d}z) - I_\nu(z) = \epsilon_\nu \, \mathrm{d}z - \chi_\nu \, I_\nu \mathrm{d}z
\tag{3.6}
$$

with z measured along the beam in the propagation direction, I_ν is the specific monochromatic intesity at the frequency ν, χ_ν is opacity and ϵ_ν is emissivity.

Specific intensity (or surface brightness) I_ν is the proportional coefficient in:

$$
\begin{aligned}
\mathrm{d}E_\nu &\equiv I_\nu(\boldsymbol{r}, \boldsymbol{l}, t) \, (\boldsymbol{l} \cdot \boldsymbol{n}) \, \mathrm{d}S \, \mathrm{d}t \, \mathrm{d}\nu \, \mathrm{d}\Omega \tag{3.7} \\
&= I_\nu(x, y, z, \theta, \varphi, t) \cos\theta \, \mathrm{d}S \, \mathrm{d}t \, \mathrm{d}\nu \, \mathrm{d}\Omega \tag{3.8}
\end{aligned}
$$

with $\mathrm{d}E_\nu$ the amount of energy transported through the area $\mathrm{d}S$, at the location $\boldsymbol{r}$, with $\boldsymbol{n}$ the normal to $\mathrm{d}S$, between times t and $t + \mathrm{d}t$, in the frequency band between ν and $\nu + \mathrm{d}\nu$, over the solid angle $\mathrm{d}\Omega$ around the direction $\boldsymbol{l}$ with polar coordinates θ and φ. The total intensity is

$$
I \equiv \int_0^\infty I_\nu \, \mathrm{d}\nu.
\tag{3.9}
$$

I_ν represents the macroscopic counterpart to specifying the energy carried by a bunch of identical photons along a single "ray". Since photons are the basic carrier of electromagnetic interactions, intensity is the basic macroscopic quantity to use in formulating radiative transfer.

Emissivity is also known under name emission coefficient and describes the emission of radiation from the stellar material. The coefficient is defined as

$$
\delta E \equiv \epsilon_\nu(\boldsymbol{r}, \boldsymbol{n}, t) \, \mathrm{d}S \, \mathrm{d}s \, \mathrm{d}\Omega \, \mathrm{d}\nu \, \mathrm{d}t.
\tag{3.10}
$$

Opacity is also known as the extinction coefficient and describes the removal of energy from the radiation field by matter (Mihalas 1978). The coefficient is defined as

$$
\delta E \equiv \chi_\nu(\boldsymbol{r}, \boldsymbol{n}, t) \, I_\nu(\boldsymbol{r}, \boldsymbol{n}, t) \, \mathrm{d}S \, \mathrm{d}s \, \mathrm{d}\Omega \, \mathrm{d}\nu \, \mathrm{d}t.
\tag{3.11}
$$

Sometimes it is useful to distinguish between "absorption" and "scattering". The total extinction is given by

$$
\chi_\nu = \kappa_\nu + \sigma_\nu
\tag{3.12}
$$

where κ_ν and σ_ν are volume coefficients that describe the rate at which energy is removed from the beam by "true absorption" and "scattering" respectively. In the

calculation of χ it is necessary to include a correction for stimulated emission[2]. In Budaj & Richards (2004) they defined line opacity corrected for a stimulated emission as

$$\chi_\nu^{line} = (1 - e^{-\frac{h\nu}{kT}})N_l\,B_{lu}\,h\,\nu\,\varphi_{lu}\,(\nu - \nu_0)(4\,\pi)^{-1} \tag{3.13}$$

where h is Planck constant , $h\,\nu$ is energy of the transition from the lower level l to upper level u, k is Boltzmann constant, T is temperature, N_l is population of the l-th state of corresponding ion, and B_{lu} is the Einstein coefficient for the whole solid angle. $\varphi_{lu}\,(\nu - \nu_0)$ is a Voigt profile where

$$\nu_0 = \nu_{lu}\left(\frac{v_z(z)}{c} + 1\right) \tag{3.14}$$

where ν_{lu} is a laboratory frequency and $v_z = \boldsymbol{v}\cdot\boldsymbol{n}$ is radial velocity. Stimulated emission occurs only when the emitting system exists in a definite upper state. There is thus no stimulated emission in Thompson scattering or Rayleigh scattering but there is stimulated emission in spectrum lines, even if they are described with a scattering coefficient. Budaj & Richards (2004) define other opacity sources as well such as HI bound-free opacity, HI free-free opacity, Thomspon scattering and Rayleigh scattering on neutral hydrogen.

In both the physical and the mathematical description of a radiation field it is useful to employ various angular averages, or often called moments. Thus for example Mihalas (1978) define the mean intensity J_ν to be the straight average (zero-order moment) of the specific itensity over all solid angles

$$J_\nu(\boldsymbol{r},t) \equiv \frac{1}{4\pi}\oint I_\nu(\boldsymbol{r},\boldsymbol{n},t)\,\mathrm{d}\Omega. \tag{3.15}$$

One of the last quantity we need to define is flux. The monochromatic flux is defined as

$$\mathcal{F}_\nu(\boldsymbol{r},t) = \oint I_\nu(\boldsymbol{r},\boldsymbol{n},t)\,\boldsymbol{n}\,\mathrm{d}\Omega. \tag{3.16}$$

This is the net flow of energy per second through an area placed at location $\boldsymbol{r}$ perpendicular to $\boldsymbol{n}$. In Cartesian coordinates (Mihalas 1978) we have

$$(\mathcal{F}_x,\mathcal{F}_y,\mathcal{F}_z) = \left(\oint I\,n_x\,\mathrm{d}\Omega, \oint I\,n_y\,\mathrm{d}\Omega, \oint I\,n_z\,\mathrm{d}\Omega\right), \tag{3.17}$$

where $\mathrm{d}\Omega = -\mathrm{d}\mu\,\mathrm{d}\varphi$, $n_x = (1 - \mu^2)^{\frac{1}{2}}\cos\varphi$, $n_y = (1 - \mu^2)^{\frac{1}{2}}\sin\varphi$, $n_z = \mu$ and $\mu \equiv \cos\theta$. For a planar atmosphere homogeneous in x and y, only $\mathcal{F}_z$ can be zero; we shall therefore require only this component of the flux, and shall refer to it as the flux, as if it were a scalar and write

$$\mathcal{F}_\nu(z,t) \equiv \oint I_\nu\cos\theta\,\mathrm{d}\Omega = \int_0^{2\pi}\int_0^{\pi} I_\nu\cos\theta\sin\theta\,\mathrm{d}\theta\,\mathrm{d}\varphi. \tag{3.18}$$

---

[2] From Mihalas (1978) we know that this is a quantum process in which radiation induces a downward transition from the upper state at a rate proportional to the product of a cross-section, the upper-state population, and the specific intensity. Because the process is proportional to I_ν and effectively cancels out some of the opacity, it is convenient to include it in the definition of χ.

Rutten (2003) presents the flux as the quantity to use for specifying the energetics of radiation transfer, through stellar interiors, stellar atmospheres, planetary atmospheres or space. In principle, flux is a vector. In stellar-atmosphere practice, the radial direction is always implied, outward positive, so that

$$
\begin{aligned}
\mathcal{F}_\nu(z) &= \int_0^{2\pi}\int_0^{\pi/2} I_\nu \cos\theta \sin\theta\, \mathrm{d}\theta\, \mathrm{d}\varphi + \int_0^{2\pi}\int_{\pi/2}^{\pi} I_\nu \cos\theta \sin\theta\, \mathrm{d}\theta\, \mathrm{d}\varphi \\
&= \int_0^{2\pi}\int_0^{\pi/2} I_\nu \cos\theta \sin\theta\, \mathrm{d}\theta\, \mathrm{d}\varphi - \int_0^{2\pi}\int_0^{\pi/2} I_\nu(\pi-\theta) \cos\theta \sin\theta\, \mathrm{d}\theta\, \mathrm{d}\varphi \\
&\equiv \mathcal{F}_\nu^+(z) - \mathcal{F}_\nu^-(z)
\end{aligned}
\tag{3.19}
$$

with both the outward flux $\mathcal{F}_\nu^+$ and the inward flux $\mathcal{F}_\nu^-$ possitive. Isotropic radiation has $\mathcal{F}_\nu^+ = \mathcal{F}_\nu^- = \pi I_\nu$ and $\mathcal{F}_\nu = 0$

We also need to define the total source function

$$
S_\nu \equiv \frac{\epsilon_\nu}{\chi_\nu}.
\tag{3.20}
$$

When multiple processes contribute to the local emission and extinction the total source function is

$$
S_\nu^{tot} = \frac{\sum \epsilon_\nu}{\sum \chi_\nu}.
\tag{3.21}
$$

Since we know source function we can rewrite the Eq. 3.6 as follows

$$
\frac{\mathrm{d}I_\nu}{\chi_\nu} = S_\nu - I_\nu.
\tag{3.22}
$$

The versions of equation Eq. 3.6 and Eq. 3.22 differ trivially in notation but drastically in their domain of application. In stellar photospheres one often meets LTE or near-LTE conditions having $S_\nu = B_\nu(T)$ or $S_\nu \approx B_\nu(T)$ with B_ν the Planck function.

3.4   Output of the Shellspec code

Shellspec code has several output files, user can find for example lightcurve or trailed spectrogram (*lightcurve* file), spectrum of a shell (*shellspectrum* file), 2D images at some frequency (*fort.xx* file) or detailed output of various quantities (*shellspec.out* file).

In our work we need to compare observed spectrum with the synthetic one. In that reason we use output file called *shellspectrum* which contains several blocks separated by a blank line with values for synthetic spectra. Each block corresponds to one rotation of the shell. Blocks have 6 columns, where among others are columns with wavelength [] (column #1) and normalized flux (column #5), these two columns correspond to those from file which includes data for observed spectrum. This gives us the way to compare these two spectra. More about method dealing with the comparison of synthetic and observed spectra can be found in Chapter 5.

Genetic algorithms and PIKAIA

A genetic algorithm (GA) is great for finding solutions to complex search problems. They are often used in fields such as engineering to create incredibly high quality products thanks to their ability to search through a huge combination of parameters to find the best match. For example, they can search through different combinations of materials and designs to find the perfect combination of both which could result in a stronger, lighter and overall, better final product. They can also be used to design computer algorithms, to schedule tasks, and to solve other optimization problems (Jacobson 2012).

4.1 Introduction

GA are search and optimization procedures that are motivated by the principles of natural genetics and natural selection. Some fundamental ideas of genetics are borrowed and used artificially to construct search algorithms that are robust and require minimal problem information (Deb 1999).

The GA can be thought as a classifier system that continuously sorts out and combines the most advantageous substrings that happen to be present across the whole population at a given time (Metcalfe & Charbonneau 2003).

GA create initial population of the individuals then make crossing of the individual and at the end mutate it and find the most powerful ones and create new population. Selection pressure is imposed in between generation based on the quality of the solutions, their so called fitness. A higher fitness implies a higher probability the solution will be selected for reproduction. Consequently, only a selected set of individuals will pass on their genetic material to subsequent new generations. This procedure is done several times and as a result is the most precise individual. Each cell of each individual (or phenotype) contains a complete set of instructions effectively defining its physical makeup. This information is encoded in the form of linear gene sequences stored on pairs of homologous chromosomes, which constitute the individual's genotype, see Fig. 4.1.

To create the new populations require a reproduction mechanism. In its most form this mechanism consists of two operators. These are the crossover operator[1], simulating sexual reproduction, and the mutation operator, simulating copying errors and random effects affecting a gene in isolation. An important benefit of these two operators is the fact that they also introduce new genetic material into the population. This allows the GA to explore new regions of parameters space, which is important in view of the existence of local extremes.

When the optimization runs into a local optimum, these two operators, where usually mutation has the strongest effect, allow for the construction of individuals outside of this optimum, thereby allowing it to find a path out of the local optimum (Mokiem et al. 2005).

---

[1]The crossover operator is, in essence, what distinguishes genetic algorithms from other heuristic search techniques.
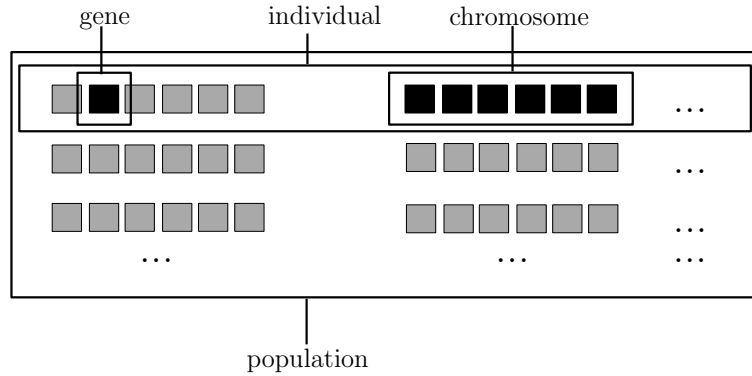
Figure 4.1: *Scheme of a population; number of individuals and population or number and size of the chromosomes is defined by user.*

To summarize, the basic processes for genetic algorithms are:

- Initialization - create an initial population

- Evaluation - each member of the population is then evaluated and we calculate a fitness for that individual

- Selection - an idea is to make it more likely that fitter individuals will be selected for our next generation.

- Crossover - a method for mixing fragments of the better solutions to form new, on average even better solutions

- Mutation - to avoid permanent loss of diversity within the solutions

A basic scheme of GA

In Charbonneau & Knapp (1995) they presented an example generic optimization problem where basic genetic algorithm is introduced. It follows, one is given a "model" that depends on a set of parameters $\mathbf{a}$, and a function relation $f(\mathbf{a})$ that returns a measure of quality for the corresponding model. The optimization task consists in finding the "point" $\mathbf{a}^*$ defining a model that maximizes the quality measure $f(\mathbf{a})$. For the sake of the argument suppose that one has available a target value F and define a tolerance criterion $\varepsilon(>0)$ such that a "solution" $\mathbf{a}^*$ satisfying

$$|F - f(\mathbf{a}^*)| \leq \varepsilon \tag{4.1}$$

corresponds to a model deemed acceptable. Define now a population A as a set of K realization of the parameters $\mathbf{a}$:

$$A \equiv \{\mathbf{a}_k\}, \qquad k = 1, 2, \ldots, K \tag{4.2}$$

and an operator $\mathcal{R}$ that, when applied to a given population A^{n-1}, produces a new population A^n. From these building blocks a basic genetic algorithm could be constructed as follows:

$$\text{Initialize}: \quad A^0 \equiv \mathbf{a}_k^0, \qquad k = 1, \ldots, K$$
$$\text{Compute}: \quad f_k^0 \equiv f(\mathbf{a}_k^0)$$
$$n := 0$$
$$\textbf{do while} \quad |F - max(f_k^n)| \geq \varepsilon$$
$$\quad n := n + 1$$
$$\quad A^n = \mathcal{R}(A^{n-1})$$
$$\quad \text{Compute}: \quad f_k^n, \qquad k = 1, \ldots, K$$
$$\textbf{end do}$$
$$\mathbf{a}^* = \mathbf{a}_{k(max)}^n$$

4.2 PIKAIA

For our modification we decided to use genetic module PIKAIA. PIKAIA is a general purpose function optimization module based on a genetic algorithm. The module is written in Fortran and uses decimal encoding. The module is particularly useful (and robust) in treating multimodal optimization problems. It is possible to download this subroutine freely[2], manual is available as well, see Charbonneau & Knapp (1995).

From the manual we learn that internally, PIKAIA seeks to maximize a (user-defined) function $f(\mathbf{x})$, the name of which is passed in as an argument, in a bounded **n**-dimensional space, i.e.,

$$\mathbf{x} \equiv (x_1, x_2, \ldots, x_n), \qquad x_k \in [0.0, 1.0] \quad \forall k \tag{4.3}$$

The restriction of parameter values in the range $[0.0, 1.0]$ allows greater flexibility and portability across problem domain.

To call PIKAIA user has to use command

```
call PIKAIA(ff,n,ctrl,xb,fb,status)
```

where *ff* is fitness function which is to be maximized, n is a dimension of the space, *ctrl* is a control vector by which algorithm behavior is described, *xb* contains the optimal solution parameters, namely the best solution of the final population at the end of the evolution, *fb* is the fitness of the solution and *status* contains a numerical value coding error conditions or successful termination.

PIKAIA requires a random number generator function that returns random or pseudo-random deviates from a uniformly distributed sequences in the interval $[0.0, 1.0]$. PIKAIA is distributed with a simple random number generator based on the "minimal standard" Lehmer multiplicative linear congruential generator of Park

---

[2]http://www.hao.ucar.edu/modeling/pikaia/pikaia.php

& Miller (1988). Charbonneau & Knapp (1995) chose the Park-Miller generator because of its simplicity and portability: for a given `seed` values, it will produce the same sequence of uniform random deviates. In our work we used `seed=clock` with connection of using subroutine *system_ clock(clock).*

Modification of Shellspec code

The goal of this work is to find out the characteristics of a disk around the star, this is called inverse problem. An inverse problem is a general framework that is used to convert observed measurements with the help of the model into information about a physical object or system that we are interested in. For this problem we use Shellspec code. We nicely ask user to read original manual of the Shellspec code at first even though brief summary of this program was made in Chapter 3. User can find it at Budaj & Richards (2004). We present here description of the modification of the Shellspec code. To understand modification more it is also necessary to know something about genetic algorithms (previous Chapter).

5.1 Motivation

The motivation to modify Shellspec was to optimize the code. Shellspec code contains several input and output files. The main input file where we must set physical parameters of the disk is called *shellspec.in.* As an output for given set of parameters like inner(outer) radius, opening angle, density and inclination angle we get synthetic spectrum stored in the file *shellspectrum* which we can compare with the observed spectrum.

Our goal is to estimate some physical parameters of the Be star disk, like outer radius, from observed spectra. But the original version of the Shellspec is not proper for this goal. Namely, physical parameters are input parameters for the code and you must enter them manually.

It is clear that for an inverse problem "to find the best estimation of the physical parameters describing a disk from a spectra" we must modify the code. Our modification must allow automatic systematic search through parameters space and thus to find optimal set of parameters.

We decided to input some algorithm which would search through this parameters space and also compare synthetic and observed spectrum.

5.2 First attempts

After our first attempts with pure grid method for systematic search in the parameters space (Šejnová et al. 2012b; Šejnová 2010), which were struggled with its computational heftiness and ineffectivity, we decided to use genetic algorithms (GA) due to their robustness. GA can also enable to increase the number of parameters, which we can estimate from observed spectra.

In the next step we include automatic entering of the input free parameters and optimization algorithm to the Shellspec code. For our study of 60 Cyg we used inner radius, outer radius, density, opening angle and only partially (explained later) inclination as the free parameters which we want to estimate from spectra. But it is possible to choose different parameters (Šejnová et al. 2012a). Consequently we

implemented optimization algorithm based on GA to the code. This allows us to find optimal values of the free parameters.

We chose GA as an algorithms which search through the parameters field. Subroutine PIKAIA is called by program *shellspec17gen1* where user can define number of the individuals in population, generations and number of free parameters. More about GA and PIKAIA is in previous Chapter 4. Name *shellspec17gen1* refers to original version Shellspec code number 17 and the first version of the modified code.

5.3   Description of the code

Firstly we translated the code into programing language Fortran 90 (Metcalf et al. 2004) which improved the readability and usability of the code and made it more effective in combination with GA subroutine PIKAIA (explained below). This translation also enable the code to be more efficient in the respect of the upgrading the compilators which still count with the programming language Fortran 90 unlike Fortran 77.

The original program code was transformed into function *shell_calculation* which is contained in module called *shellgen* and calculates normalized synthetic spectrum. The *shellgen* module is used by the program *shellspec17gen1* which is the main program after modification.

We also changed some of the subroutine (instead *shellspec.in* we defined module *initsh.f90* - the concept of the new file is the same as before, only the definition and values of parameters are in the same folder, so it is more clear), we also put some subroutine into the module (*raphson.f90, shellfunc.f90, statfun.f90*) and made it more systematic.

In *shellgen* module user can define free parameters and boundaries for parameters. PIKAIA subroutine then choose random number in interval of boundaries (for example `rinmax = 5.D0, rindc=rstar+xpar(1)*rinmax`, where `xpar` lies in the interval $[0, 1]$) and run original shellspec code. When the run is over results are saved (for this moment we are interested in synthetic spectrum (flux, wavelength) but user can choose different output if necessary), observed spectrum is read.

Modified code follows simple computational scheme, see Fig. 5.1. Namely in the initial run we have population of n_i individuals with randomly generated set of parameters (genome). For every individual from population we calculate normalized synthetic spectrum F_{synth} using modified Shellspec code and compare it with normalized observed spectrum F_{obs}. The subroutine *chii(matice,inter,chi2)* determine value of the fitness for synthetic and observed spectrum. As a measure of the quality of the fit we define fitness function (which PIKAIA seeks) f_{fit}, this function is called *shell_calculation*.

$$f_{\text{fit}} = \frac{1}{1 + \chi^2}, \tag{5.1}$$

based on the χ^2 merit function

$$\chi^2(A) = \sum_{i=1}^{N} \left(\frac{F_{\text{obs}}(x_i) - F_{\text{synth}}(x_i; A)}{\sigma_i} \right)^2, \tag{5.2}$$
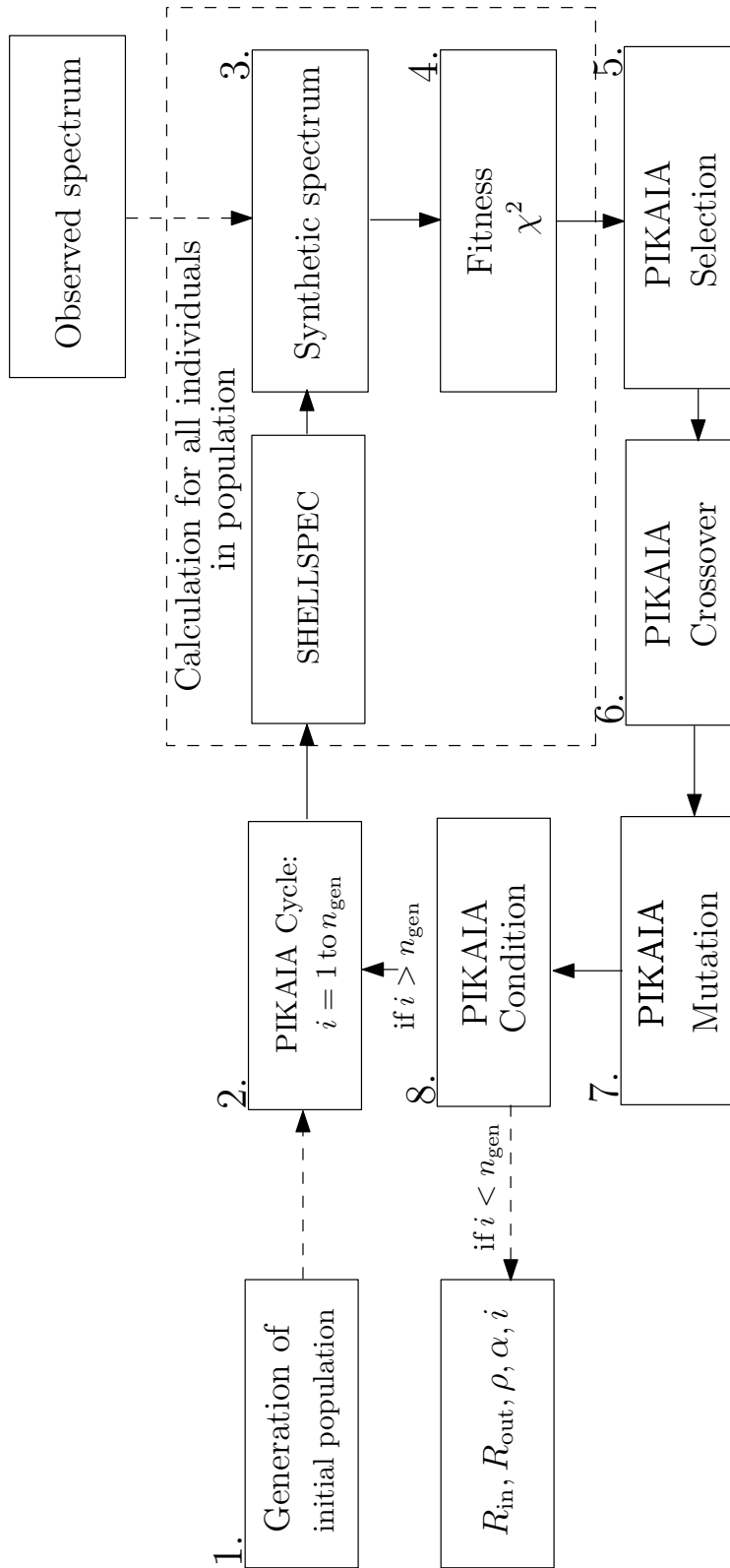
Figure 5.1: *Layout chart of the code: 1. Creation of the initial population (generation zero) of n_i individuals with the different set of parameters. 2. Starting the generation cycle 3. For every individuals we calculate synthetic spectrum using modified SHELLSPEC 4. This synthetic spectrum is compared with the observed spectrum using fitness function 5. Selection of the best individuals using fitness values. 6. Reproduction for the new generation using crossover applied on the best individuals. 7. Mutation applied on the individuals from the new generation. 8. If the number of the generation is greater than n_{gen} then cycle will end else cycle will continue.*

where $F_{\mathrm{obs}}(x_i)$ is the flux of the observed spectrum at the wavelength x_i, N is the number of points in the observed spectrum and $A(a_1, \ldots, a_j)$ is set of free input parameters like outer disk radius, density of the disk, opening angle or inclination and σ_i is the standard deviation. For determination of merit function (5.2) it was necessary to interpolate calculated synthetic spectrum to the same wavelengths as the observed spectrum. Subroutine *interpolace* includes these determination:

$$F_{\mathrm{obs}}(\lambda) = F_{\mathrm{obs}0} + \frac{(F_{\mathrm{obs}1} - F_{\mathrm{obs}0})}{(\lambda_1 - \lambda_0)}(\lambda - \lambda_0) \qquad (5.3)$$

where $F_{\mathrm{obs}1}$, $F_{\mathrm{obs}0}$ is synthetic flux, λ_1, λ_0 synthetic wavelength and $F_{\mathrm{obs}}(\lambda)$ flux at the wavelength. This procedure is done several times (it depends how big number of generations user defines) and the result is the best fit. All the preliminary results are saved into the file *vysledky.dat*. Again user can define what should be saved here.

In the next step, input parameters describing the geometry and the physics of the problem are optimized via genetic algorithms PIKAIA. Namely, all individuals (every individual represents different combination of parameters) from the given population are sorted according to their value of fitness function (Eq. (5.1)) from the best to the worst individual. Only the best individuals survive and generate new population via mutation and crossover operations and thus generated the new sets of parameters. Loop continue until the best match is found. Values of the estimated free parameters and χ^2 are saved to the output file. Number of individuals in the population n_{i} and number of generation n_{gen} which are driving behavior of PIKAIA genetic algorithm must be defined before calculation and are stored in the control vector `ctrl`. Users can also define boundaries for their own free parameters if it is necessary.

As it is clear from the above, to use our modified code user needs to have observed spectrum of the studied star. Shellspec code itself has not needed it before but the modified code uses the observed spectrum as an input.

Detailed description of changes together with the complete manual of the code can be found in package at http://physics.muni.cz/~klarka/shellspecen.html.

5.4   First run

We started with only two free parameters (R_{in}, R_{out}). Firstly we studied how the code behave with two free parameters (used for a model example TT Hya and first study of 60 Cyg). We tried to improve computational heftiness so the code runtime would be as fast as possible. Then we increased the number of free parameters to three (only for 60 Cyg study) and obtained similar results. Currently there are up to six free parameters and the runtime is about 1 day and a half, it depends mostly on the number of generations, individuals in the generation, and also grid points.

PIKAIA creates population of the individuals, number of the individuals can be defined by user as well as the number of the generation by the input control vector `ctrl`. Default values are 150 generations and 100 individuals. We sticked with this value, since smaller number of generations (for example 30 generations) converge to smaller value for f_{fit} and bigger number (for example 1000 generations) converge to almost the same value as if we have only 150 generations.

5.5 How to use the modified code

- In *shellspec17gen1.f90* user can define number of the individuals in population `ctrl(1)` and number of the generation `ctrl(2)`. The meaning of the control vector can be found in the manual for PIKAIA. User can define other properties by this vector. The bigger the number of the generation the longer the computing time. With increasing number of the generation the fitness is getting better but it is not that much significant. In our experience it is not necessary to have big number of the generation (more about this problem can be found in one of the next chapter on page 52). User can also define number of the free parameters by `npar`.

- In *shellgen.f90* user defines free parameters and their intervals. For example to define opening angle of a disk we use

$$\texttt{adisc=1.D0+xpar(4)* adiscmax,}$$

where `xpar()` lies in the interval $[0, 1]$. This also means that lower boundary for opening angle is $1°$ and upper boundary is $1°+$`adiscmax` and `adiscmax` is defined by user. Caution must be made when defining `adicsmax`. If the lower boundary is not zero then the value for `adicsmax` does not mean upper boundary, the upper boundary is lower boundary plus `adiscmax`. Number 4 in `xpar(4)` means that it is the fourth free parameter, this information is useful for reading the results.

- In file *initsh.f90* user defines values for the object to be study, usually parameters which are known, values for free parameters do not have to be filled up.

- **Example**
  The example is a model presented by a star with a disk, the properties of the primary star are usually known unlike the properties of the disk. Thus the parameters of the primary star are defined in file *initsh.f90*. And as the free parameters we choose the inner, outer radius of the disk, the density, the angular halfwidth of the disk wedge, the microturbulent velocity which are defined in module *shellgen*. The boundaries of some of these parameters can be found in articles. User should find its own boundaries for different type of the model. We have five free parameters in this example model $\Rightarrow$ `npar`$= 5$. Number of the individuals is $100 \Rightarrow$ `ctrl(1)`$= 100$ and number of generations is $30 \Rightarrow$ `ctrl(2)`$= 30$. As was mentioned before these free values can be defined in *shellspec17gen1.f90*. Definition of the free parameters is in the beginning of the module *shellgen.f90*:

  Restrictions of free parameters for optimization problem (maximal value of the parameter)

  `rinmax = 5.D0` . . . the innner radius

```
drmax = 12.D0 ...the width of the disk
densmax=1.D-10 ...the disk density
adiscmax=45.D0 ...the angular halfwidth of the disk wedge
vtrbdcmax=150.D0 ...the microturbulent velocity
```

Definition of free parameters

```
rindc = rstar + xpar(1)*rinmax
dr = 1.D0 + xpar(2)*drmax
routdc = rindc+dr
densdc=1.D-13+xpar(3)*densmax
adisc=1.D0+xpar(4)*adiscmax
vtrbdc=10.D0+xpar(5)*vtrbdcmax
```

- To run the code we have prepared *Makefile* with further instruction:

```
make clean
make mod
make shellspecgen
./shellspecgen
```

- If user would like to save all the output from PIKAIA then do command `./shellspecgen > results.txt` and the output will be saved to the file *results.txt*. To understand all of the output from PIKAIA please see Charbonneau & Knapp (1995) here we present only the most important output. Example of the *results.txt* file follows:

```
************************************************************
*             PIKAIA Genetic Algorithm Report             *
************************************************************

   Number of Generations evolving:   30
       Individuals per generation:  100
   Number of Chromosome segments:     5
   Length of Chromosome segments:     6
            Crossover probability:    0.8500
            Initial mutation rate:    0.0500
            Minimum mutation rate:    0.0005
            Maximum mutation rate:    0.2500
   Relative fitness differential:     1.0000
                   Mutation Mode:
Variable                                    input and values of free parameters ←
               Reproduction Plan:                                               |
Full generational replacement                                                   |
 Parameters :            5  /   0.775036097    0.766041458     0.58724206_____|
 0.761822581      0.939142346       0.00000000      0.00000000      0.00000000   |
 0.00000000       0.00000000        0.00000000      0.00000000      0.00000000   |
 0.00000000       0.00000000        0.00000000      0.00000000      0.00000000   |
 0.00000000       0.00000000        0.00000000      0.00000000      0.00000000   |
 0.00000000       0.00000000        0.00000000      0.00000000      0.00000000   |
 0.00000000       0.00000000        0.00000000      0.00000000                   |
 Test :    19.167677736282350    8.9751804828643795   5.8824206053462074E-011_____|
 35.282016754150391        150.87135314941406

                 Shellspec
```

```
        INPUT:
shellspec.in - main input (geometry,objects...)
line.dat - atomic data for the lines
shellspec.mod - 3D model of the shell
                        (optional IF imodel=2)
abundances  - abundances (optional IF ichemc=1)
phases - orbital phases (optional IF nphase=0)
starspec1 - star spectrum (optional IF lunt1>0)
starspec2 - star spectrum (optional IF lunt2>0)        → start of Shellspec
starspec3 - star spectrum (optional IF lunt3>0)
albedo1 - albedo (optional IF albst<0)
albedo2 - albedo (optional IF albcs<0)
        OUTPUT:
shellspec.out - more detail output
fort.xx - 2D images at some frequency
shellspectrum - spectrum of the shell
lightcurve - LC or trailed spectrogram

 nphase=            1
 No. of sp. lines READ from line.dat=            1
 nstar1=            1      31006
i=  40.50  alpha=   0.00
 chi2   38.263639636012677      0.960224926  → fitness of the syntetic
                                                and observed spectrum
                                                with input parameters
                                    .
                                    .   → shellspec runs several times
                                    .
                    656609     657335     636841
                    358352     354352     423062
                     12089      12089     110006
                    603457     808037     367174
                    403011     346258     408248
 status:            0
 x:   0.656608999 0.358352005 1.20890001E-02 0.603456974 0.403010994
 f:   0.998377800   → this is the result with the value of the best
                      individual (x:) and its fitness function (f:)


 ctrl:  100.000000  30.000000   6.000000   0.850000   2.000000   0.050000
          0.000500   0.250000   1.000000   1.000000   1.000000   3.000000
                    →these are just values for ctrl vector
```

- Values for the best individuals are saved into the file *generace.dat*. By plotting the first and the fourth column of the file user will be able to see how the best individual for each generation varies and getting better by each generation. This file is generated by the `write` command in module *pikaia.f90* (`/home/shellspecf90/source`). Example of the *generace.dat* is below (in columns from the first: generation, individuals, initial mutation rate, fitness of the first best, second best, and the average) and data of the first and the fourth column (number of generation and fitness of the first best individual for the generation) are plotted in the Fig. 5.1.

```
            #generace.dat

        1    99 0.0033333 0.3286170 0.3286168 0.0252947

        2    99 0.0022222 0.3286170 0.1962448 0.0554000

        3    99 0.0014815 0.3286170 0.3286168 0.0736583
```
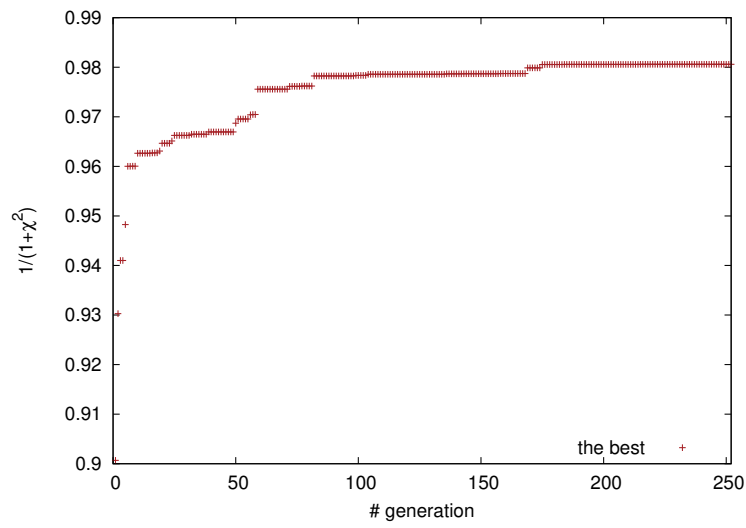
Table 5.1: *Evolution of the value for $1/(1 + \chi^2)$ for the best individuals for each generation*

4	99	0.0009877	0.4598798	0.3485152	0.0920731
5	99	0.0006584	0.5018177	0.4845585	0.1004014
6	99	0.0005000	0.5018177	0.4845585	0.1254106
		. . .			
495	99	0.0432488	0.8062923	0.8056455	0.5158235
496	99	0.0432488	0.8062923	0.8062890	0.5158592
497	99	0.0432488	0.8062923	0.8062800	0.6942428
498	99	0.0432488	0.8063483	0.8063009	0.7174796
499	99	0.0648732	0.8063483	0.8063152	0.7344757
500	99	0.0648732	0.8063483	0.8062189	0.6891267

Model examples - TT Hydrae, κ Draconis

To verify that our modified code works correctly we decided to use it at first to model well studied stars where properties describing the stellar system were known. As a model examples we chose two stars, TT Hya which was studied by Budaj et al. (2005) using the original Shellspec code and κ Dra which is one of the brightest and frequently studied Northern Hesmisphere Be star.

6.1   TT Hydrae

TT Hya (HD 97528, HIP 54807, SAO 179648, $V = 7.27\,\mathrm{mag}$, $\alpha = 11^\mathrm{h}13^\mathrm{m}$, $\delta = -26°28'$) which was studied by Budaj et al. (2005)[1], Miller et al. (2007)[2], Etzel (1988) and others. TT Hya was discovered to be an eclipsing variable of the Algol type by Wood (1926).

6.2   Settings of the model for the star TT Hya

At first we have randomly chosen one of the Hα line profile which was also studied by Budaj et al. (2005). We used Budaj et al. (2005) data with author permission to compare their resulting synthetic spectrum with our results.

For this example star we used model set up from STAR + COMPANION + STREAM + DISK. User definition of the modeling objects was stored in the file *initsh.f90* (originally *shellspec.in* file). Since this example is not Be star, the temperature was not redefined and the original one (equation (3.2)) was used but Budaj in his setting utilized *itdc*[3] to be 1 which signifies that temperature of the disk is constant.

To be noted, our model is rather simplified. In original work by Budaj et al. (2005) they had free parameters for secondary star and the disk. Since we were seeking for the verification of the modified code we used only five free parameters (inner and outer radius of the disk, density, microturbulent velocity and temperature), we picked up the most important properties which are describing the disk.

We adopted values of the properties for the primary star, the secondary star and the disk (except the parameters we chose to find by the modified code) from Budaj et al. (2005). Adopted properties describing the disk which we used are gathered in the first part of Tab. 6.1, except the inner and outer radius of the disk, disk density, microturbulent velocity and temperature of the disk which we found out by modified code and verified that the parameters are in good agreement. The confirmation whether the code runs correctly consisted in to get the same values for inner and outer radius, density, microturbulent velocity and temperature as in Budaj et al. (2005).

Free parameters restriction can be found in Tab. 6.2.

---

[1] They used original Shellspec code to study star TT Hya

[2] For part of the study original Shellspec code was used as well

[3] This parameter can be set in module *shellspec.in* or in modified version of the Shellspec in module *initsh.f90*

Table 6.1: *Adopted properties of TT Hya disk (first part of the table) and our results for disk radiuses (second part of the table) for TT Hya at 3606.071 phase*

Parameter	Value	
i	82°84	
α'	$2\,R_\odot$	
R_{in}	$2\,R_\odot$	
R_{out}	$10\,R_\odot$	
$\rho\,(R_{\mathrm{in}})$	$5 \times 10^{-14}\,\mathrm{g\,cm^{-3}}$	Budaj et al. (2005)
$n_{\mathrm{e}}\,(R_{\mathrm{in}})$	$2 \times 10^{10}\,\mathrm{cm^{-3}}$	
T	$7\,000\,\mathrm{K}$	
η	-1	
v_{trb}	$30\,\mathrm{km\,s^{-1}}$	
R_{in}	$2\,R_\odot$	
R_{out}	$9.7\,R_\odot$	
$\rho\,(R_{\mathrm{in}})$	$3.6 \times 10^{-14}\,\mathrm{g\,cm^{-3}}$	Our results
v_{trb}	$10.2\,\mathrm{km\,s^{-1}}$	
T	$5801\,\mathrm{K}$	

Notes: *i is an angle between rotation axis of the model and the line of sight, α' is angular halfwidth of the disc wedge, R_{in} inner radius, R_{out} outer radius, ρ is density, n_{e} electron number density, T temperature of the disc, η density dependence exponent and v_{trb} micro-turbulent velocity*

Table 6.2: *Free parameters restriction*

Free parameter	Interval of restriction
R_{in}	$(R_*, R_* + 5]\,R_\odot$
R_{out}	$(R_{\mathrm{in}}, R_{\mathrm{in}} + 15R_*]\,R_\odot$
$\rho(R_{\mathrm{in}})$	$[10^{-15}, 10^{-12}]\,\mathrm{g\,cm^{-3}}$
T	$[1\,000, 9\,000]\,\mathrm{K}$
v_{trb}	$[10, 160]\,\mathrm{km\,s^{-1}}$

Notes: *The restriction for R_{out} strongly depends on the value of inner radius R_{in}, $R_* = 1.95\,R_\odot$*

6.3 Results of the modeling for TT Hya

The second part of Tab. 6.1 presents obtained values for outer and inner radius of the disk, density, microturbulent velocity and temperature. These parameters are in good agreement with results in Budaj et al. (2005). Especially values for the inner radius and the temperature of the disk are the same.

At Fig. 6.1 you can see our and Budaj's fit of the observed spectrum (reproduced with permission). More results for TT Hya can be found in Budaj et al. (2005). The synthetic spectrum does not fit the observed one that well but the same inaccuracy is seen in the article outcome. Since our synthetic spectrum fits observed spectrum in the analogous way as Budaj's we can judge of the correctness of our results as well.

These results show that our modified code works in the analogous way as the original Shellspec code and the optimization of the input successfully replaced manual setting of the input parameters. This verified that the code runs correctly and we can use it to model other stars but we wanted to be more sure about this so we implemented the code to model well studied Be star (in this case κ Dra), since we focus on the circumstellar disks of Be stars, with the same purpose to get the same results for the disk parameters.
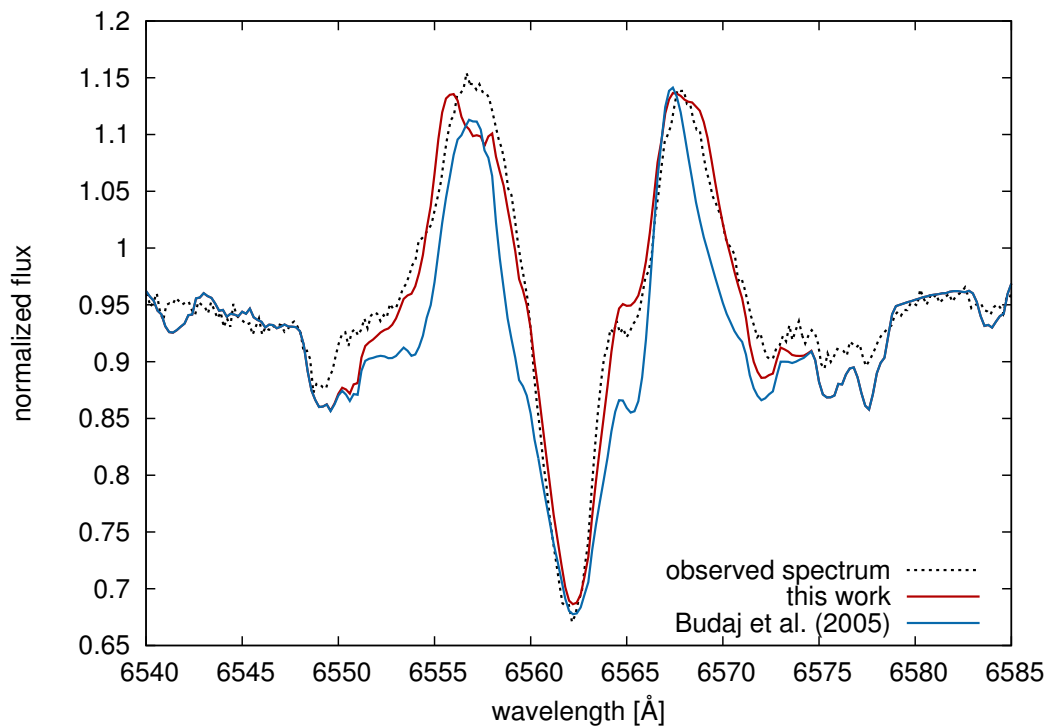
Figure 6.1: *Comparison of the synthetic (ours and Budaj's fit) and observed spectrum for TT Hya at 3606.217 phase.*

6.4 κ Draconis

κ Dra (5 Dra, HD 10 9387, HR 4 787, HIP 61 281, $V = 3.75 - 3.95$ mag) is one of the brightest variable Northern Hemisphere Be stars. It is also a known spectroscopic binary. It is variable on a variety of timescales. From Saad et al. (2004) we know that an analysis of time variations of the line strength and intensity of Hα and Hβ over the last thirty years show that κ Dra undergoes cyclic long-term variations with an average cycle of 22 years. These cyclic changes are most probably caused by a steep rise and a gradual decrease of the dimensions of a rapidly rotating circumstellar disk.

We chose this star as the model example because the radius of the disk of the star is known. Gies et al. (2007) and Touhami et al. (2013) presented values for the disk radius. Size estimates come from fitting the interferometric data with a geometrical model. Gies et al. (2007) estimated the size of the disk for K'-band continuum and Touhami et al. (2013) estimated the size for K-band and Hα. Their estimations are summarized in Table 6.3. These and other estimations for other Be stars can be found in Table 2 in Rivinius et al. (2013).

This star was also studied by Silaj et al. (2010), they estimated values for inclination $i = 45°$ and density $\rho_0 = 5 \times 10^{-10}$g cm^{-3} with index $n = 4$. In Fig. 6.2 we can see their best fit for the observed spectrum, adopted from Silaj et al. (2010). Their observed Hα line profile has the equivalent width $EW = -20.99$ (we explain theory of EW on page 72).

Figure 6.2: *Observed Hα line emission spectrum (solid line) along with the theoretical line profile (dotted line) for κ Dra, adopted from Silaj et al. (2010).*

Another study focusing on κ Dra is by Jones et al. (2008) who computed theoretical models of circumstellar disks for the classical Be stars, κ Dra included. They obtained value for the inclination, $i = 35°$, and by combining results from spectroscopy and interferometry, they found values for density ρ_0 and index n ($\rho_0 = 1.5 \times 10^{-10}$ g cm^{-3}, $n = 4.2$). Their resultant fits can be seen in Fig. 6.3, adopted from Jones et al. (2008). Their observed Hα line profile has $EW = -22.2$.

Modeling of κ Dra

We would like to note here that we model spectroscopically observed spectrum (Hα line profile) and thus we compare results obtained by two different methods, interferometry and spectroscopy.

Touhami et al. (2013) used observations from the period 2007 – 2010. Thus we used spectrum observed in this period for our modeling.
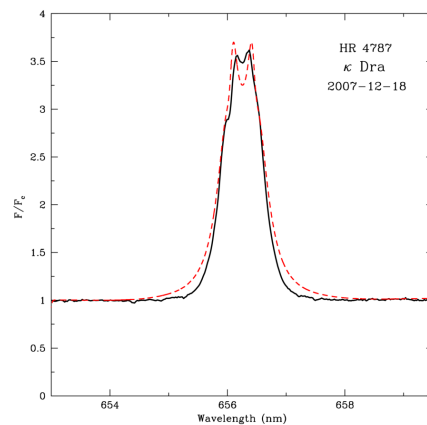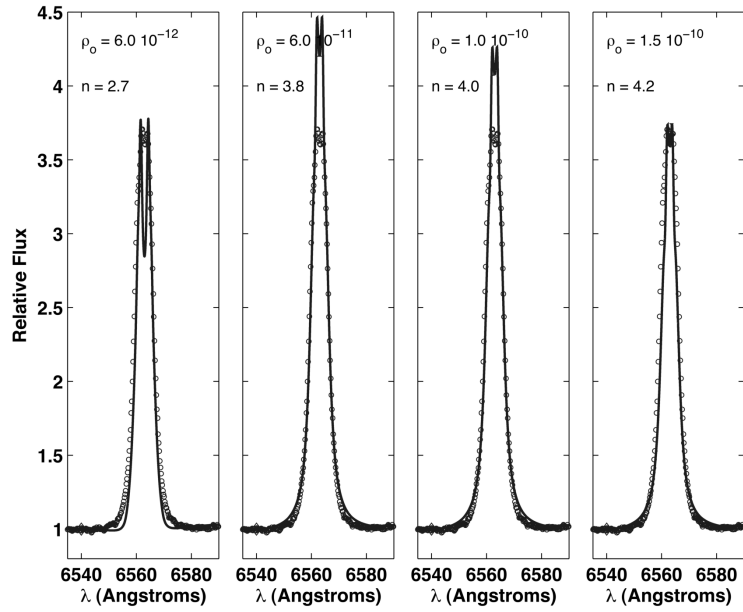
Figure 6.3: *Observed Hα line for κ Dra compared with 4 models with different values for n and ρ_0, adopted from Jones et al. (2008).*

The spectrum, we model, was observed on the 1st May 2008 at the Ondřejov Observatory and equivalent width of this spectrum is $EW(\text{H}\alpha) = -18.619$. As a model we used star + disk. We adopted values for the central star from Saad et al. (2004), see Table 6.4 with M the stellar mass, R_* the stellar radius, $\log g$ the surface gravity, T_{eff} the effective temperature, $v \sin i$ the rotational velocity and d the distance to the star.

Since there is several papers studying κ Dra and each uses different n index in the density distribution in its model, we present results for three models for three different indexes. We used model set up from

Table 6.4: *Stellar properties for κ Dra*

Parameter	Value
M	$4.8\,\text{M}_\odot$
R_*	$6.4\,\text{R}_\odot$
$\log g$	3.5
T_{eff}	$14\,000\,\text{K}$
$v \sin i$	$170\,\text{km}\,\text{s}^{-1}$
d	$150\,\text{pc}$

Table 6.3: *Size of the emitting region estimated from Gaussian fits, for different wavelengths*

Article	Wavelength	Disk radius [R_*]
Touhami et al. (2013)	Hα	5.1 ± 0.8
Touhami et al. (2013)	K	7.9 ± 1.9
Gies et al. (2007)	K'	4.62 ± 0.28

Table 6.5: *Summary of restriction for free parameters for modeling κ Dra.*

free parameter	interval of restriction
R_{out}	$(\mathrm{R}_*, 15\,\mathrm{R}_*]$
ρ_0	$[10^{-13}, 10^{-9}]\,\mathrm{g\,cm^{-3}}$
α	$[0, 20]°$
i	$[10, 90]°$
v_{trb}	$[10, 160]\,\mathrm{km\,s^{-1}}$

star + disk. We were looking for the disk parameters, their restrictions are summarized in Table 6.5.

6.5   Results of the modeling of κ Dra

Resulting values for the disk parameters can be found in Table 6.6. The fit of the observed spectrum for each model can be seen in Fig. 6.4. From the plots we can see that the best fits for all the models are approximately the same (see Fig. 6.5, difference between fitness function, $1/(1 + \chi^2)$, for these models is negligible). For these model we also obtained the same values for the parameters, except the density and the opening angle.

Using modified code we obtained values for the disk radius, $7.7\,\mathrm{R}_*$, $7.6\,\mathrm{R}_*$ and $6.7\,\mathrm{R}_*$ for n to be 3.5, 4 and 4.2 respectively. We can see that all the values are close to the values obtained by Gies et al. (2007) and are in a good agreement to those estimated by Touhami et al. (2013).

For the model with $n = 3.5$, $n = 4$ and $n = 4.2$ we get the value for the opening angle 9.4°, 10.4° and 19° respectively and the inclination of the system, $i = 66.1°$, $i = 66.4°$ and $i = 64.3°$ respectively.

These results also verified that our modified code is a good tool to model Be stars disks and a good method which gives the comparable results as the interferometry.

The differences between ours and Jones et al. (2008) resultant values for the inclination and the density, for the model with $n = 4.2$, can be caused due to the fact that we used more simple density distribution, the density distribution is not dependent on the vertical distance Z (height above the equatorial plane) and that we used a single star with a disk as a model unlike Jones et al. (2008) who used a binary model.

We neglected this possibility since the secondary star is assumed to be faint and also how Touhami et al. (2013) pointed out: Gies et al. (2007) improved their fit of K'-band by adding the hot companion, but Jones et al. (2008) noticed that their density exponent determined from Hα interferometry is much higher than the one determined by Gies et al. (2007) from K'-band interferometry. Touhami et al. (2013) made an observation that this discrepancy casts some doubt about the detection of the companion and that there are no published speckle measurements of this star.
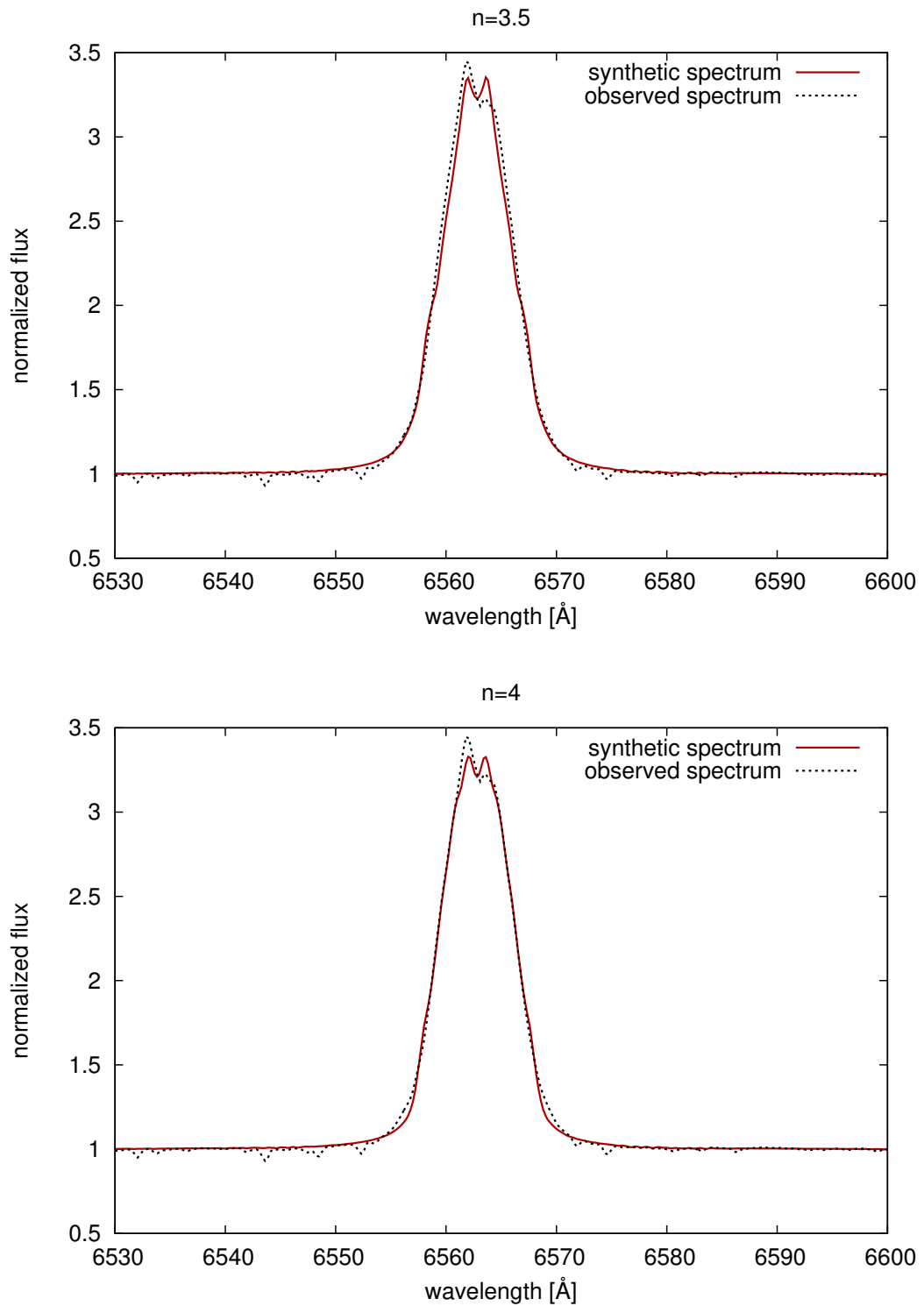
Figure 6.4: *Comparison of the synthetic (solid red line) and observed spectrum (dashed black line) for κ Dra for three models with different n indexes (n = 3.5, 4, 4.2).*
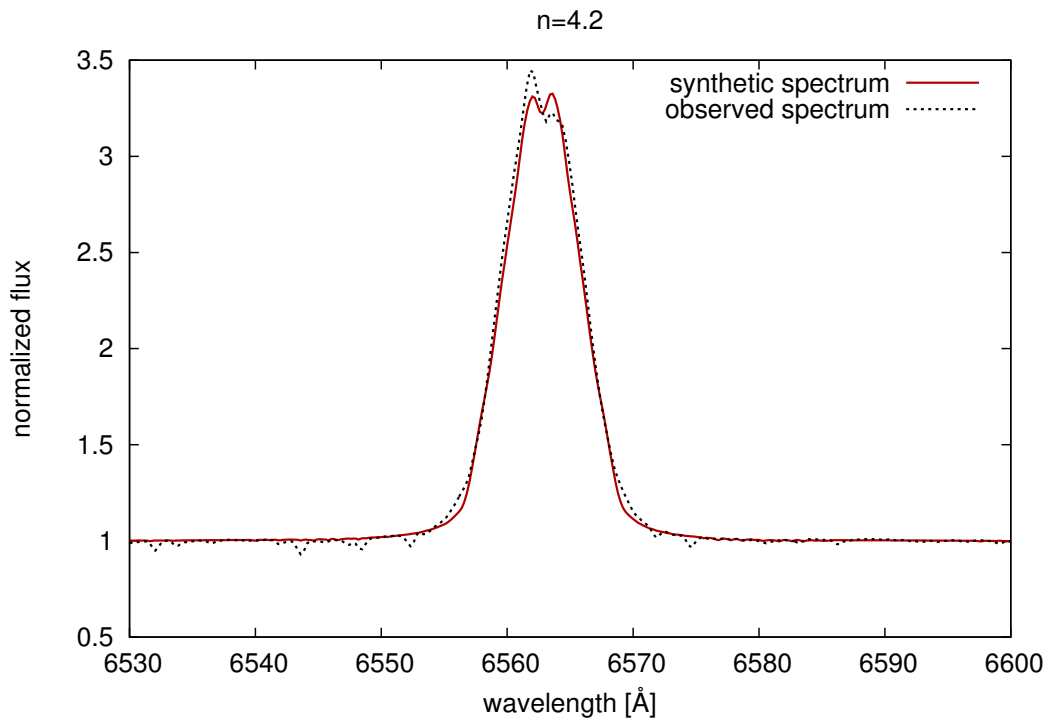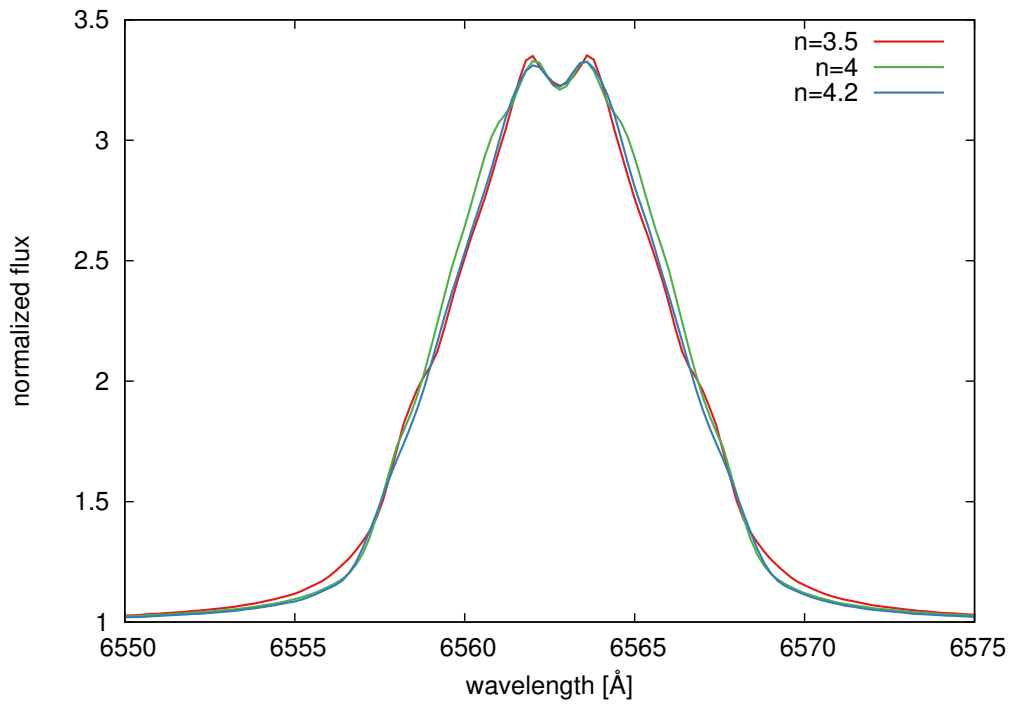
Figure 6.4: *(Continued)*

Figure 6.5: *Comparison of all the synthetic spectra for three models with three different n indexes.*

Table 6.6: *Resultant values for the circumstellar disk parameters of the star κ Dra*

Parameter	$n = 3.5$	$n = 4$	$n = 4.2$
$R_{\mathrm{out}} \, [\mathrm{R}_*]$	7.7	7.6	6.7
$i \, [°]$	66.1	66.4	64.3
$\rho_0(R_{\mathrm{in}}) \, [\mathrm{g\,cm}^{-3}]$	3.5×10^{-10}	8.6×10^{-10}	6×10^{-10}
$v_{\mathrm{trb}} \, [\mathrm{km\,s}^{-1}]$	34.1	38.1	40.9
$\alpha' \, [°]$	4.7	5.2	9.5
$1/(1 + \chi^2)$	0.85	0.83	0.84

60 Cygni

Be shell star 60 Cyg (according to Bright Star Catalogue (Hoffleit & Jaschek 1982): V1931 Cyg, HD 200310, HR 8053, MWC 360; B1 Ve, $V = 5^{\mathrm{m}}37$ (var.), $v \sin i = 320\,\mathrm{km\,s^{-1}}$). 60 Cygni exhibits pronounced long-term spectral variations characterized by the B $\rightleftharpoons$ Be phase transitions.

7.1 History of 60 Cygni study

There are four main articles studying 60 Cygni star: Koubský et al. (2000), Wisniewski et al. (2010), Draper et al. (2011) and Draper et al. (2014).

The first article analyzed electronic spectra secured between 1992 and 1999 at the Haute Provence, Ondřejov and Dominion Astrophysical Observatories and of differential UBV measurements of 60 Cyg obtained between 1984 and 1999 at Hvar, San Pedro Mártir, Toronto and Xinglong Observatories, the all-sky Hipparcos satellite H_p photometry transformed to Johnson V and B magnitudes, and all-sky UBV observations and found changes on long, medium and rapid time-scales.

Koubský et al. (2000) presented evidence that the star has experienced disk-loss and subsequent regeneration in the past. Their study of periodic radial velocity variations of Hα and He I 6678 suggest that the star might be a spectroscopic binary having a period of 146.6 ± 0.6 days, while 1.064 day line profile variations and 0.2997 day photometric variations may be caused by non-radial pulsations.

At Fig. 7.1, adopted from (Koubský et al. 2000), it is possible to see the schematic of how the emission in Hα line profile progresses between years 1953 and 1999.
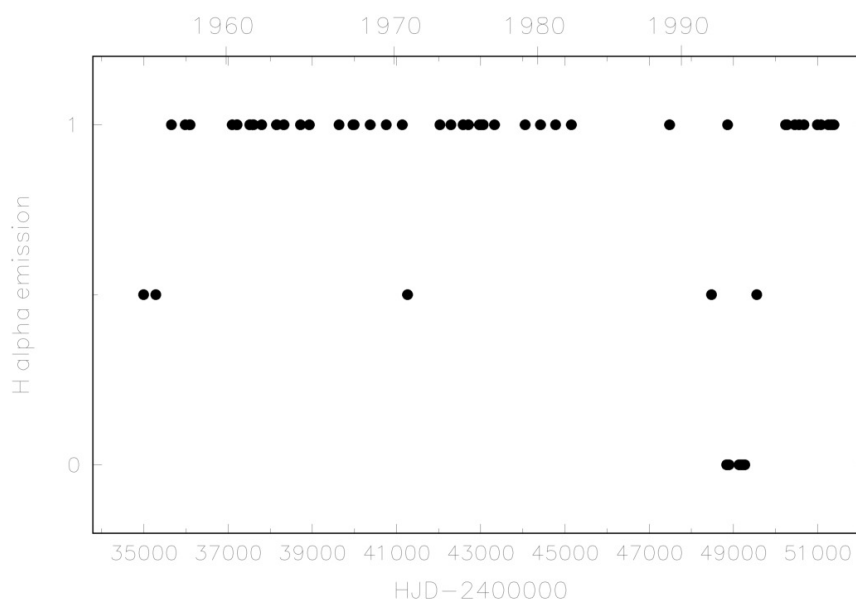
Figure 7.1: *Schematic representation of Hα vs time; 1 denotes strong emission, 0.5 an intermediate state, and 0 a "pure" absorption.*

The characteristics of the primary star are also presented in the article, we summarized them in Table 7.1 (the explanation of the characteristics is the same as in Table 6.4). Synthetic spectrum for this primary star can be seen in Fig. 3.1 on page 20.

The second article analyzed about 15 years of spectropolarimetric observations of the classical Be stars 60 Cygni and π Aquarii, which covered one disk-loss episode in each star, and discussed the timescale and overall evolution of these events.

In Wisniewski et al. (2010), they presented one of the most comprehensive spectropolarimetric view of transition from Be phase to normal B-star phase to date. They presented 35 spectropolarimetric and 65 Hα spectroscopic observations of Be star 60 Cyg spanning 14 years. They found that the timescale of the disk-loss events in 60 Cyg corresponds to almost 6 complete orbits of star's binary companion. This suggest that star's binary companion does not influence the primary star (or its disk). From Wisniewski et al. (2010) we also know that the position angle[1] of intrinsic polarization arising from 60 Cyg's disk is $\theta_* = 107°\!.7 \pm 0°\!.4$ indicating that the disk situated in the equatorial plane is oriented on the sky at a position angle of $\theta_{disk} = 17°\!.7$ (measured North to East).

In the last article, they present a first look at the behavior of the intrinsic polarization during these events. Draper et al. (2011) analyzed the intrinsic polarization in the process of losing its circumstellar disk via Be to normal B star transition. They observed 60 Cygni 35 times between 1992 and 2004 with the University of Wisconsin's HPOL spectropolarimeter, all these data are the same as in Wisniewski et al. (2010).

Table 7.1: *Stellar properties for 60 Cyg*

Parameter	Value
M	$11.3\,\mathrm{M_\odot}$
R	$5.1\,\mathrm{R_\odot}$
$\log g$	4
T_{eff}	$27\,000\,\mathrm{K}$
$v \sin i$	$320\,\mathrm{km\,s^{-1}}$

7.2 Modeling of the Be star 60 Cygni

Since we knew from Koubský et al. (2000) and Wisniewski et al. (2010) that the star's binary companion does not influence the primary star (or its disk) and we wanted to study evolution of the star's disk, we defined in Shellspec code model STAR + DISK. The characteristics for primary star were adopted from Koubský et al. (2000), we summarized them in Table 7.1. In this work we modeled only Hα line profiles.

7.3 Data

For our modeling we used some of the results which Doubek (2006) gained in his master thesis, where he had the same spectra as in Koubský et al. (2000) at his disposal. He divided spectra into five Hα profile types (P1, P2, P23, P233, P3), see

---

[1]The position angle of polarization θ is the angle of orientation of the ellipse relative to the two chosen orthogonal bases (say, the vertical and horizontal axes of your telescope field of view). If you observed linear polarization, the angle of the linear polarization would also be θ.

Fig. 7.2. These spectra are not real observed one but they are smoothed to see what kind of Hα profiles 60 Cygni had during years 1992 and 1999. In Fig. 7.2 we can also see how the emission activity changes. Profile P1 shows the highest emission, profile P2 is interested by its double peaked emission line, other profiles show lower emission activity and the last profile P3 seemed not to have the emission at all.

We also had several real observed spectra of 60 Cygni which we modeled as well. These spectra were observed at Ondřejov Observatory in the period from 2003 to 2011. We modeled 38 of the observed spectra. Results of the modeling of these spectra are more important in understanding the dynamical evolution of the Be star 60 Cygni.
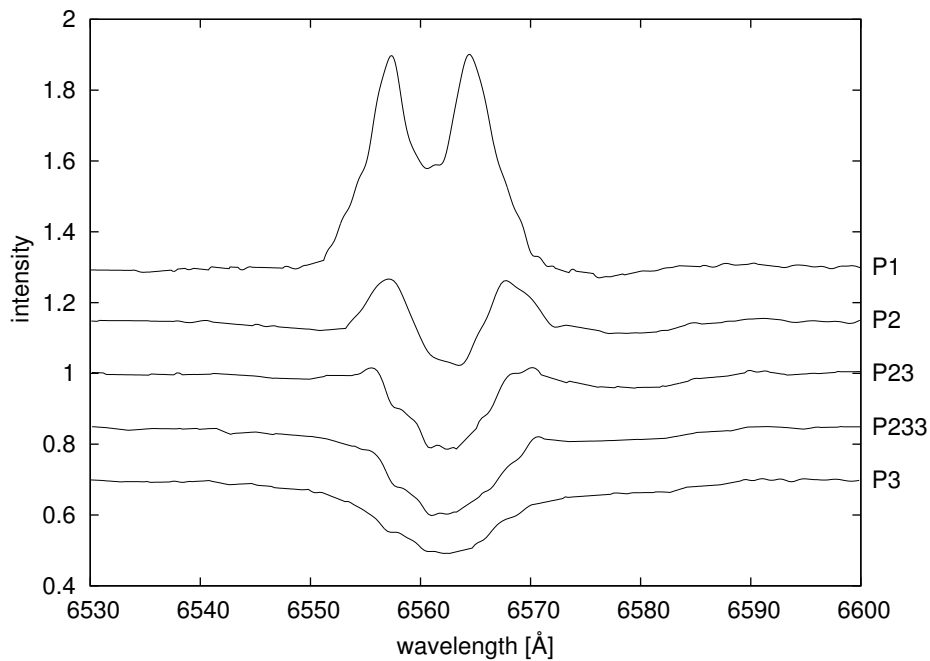
Figure 7.2: *Smoothed Hα profiles for 60 Cyg*

7.4 Set up of the subroutine PIKAIA

One of the most important point to set up PIKAIA is to choose number of free parameters. In this study we used 5 free parameters in the beginning. They were outer radius, density, opening angle, turbulent velocity and inclination.

It is also necessary to choose a number of generation and individuals (population number) or in other words set values for control vectors which we introduced in Chapter 5 on page 35. After discussing examples in PIKAIA manual (Charbonneau & Knapp 1995) we decided to point number of generation to be 150 and number of individuals to be 100. We tried different combination but this one seemed to be the best in the way of computational time and getting the best individual. To choose
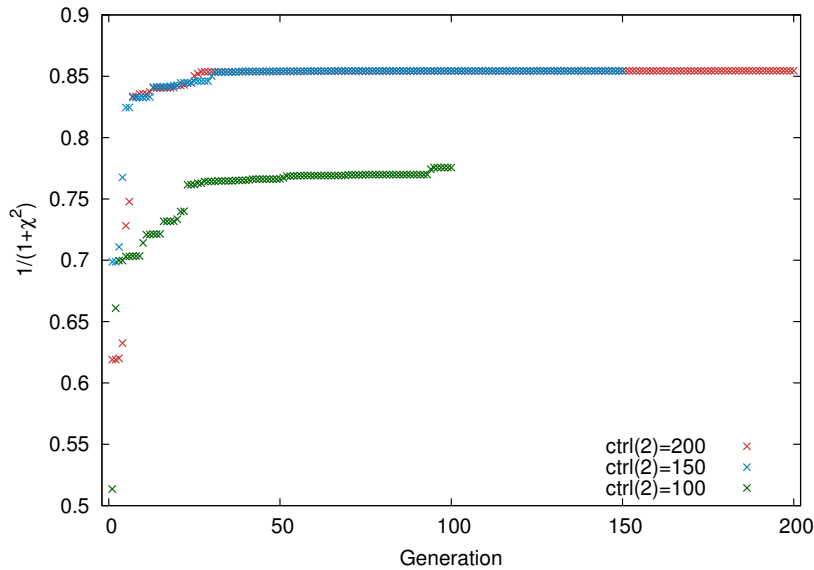
Figure 7.3: *Evolution of the $1/(1 + \chi^2)$ associated with the best individual of a given generation, for three genetic solutions*

bigger number of generations means longer time and the best individual which does not differ that much from the best individual which we got with lower number of the generation. In Fig. 7.3 we present evolution of the $1/(1 + \chi^2)$ associated with the best individual of a given generation, for three genetic solutions.

Values for other control vectors such as encoding accuracy, crossover rate, mutation mode etc. were left default, see (Charbonneau & Knapp 1995). The most important settings are collected in Table 7.2

Table 7.2: *Set up of PIKAIA*

	value
npar	5
ctrl(1)	100
ctrl(2)	150

Notes: *npar is number of free parameters, ctrl(1) is number of individuals, ctrl(2) is number of generation, other control vectors were left default*

7.5   Free parameters restriction

There are physical and observed restriction for free parameters describing disk of a Be star. In our case there is restriction namely for inner and outer radius of the disk, density, inclination and opening angle of the disk.

We know that double-peaked emission lines (typical for Be-shell stars) are formed when the inclination angle i is sufficiently large and we know that star 60 Cygni is Be-shell star (for example Silaj et al. (2010) mentioned 60 Cyg to be the Be-shell star). Due to that boundaries for inclination were defined with the assumption that the star 60 Cygni is Be-shell star whose value of the inclination lies in the range $i \, \epsilon \, [70°, 90°]$.

Table 7.3: *Summary of restriction for free parameters*

free parameter	interval of restriction
R_{out}	$(5.2, 91.8] \, \mathrm{R}_\odot$
ρ_0	$[10^{-13}, 10^{-10}] \, \mathrm{g} \, \mathrm{cm}^{-3}$
α	$[0, 20]^\circ$
i	$[70, 90]^\circ$

From Quirrenbach et al. (1997) we know that an opening angle should be smaller than 20° ($\alpha < 20°$), we explained this problem in more detail on page 12. We adopted this boundary for our model.

Boundaries for density ρ_0 were chosen dependently on several articles (for example Carciofi & Bjorkman (2006), Silaj et al. (2010), Porter (1999), etc.), where the typical values for densities were in the interval $\rho_0 \, \epsilon \, [10^{-13}, 10^{-10}] \, \mathrm{g} \, \mathrm{cm}^{-3}$. Density distribution was defined as

$$\rho(R_{\mathrm{in}}) = \rho_0 \left(\frac{r}{R_{\mathrm{in}}} \right)^{-n} .$$

Since determination of the density slope n from Silaj et al. (2010) showed that it is in the range of $1.5 - 4$ with a statistically significant peak at 3.5, we defined $n = 3.5$.

As was mentioned before (see more in Chapter 2 on page 13) Rivinius et al. (1998) revived the idea of a ring, suggesting that in some cases the disk might be detached from the star, instead of starting right at its photosphere, and be separated from it by a relative minimum in density. Rivinius et al. (2001) observed, mainly in the optically thin metal and helium lines, graduate disappearance of the high velocity components of the line, which indicates that the high velocity material close to the star has been partially depleted. However Rivinius et al. (2013) mentioned that the suggestion that this was due to the formation of an inner ringlike void is inadequate, as this would be dynamically unstable in a viscous disk. Due to this reason we defined the inner radius to be constant during modeling real observed spectra, starting right next to the star $R_{\mathrm{in}} = R_* + 0.1 \, \mathrm{R}_\odot$ (inner radius cannot have the same value as the radius of the star, Shellspec would notify an error). For smoothed spectra we present both cases: with inner radius as a free parameter and as a constant parameter, just for a curiosity how would results for these two cases differ.

We defined lower boundary for width of the disk, dr, as $0.1 \, \mathrm{R}_\odot$. The upper boundary for R_{out} was more difficult to define. Doubek (2006) tried to determine distance r_{r} where the disk falls apart. He assumed that the disk is Keplerian, and has a shape of a ring and he found $r_{\mathrm{r}} \simeq 5 - 6 \, \mathrm{R}_*$. Since this value has not been verified yet we defined this boundary to be $18 \, \mathrm{R}_* = 91.8 \, \mathrm{R}_\odot$ at the beginning.

The summary of the restriction for outer radius, density, opening angle and inclination can be seen in Table 7.3.

7.6   Grid

We also searched for the best choice of the grid. At first we used sparse gain with bigger boundary for radius of the disk. Then we continued iteratively, we got results for radiuses and if the results are smaller we decrease the boundary for outer radius and make the grid denser which gives us more precise results. Using sparse grid we noticed oscillation in the wings of a line (see Fig. 7.4) which is due to a numerical problem. Due to this we found that for large disk, for example larger than $15\,R_*$, we do not get too good results. Moreover if we want

Figure 7.4: *Example of the oscillation using sparse grid in Shellspec code*

to make a denser grid for such a large disk we got error because of the computer memory so we were not able to get rid of the oscillation. In that reason some of the synthetic profiles can show a features in form of the oscillations. This is one of the goal for our future work to improve the description of the grid.

7.7   Results for smoothed profiles

At first we present results for smoothed profiles P1, P2, P23, P233, P3. We present here two results for two cases of the problem as was discussed before. Results for these profiles are not relevant in understanding the dynamical evolution of the Be star 60 Cyg but it gives us an idea of values of parameters for modeling real spectra.

First model was with inner radius as a free parameter. Final value for each free parameter can be found in Table 7.4 and fit of the synthetic and observed spectra can be seen in Fig. 7.5.

Second model was with disk rises from the star, $R_{\mathrm{in}} = R_* + 0.1\,R_\odot$ (inner radius cannot have the same value as the radius of the star, Shellspec would notify an error). Results for values of the free parameters can be seen in Table 7.5 and the best fits of the synthetic spectra can be seen in Fig. 7.6. We can see from Table 7.5 that with increasing emissivity activity the outer radius increases as well.

If we compare results for the case when inner radius was free parameter and the case where it was a constant we can say that for the later case results are much better, values for inclination or opening angle are more constant, we do not see such a big dispersion as in the first case. Thus we believe that this shows that using constant inner radius rising right from the star is the relevant method.
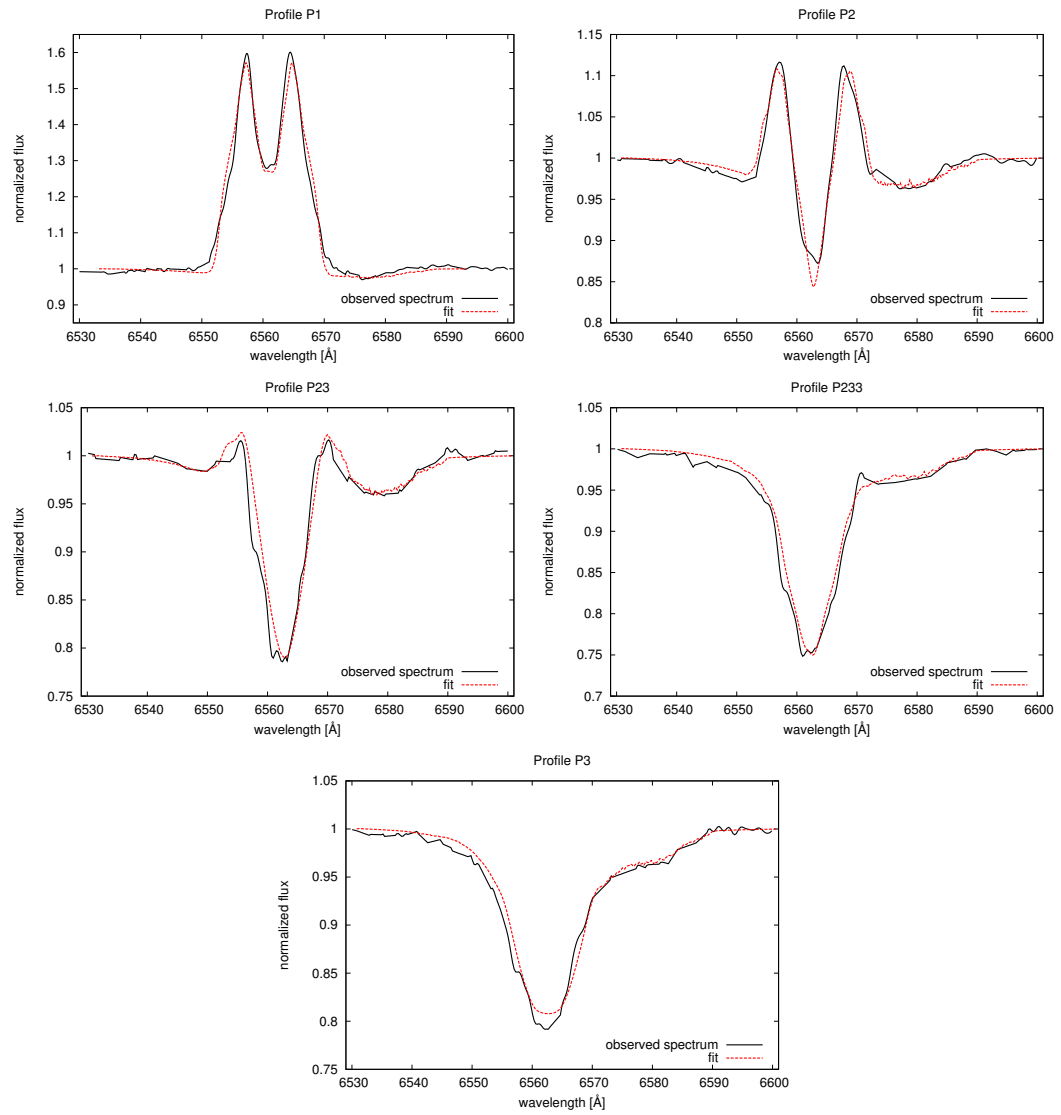
Figure 7.5: *Fit of the synthetic spectra for Hα profiles P1 – P3, for synthetic spectra parameters from Table 7.4 were used*
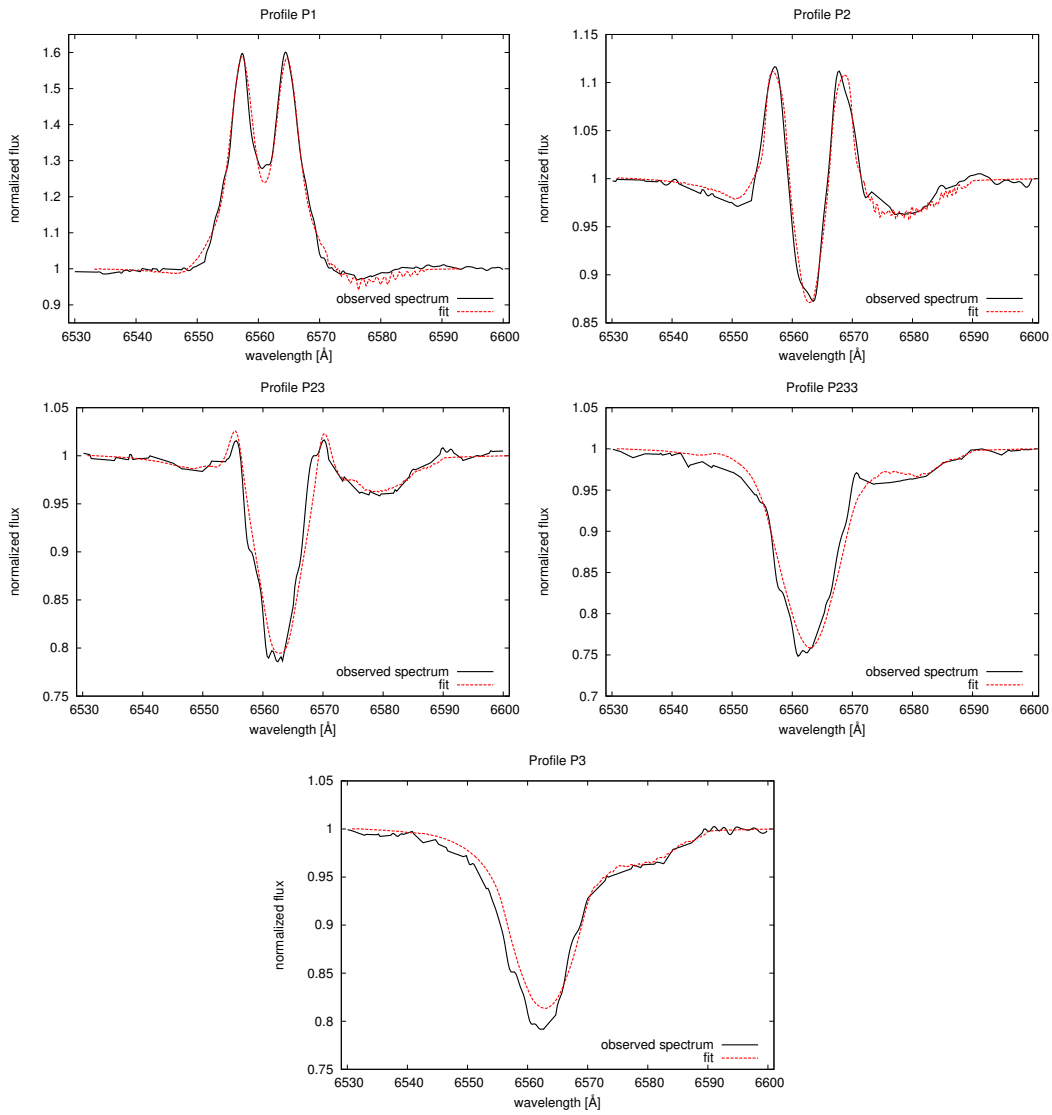
Figure 7.6: *Fit of the synthetic spectra for Hα profiles P1 – P3, for synthetic spectra parameters from Table 7.5 were used*

7.8   Results for observed spectra

We had 38 real observed spectra in disposal which we modeled. We chose spectra rather randomly with regard to a shape of the Hα profile. We wanted to cover all the possibilities for the shape of the line profile in our modeling. Spectra were observed at Ondřejov observatory during the period from 2003 to 2011. During this period the Hα line profile changed a lot, from the absorption to emission line profile.

At first we modeled five profiles with the highest emission activity whose disk structure can be easily recognize. For these five profiles inclination was free parameter. The final value for inclination which correspond to the best fit for each profile is $i = 88.9°$. This value was adopted and fixed for the rest of the profiles. As we mentioned before (page 51) in the beginning we used 5 free parameters but after the value of the inclination was fixed number of free parameters reduced to 4.

Table 7.4: *Results for smoothed profiles with inner radius as a free parameter and $R_* = 5.1\,\mathrm{R_\odot}$*

profile	$R_{\mathrm{in}}\,[\mathrm{R_\odot}]$	$R_{\mathrm{out}}\,[\mathrm{R_*}]$	$i\,[°]$	$\rho_0\,[\mathrm{g\,cm^{-3}}]$	$\alpha\,[°]$
P1	10.1	6.4	91.4	1×10^{-10}	2.9
P2	9.6	4.2	93.9	3.8×10^{-11}	1.2
P23	8.7	3.3	87.1	3.9×10^{-12}	1.3
P233	9.6	2.1	89.6	2.5×10^{-11}	6.6
P3	7.8	1.8	91.1	2.8×10^{-11}	3.2

Notes: R_{in} and R_{out} are inner and outer radius, i is inclination, ρ_0 is density and α is opening angle

Table 7.5: *Results for smoothed profiles with constant inner radius $R_{\mathrm{in}} = 5.2\,\mathrm{R_\odot}$ and $R_* = 5.1\,\mathrm{R_\odot}$*

profile	$R_{\mathrm{in}}\,[\mathrm{R_\odot}]$	$R_{\mathrm{out}}\,[\mathrm{R_*}]$	$i\,[°]$	$\rho_0\,[\mathrm{g\,cm^{-3}}]$	$\alpha\,[°]$
P1	5.2	15.71	88.8	$8.6 \cdot 10^{-11}$	1.4
P2	5.2	5.45	88.8	$9.8 \cdot 10^{-11}$	1.1
P23	5.2	4.94	87.1	$7.5 \cdot 10^{-12}$	1.2
P233	5.2	2.19	89.9	$3.7 \cdot 10^{-11}$	3.2
P3	5.2	1.58	89.3	$1.5 \cdot 10^{-11}$	1.4

Notes: R_{in} and R_{out} are inner and outer radius, i is inclination, ρ_0 is density and α is opening angle

Resulting values for more free parameters describing disk properties of 38 observed line profiles can be seen in Table 7.6. Fits of the observed line profiles are plotted in Fig. 7.7, in Appendix A it is possible to see them in more detail. Unlike Fig. 7.7 in Table 7.6 we did not sort the results in terms of time of the observation but we separated observed profiles into six groups according to the shape of the line profile. This sorting is rather subjective.

We plotted the resulting values of the density, the outer radius, the angular halfwidth of the disk wedge (half of the opening angle) and the microturbulent velocity for each observed line profile depending on the Heliocentric Julian date in Fig. 7.9.

In each graph we added two vertical lines. The left one notes the first time when the emission line profile of Hα was observed. The second line notes the moment since only emission line profiles were observed. We also used different colors to distinguish the results for emission and absorption line profiles. It could be noted that resulting values for density, angular halfwidth of the disk wedge and the microturbulent velocity for the absorption line profiles do not show any dependency, unlike the values for the outer radius of the disk which are rather constant around the value $1.5\,\mathrm{R}_*$.

It is assumed if we observe absorption line profile no disk is present around the star. Hence it is clear that the values of parameters of the disk are expected to be dispersed which clarify the random fluctuations in our graphs (these fluctuations can be seen especially for opening angle, density and microturbulent velocity values).

We believe that for the future modeling of stars it would not be necessary to model absorption profiles. The absorption lines do not bring any information about the disk and our code is not suited to model them. This assumption can also explain the constant values of R_{out} for absorption line profiles, these values show that there is almost no disk.

But on the other hand results for emission line profiles show clear dependency. For example density shows linear increase in time.

From Table 7.6 we can also say that with increasing emission activity the outer radius of the disk increases. There is no smooth expansion of the disk we can see several events when the disk decreased a little bit. Value of the outer radius for the profile with the highest emission activity is $R_{\mathrm{out}} = 18.68\,\mathrm{R}_*$.

If we took into account only results for emission line profiles we could say that the average value of the angular halfwidth of the disk wedge α' is about $1.75°$ and thus the opening angle is $\alpha = 2\alpha' = 3.5°$.

For profiles for which emission activity is evident we tried to found if there is any dependency of density on outer radius of the disk. Just by eye we can say that there is an dependency. Thus we fitted the data by an power law function, we used Gnuplot program (Williams et al. 2013) for the fitting. The result can be seen in Fig. 7.13. The dependency we found is

$$f(R_{\mathrm{out}}) = 9.46 \cdot 10^{-13} \left(\frac{R_{\mathrm{out}}}{5.1} \right)^{-3.5},$$

where the value 5.1 is the stellar radius of the star 60 Cygni. This is actually the same power law used in the definition of the density in the Shellspec code $\rho(r) = \rho_0(r/R_*)^{-3.5}$.

In Fig. 7.10 we plotted correlations between equivalent width and disk parameters (the outer radius, the density, the opening angle and the microturbulent velocity). Values for EWs were determined by SPEFO code (Skoda 1996) and can be found in Tabel 7.7. Positive value of EW is commonly used for absorption line and negative value for emission line, we use the same notification. More about EW in the next section Spectral Analysis. In this plots we again noticed the same phenomenon as in the previous figure (Fig. 7.9) where for absorption profiles we get random values of the parameters except the values for the outer radius.

Fits of the polynomial curves to data points (only emission line profiles) can be seen in Fig. 7.11 (we used Gnuplot for the fits). The correlation between EW and ρ_0 can be seen in Fig. 7.10B. This correlation has the linear trend $f(x) = -0.8x + 3.0$ (see Fig. 7.11B). Further, it is interesting to note that the shapes of the functions of the time evolution for values of the equivalent width of the line profile EW and density ρ_0 (only for the profiles with the visible emission activity) are similar. $EW(t)$ and $\rho_0(t)$ can be seen in Fig. 7.12, EW with blue points and ρ_0 with red points. These two characteristics develop in the same way for the Be star 60 Cygni, which also confirms the linear trend in the correlation between the ρ_0 and EW.

Another interesting correlation for the EW is with the microturbulent velocity (Fig. 7.10D). This correlation has the polynomial trend $f(x) = -0.72x^2 - 12.76x + 52.78$ (see Fig. 7.11D). As was mentioned before values for the opening angle are constant around value $3.5°$, from the graph in Fig. 7.10C or Fig. 7.11C we can see that opening angle is independent of the equivalent width of the line.

It is necessary to model more spectra for a different time of observations to make the fits of the data points for correlations more accurate, especially for the correlation of the outer radius of the disk and the equivalent width. The fit of the polynomial curve to the data points for this correlation depends on how the outer radius of the disk will evolve, if it will increase or decrease. For this moment we plotted two different types of curve for the correlation between outer radius and equivalent width, the square root and the polynomial curve, see Fig. 7.11A. Use of the square root was inspired by Grundstrom & Gies (2006) where they estimated Be star disk radii using Hα emission equivalent widths and used expression

$$\frac{R_\mathrm{d}}{R_*} = \sqrt{\frac{I_\lambda^s}{I_\lambda^d}\frac{EW(1+\epsilon)}{\langle\Delta\lambda\rangle\cos i}}, \tag{7.1}$$

where I_λ^s is the stellar specific intensity near Hα, I_λ^d is the specific intensity of the disk, ϵ is the ratio of disk continuum flux to stellar flux in the Hα region.

In Fig. 7.8 we can see all the individuals for free parameters (R_out, ρ_0, i and α) for which the synthetic spectrum was determined and compared with observed one, these results are for spectrum named ud210026. Since the graphs are showing dependency of free parameters on the measure of the fit $1/(1+\chi^2)$ we can clearly see which values are the best to describe the observed spectrum.

We can compare our results for outer disk radius with Jaschek & Jaschek (1993) where they used simple formula to estimate outer radius which we mentioned on page 12. They determined radius only for one Hα line profile. Observation values were adopted from Andrillat (1983).

It is common to observe double-peaked emission lines of Be stars. Such a fact was interpreted by Huang (1972) in the framework of a simple model, as a consequence of a disk-like emission region around these stars. He showed that one can derive the outer radius of the emission r line forming region by using one of the formulae.

$$r_1 = \frac{2V\sin i}{\Delta v} \tag{7.2}$$

and
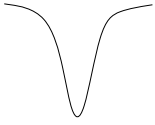
$$r_2 = \left(\frac{2V\sin i}{\Delta v}\right)^2 \tag{7.3}$$

Eq. (7.2) is used in the case that the disk rotates with conservation of an angular momentum (something that happens close to the star) and Eq. (7.3) when the disk rotates with Keplerian motion (something which happens in outer region). The resultant values by Jaschek & Jaschek (1993) are: $r_1 = 1.75\,\mathrm{R}_*$ and $r_2 = 3.1\,\mathrm{R}_*$. Authors also noted that since both $V\sin i$ and Δv are affected by observation errors, the value of r so derived have an uncertainty of the order of $\pm\,20\%$.

Since authors adopted the same Hα line profile for their estimation and some of the parameters from Andrillat (1983) we can see what type of Hα line profile they used. Value for the peak separation for the profile is $\Delta v = 343\,\mathrm{km\,s^{-1}}$ and $v\sin i = 300\,\mathrm{km\,s^{-1}}$ which differs from our value $v\sin i = 320\,\mathrm{km\,s^{-1}}$. The equivalent width for the profile is $EW = -4.4$.

The equivalent widths for our profiles are presented in Table 7.7. We can see that we found similar value for profile sg270024 . However we found outer radius to be $14.6\,\mathrm{R}_*$, which is five times bigger than Jaschek & Jaschek (1993) found, if we assume Keplerian motion.

Table 7.6: *Results for observed* Hα *profiles,* $R_{in} = 5.2 \, R_\odot$, *$i = 88.9°$; α is opening angle, R_{out} is outer radius of the disk, ρ_0 is density, v_t is microturbulent velocity, HJD is Heliocentric Julian date*

name	α [°]	R_{out} [R_*]	ρ_0 [g cm^{-3}]	v_t [km s^{-1}]	HJD	profile shape
md110022	5.2	1.45	2.6×10^{-11}	132	2741.586	
md120017	4.6	1.73	4×10^{-11}	148.3	2742.561	
mi170018	10.1	1.37	2×10^{-11}	127.5	2900.333	
ml090028	4.5	1.53	6.6×10^{-11}	152.6	2983.323	
ng210007	10.4	1.61	4.3×10^{-11}	152.9	3208.403	
nk250010	4.6	1.49	6.4×10^{-11}	120.9	3335.310	
oh300033	6.8	1.3	1.9×10^{-11}	159.8	3613.407	
oi010018	3.2	1.37	1.8×10^{-11}	160	3615.498	
mg140011	9.8	1.37	1.9×10^{-11}	109	2835.402	
mg230016	11	1.57	3.1×10^{-11}	91.4	2844.423	
oe260004	9	1.61	7×10^{-11}	93.7	3517.397	
oi050016	2.9	2.4	5.6×10^{-11}	53.9	3619.340	
mk110031	1.7	4.73	6.3×10^{-12}	10.2	2955.386	
od020047	2	9.61	8×10^{-12}	24	3463.567	
od180011	1.8	9.04	7.4×10^{-12}	10.3	3472.478	
oe200032	2	7.08	4.9×10^{-12}	10	3511.580	
oi090022	2.3	4.98	6×10^{-12}	11.5	3623.444	
pe020017	2.1	12.92	9.1×10^{-12}	11.7	3857.503	
nd280015	2	6.88	1.2×10^{-11}	10.7	3124.434	
oi190030	1.3	14.61	2.5×10^{-11}	55.5	3633.393	
oj110026	1.9	10.45	2×10^{-11}	64.1	3655.368	
oj140024	1.6	7.2	2.8×10^{-11}	61.1	3658.301	
oj160010	1.7	13.55	2.2×10^{-11}	58.3	3660.290	
oj280017	1.6	14.82	2.3×10^{-11}	37.1	3672.199	
oj310009	1.6	15.02	2.4×10^{-11}	37.2	3675.326	
ol080018	1.7	12.59	2.3×10^{-11}	48.7	3713.234	
pa090021	1.3	15.16	2.4×10^{-11}	10.1	3745.331	
qc140015	1.8	16.12	2.7×10^{-11}	63.6	4174.563	

Continued on next page

Table 7.6: *Results for observed* Hα *profiles,* $R_{\mathrm{in}} = 5.2\,\mathrm{R_\odot}$, $i = 88.9°$; α *is opening angle,* R_{out} *is outer radius of the disk,* ρ_0 *is density,* v_{t} *is microturbulent velocity, HJD is Heliocentric Julian date*

name	α [°]	R_{out} [R$_*$]	ρ_0 [g cm^{-3}]	v_{t} [km s^{-1}]	HJD	profile shape
qd040061	1.7	15.59	3.1×10^{-11}	54	4195.631	
qf230027	1.6	16.2	3.3×10^{-11}	35.5	4275.536	
re070026	1.7	14.14	3.8×10^{-11}	60.9	4594.509	
rj210042	1.5	15.22	4.5×10^{-11}	48.1	4761.302	
sg270024	1.6	14.6	6.6×10^{-11}	93.8	5040.341	
tc230053	1.6	16.2	8.7×10^{-11}	115	5279.565	
td020080	1.5	16.6	9.3×10^{-11}	110.4	5289.606	
te290038	1.7	19.2	9×10^{-11}	107.5	5346.512	
tg270022	1.5	18.37	9.6×10^{-11}	100.2	5405.430	
ud210026	1.6	18.68	1×10^{-10}	107.6	5673.429	

Continued from previous page
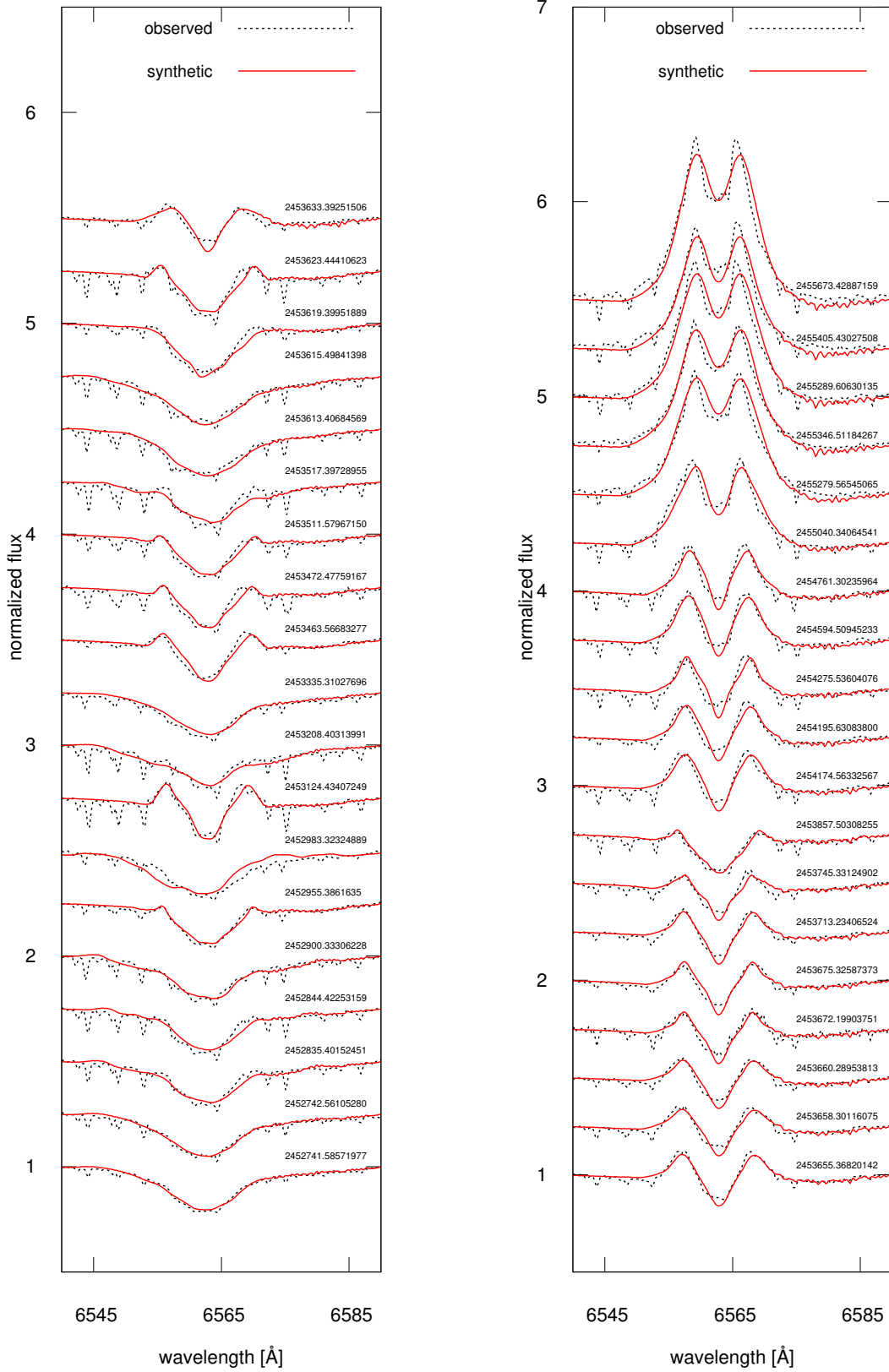
Figure 7.7: *Results of fits for 38 observed* Hα *profiles; on the right of the graphs Heliocentric Julian date for each profile is noted*
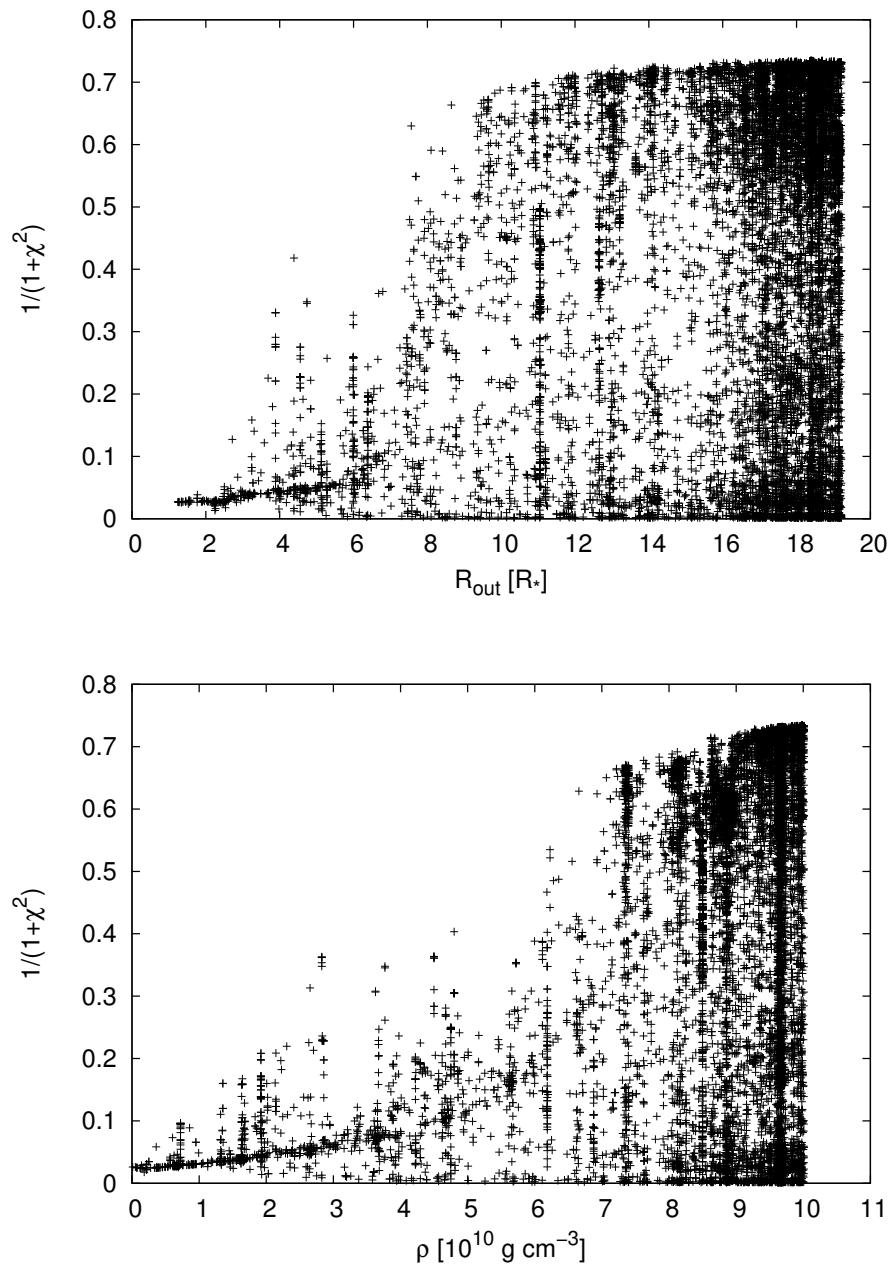
Figure 7.8: *Graphs of all the individuals from all the generations for free parameters, outer radius R_{out}, density ρ_0, inclination i, opening angle α and microturbulent velocity v_{trb} depending on $1/(1 + \chi^2)$, these results are for spectrum named ud210026, continued on next page*
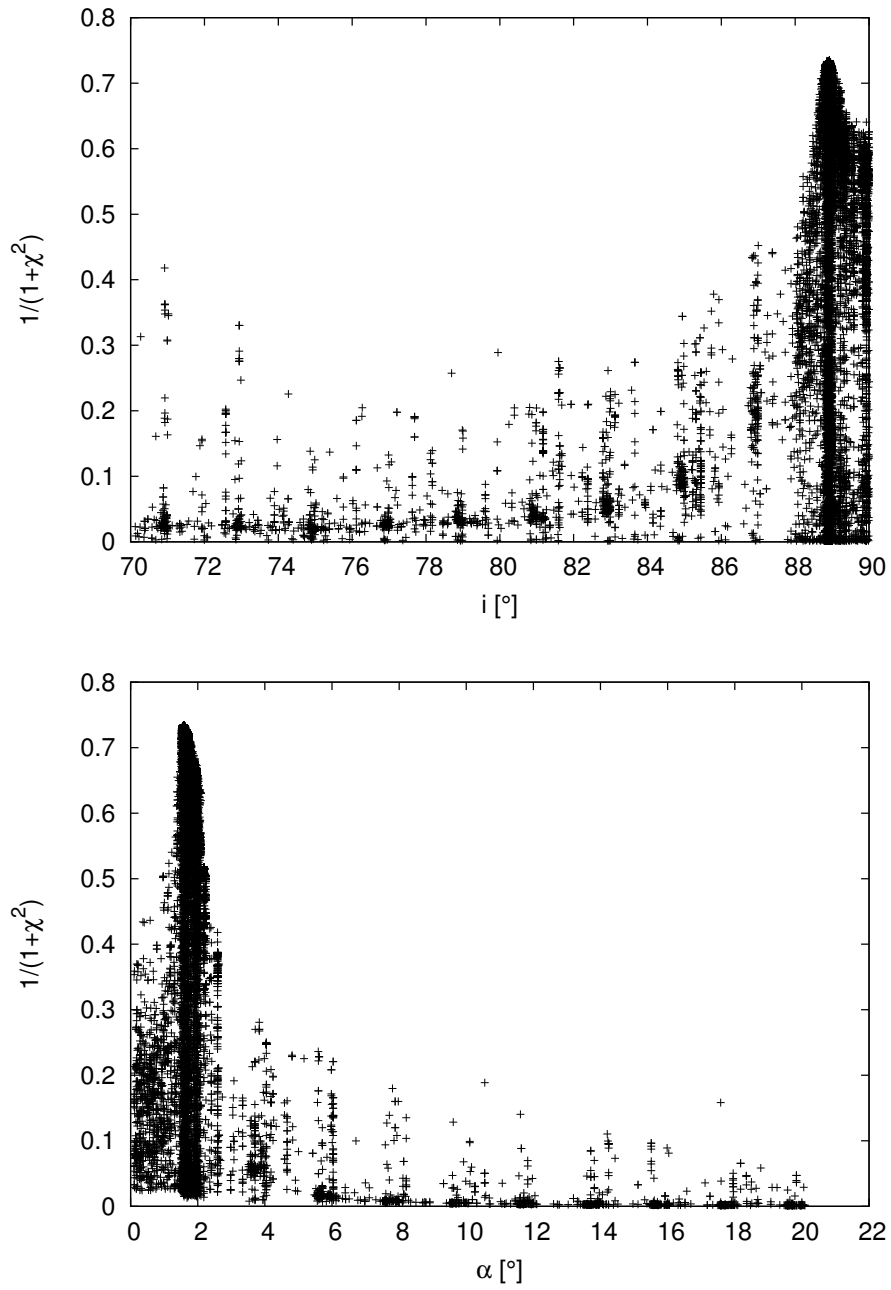
Figure 7.8: *(Continued)*
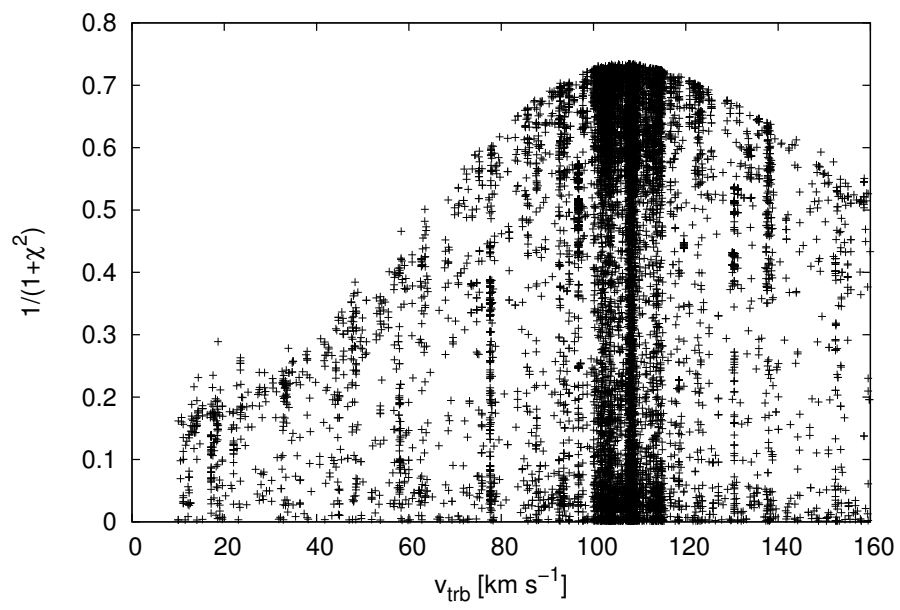
Figure 7.8: *(Continued)*
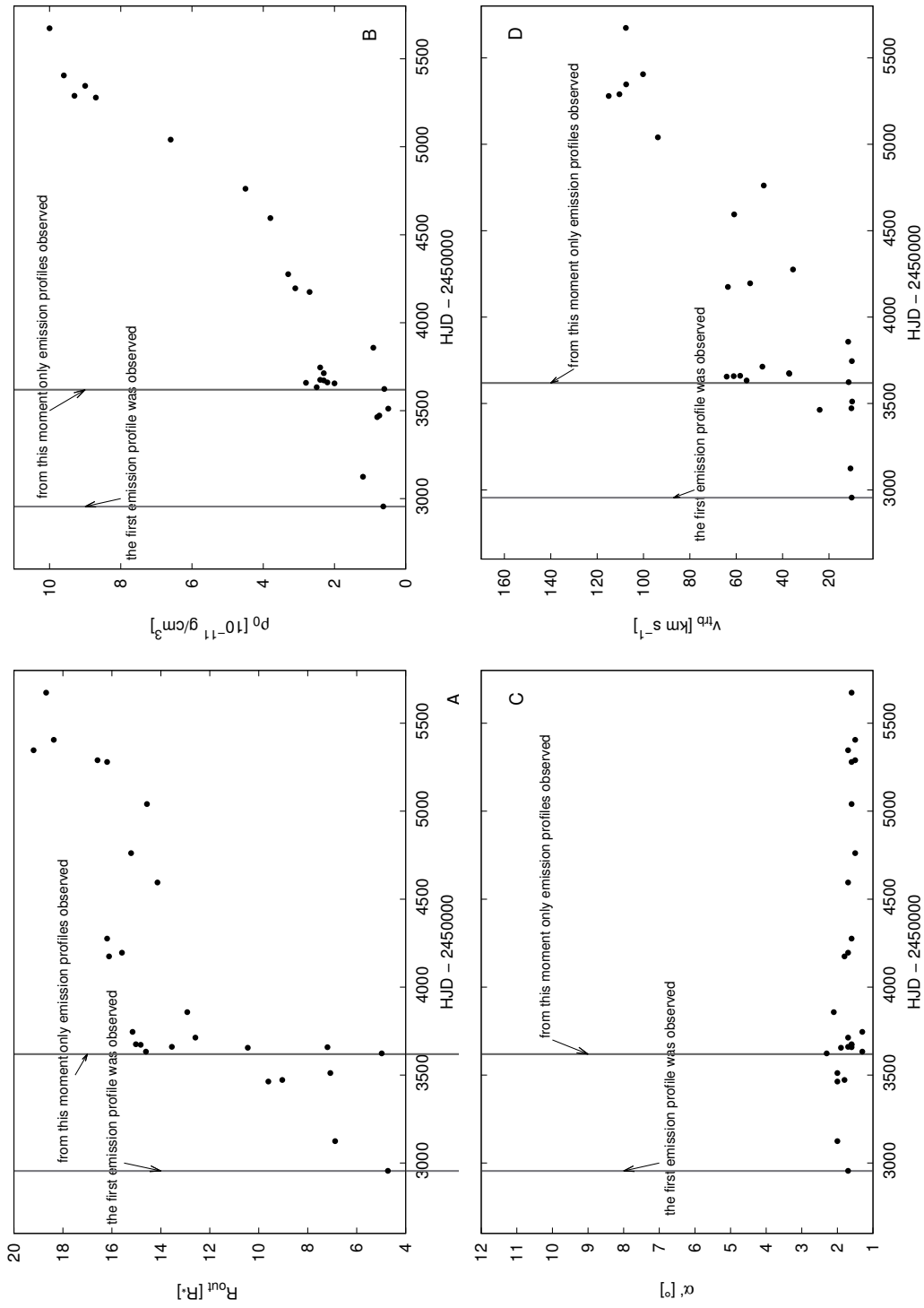
Figure 7.9: *Dependencies of the R_{out} (A), ρ_0 (B), α' (C) and v_{trb} (D) on time (HJD).*
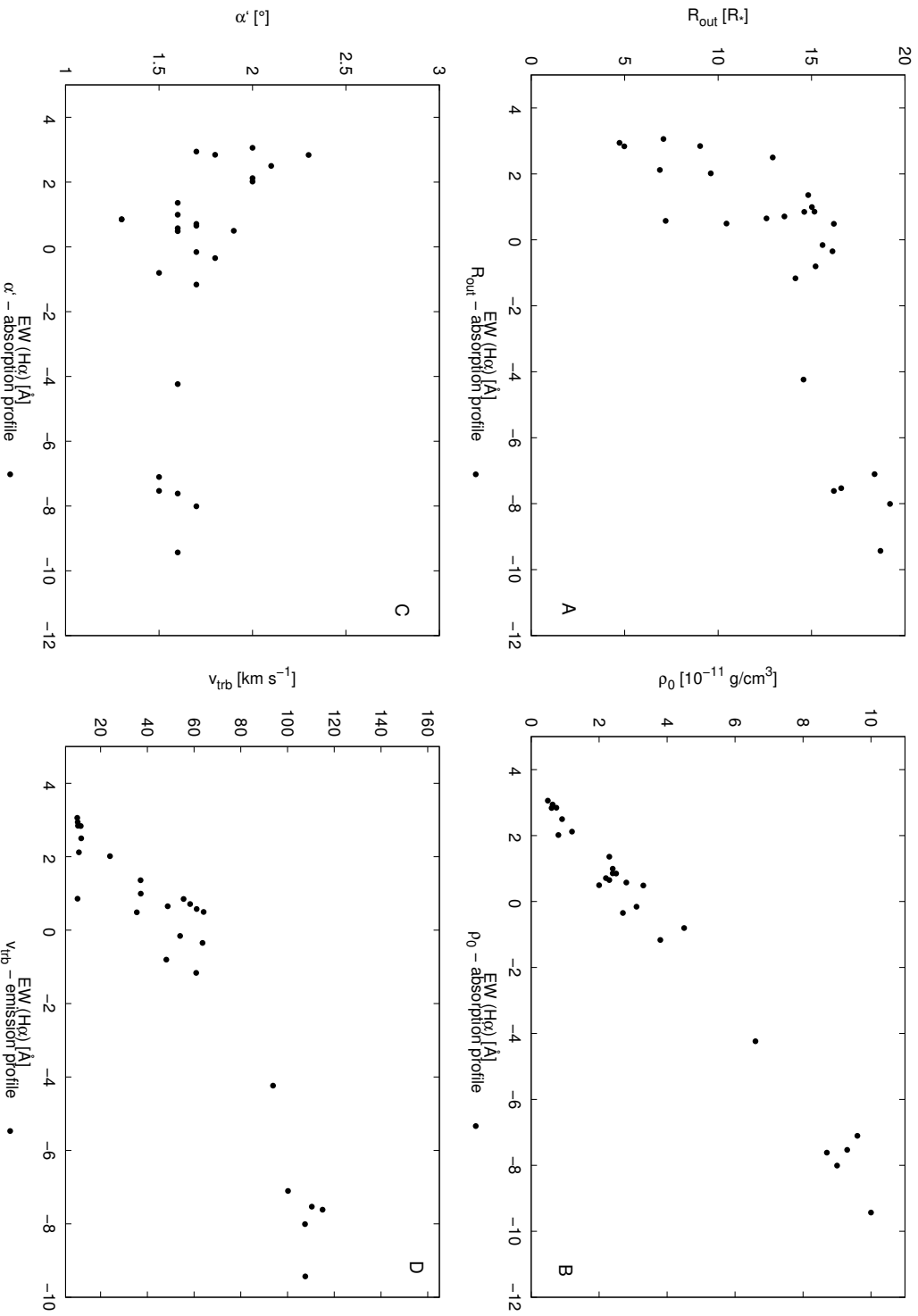
Figure 7.10: *Dependencies of the R_{out} (A), ρ_0 (B), α' (C) and v_{trb} (D) on EW.*
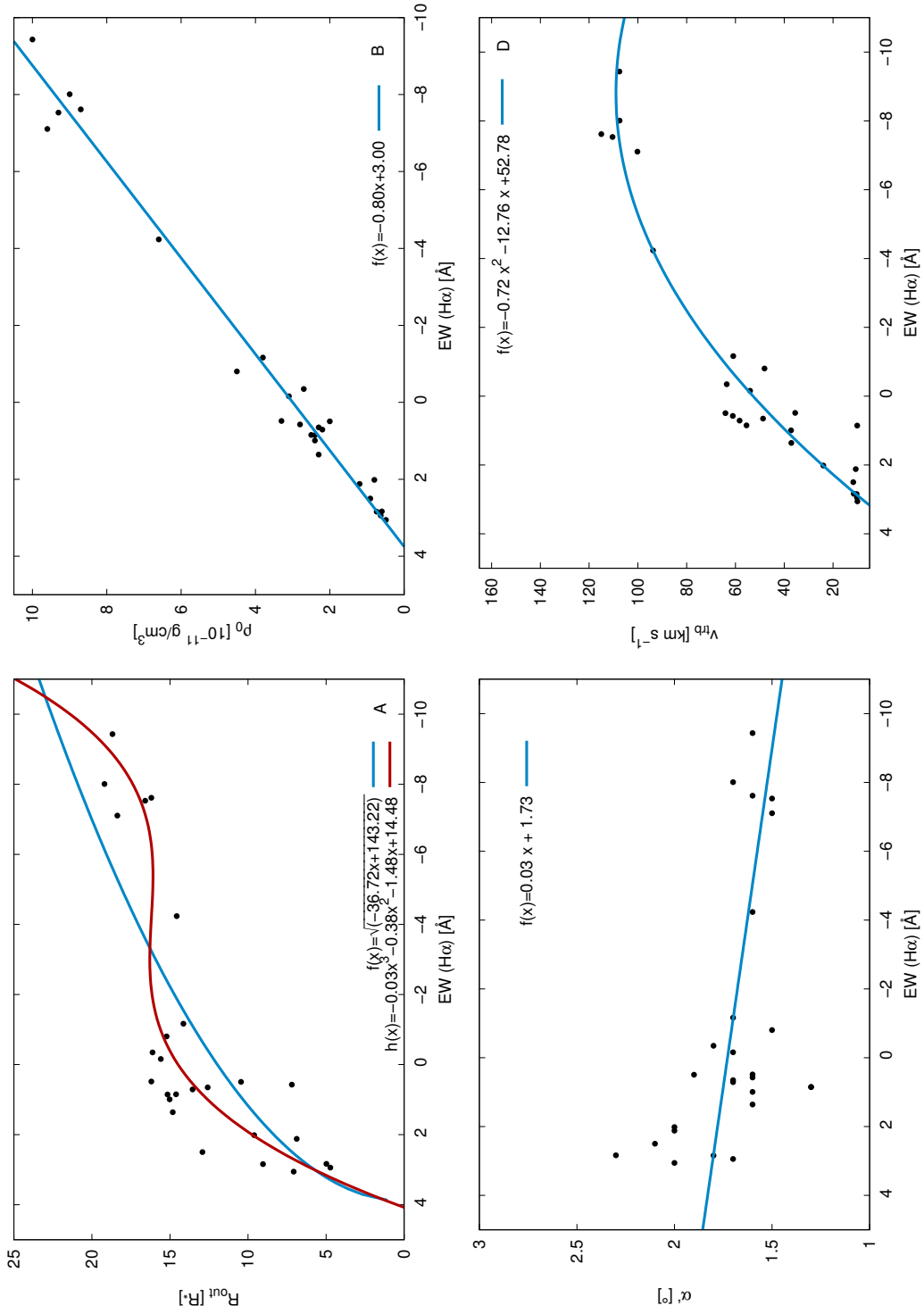
Figure 7.11: *Fits of the polynomial curves to data points: R_{out} (A), ρ_0 (B), α' (C) and v_{trb} (D) depending on EW.*
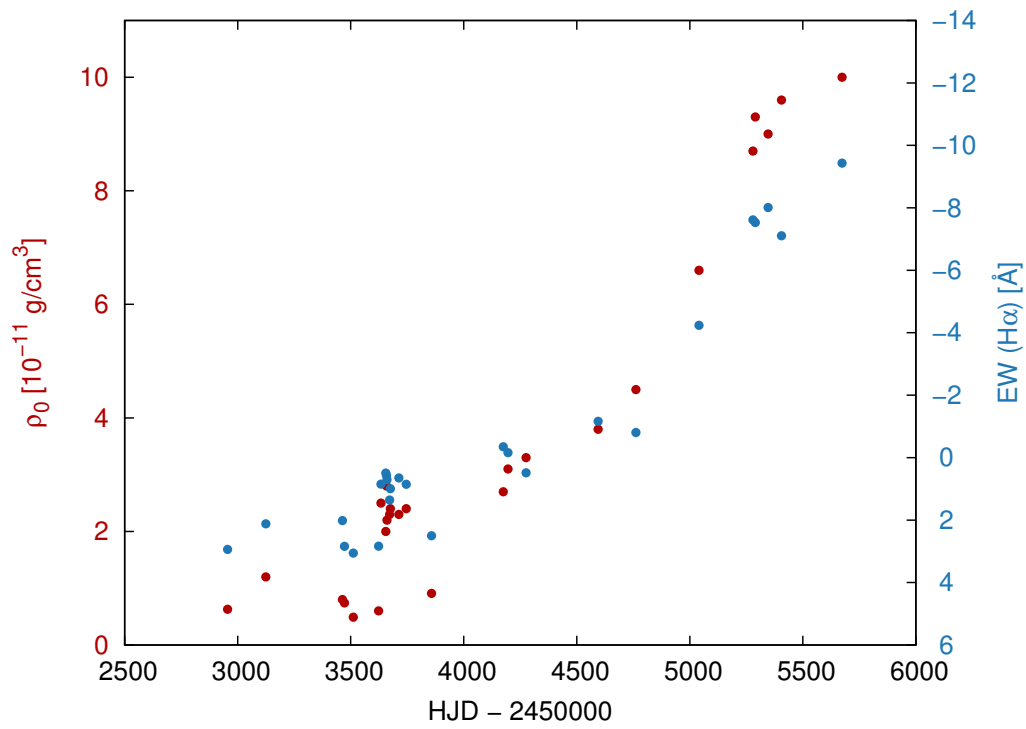
Figure 7.12: *Correlation between the evolution of the EW (blue points) and ρ_0 (red points)*
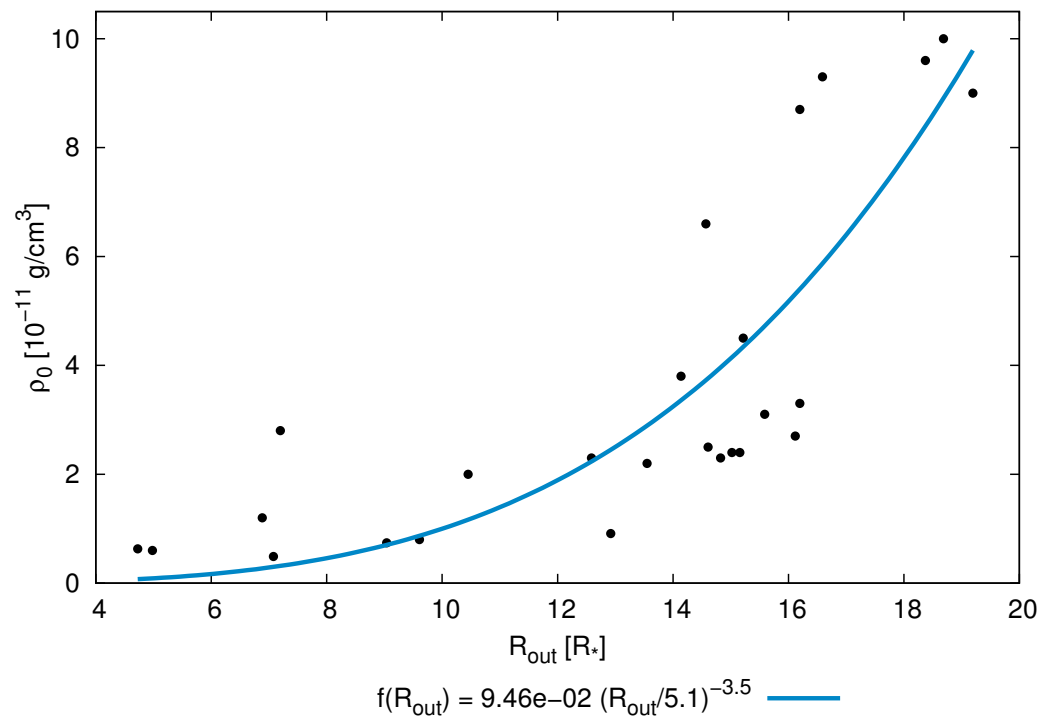
Figure 7.13: $f(R_{\text{out}}) = 9.46 \cdot 10^{-13}(R_{\text{out}}/5.1)^{-3.5}$ *is the dependency of density ρ_0 on outer radius R_{out}, where 5.1 is stellar radius of 60 Cygni*

7.9   Spectral Analysis of Hα line profiles

To have the picture of the star 60 Cygni complete we decided to present results for spectral analysis of the Hα line profiles, the same which were studied by *shell-spec17gen1* code and we also have made use of the BeSS database, operated at LESIA, Observatoire de Meudon, France (BeSS Database 2014) and study by Wisniewski et al. (2010).

In this section we present results for equivalent width (EW), V/R and ($V + R$)/2 variations for each observed spectrum of 60 Cygni. Results are summarized in Table 7.7 and Table 7.8. We try to find some dependency in this analysis and resultant values for disk properties. In previous section we showed the correlations between EW values and resulting values for the free disk parameters.

Equivalent width

The equivalent width (EW, Fig. 7.14) of a spectral line is a measure of the area of the line on a plot of intensity versus wavelength. It is found by forming a rectangle with a height equal to that of continuum emission, and finding the width such that the area of the rectangle is equal to the area in the spectral line. Positive value of EW is commonly used for absorption line and negative value for emission line, we use the same notification.
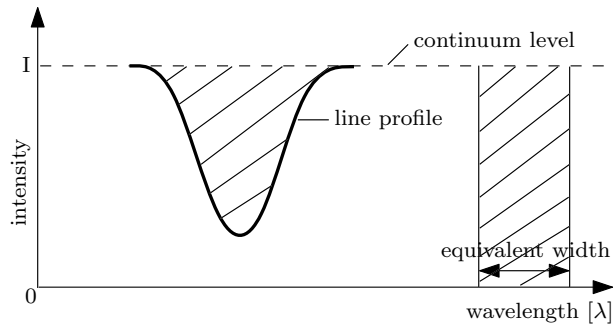
Figure 7.14: *Schematic picture for equivalent width for a line profile*

In Table 7.7 values for EW for each spectrum are presented. These are the spectra we used in our previous study and were observed at the Ondřejov Observatory. In Fig. 7.15 we can see the time evolution of the equivalent widths of Hα spectral line profile for this data (red points). We used SPEFO code (Skoda 1996) to analyze these spectra.

In Fig. 7.15 we also plotted values found in work by Wisniewski et al. (2010) (blue points). They had data from years between 1992 and 2006 and their data from the article can be found online.

We also have made use of the BeSS database (green points in Fig. 7.15). We used all the available data. These data were observed by several astronomers in period between years 1995 and 2016. In Table 7.8 values for EW for spectra adopted from BeSS Database are presented. We again used SPEFO code to determine the EW values for the Hα line profiles of the spectra. In Table 7.8 we noted observers for each spectra to be easily recognized if reader would like to see the spectra from the BeSS Database.

As it is assumed the higher the value of the $EW(\text{H}\alpha)$ the bigger the size of the circumstellar disk and for pure absorption there is no disk present. If we define that one cycle of the "life" of the disk is from the lowest state of pure absorption through the maximum strength of the Hα emission and back to the lowest state we can say from Fig. 7.15 that between years 1992 and 2016 the disk was presented twice. The second cycle is not finished since there is no further observation of the star (the last observation is from 23$^{\text{rd}}$ September 2016) and thus we cannot be sure if the value of $EW(\text{H}\alpha)$ would continue to increase or decrease. It is obvious that in the second cycle the 60 Cyg shows stronger emission activity.

Furthermore, Koubský et al. (2000) noted that observations from years 1953 – 1999 seem to indicate that the maximum strength of the Hα emission never exceeds a peak intensity of about 2.0 of the continuum level but our new observations and observations from BeSS Database show several profiles with intensity over 2.0. So it seems that 60 Cygni is showing the strongest emission activity in the last 60 years.

Wisniewski et al. (2010) presented that their data indicate that it took 870 days for 60 Cyg's disk to transform from its strongest Hα emission state to its lowest state of pure absorption, the latter of which they interpret as the time when the disk had completely dissipated. If we would do the same study for the formation of the disk we notice that it takes longer time. That means that times for formation of a disk and for dissipation of a disk are not the same.

Nevertheless from the Fig. 7.15 it is evident that a periodicity in the evolution of value of $EW(\text{H}\alpha)$ can be found. This work made use of python module pdm.py to determine the period. This module is patterned on the method of period determination using phase dispersion minimization (Stellingwerf (1978)). Phase dispersion minimization (PDM) is a data analysis technique that searches for periodic components of a time series data set. It is useful for data sets with gaps, non-sinusoidal variations, poor time coverage or other problems that would make Fourier techniques unusable. This method provides likelihood estimate in the form of theta where lower theta represents higher certainty of prediction. See Fig. 7.16 for the result of the analysis, the procedure found period 6009 ± 52 days (period for the minimal theta ($\theta = 0.15$) is 6050.1 days). pdmEquiBin carry out the PDM analysis using equidistant bins and pdmEquiBinCover carry out the PDM analysis using multiple sequences of equidistant bins.

We also used Period04 (Lenz & Breger (2005)) for period analysis and we found value for the period close to the one found by pdm.py: $P = 6172.8 \pm 86.4$ days, see Fig. 7.17. But in Fig. 7.18 we can see that the Least-Sqaures Fit does not fit data well. For better understanding of this dependency it would be convenient to watch the star closely in the future and gain more data from the past.

V/R variation

As was mentioned before on page 10, long-term cyclic changes in the V/R variation are observed in many stars, taking from a few years up to decades to complete the cycle and we can observe this phenomena in 60 Cygni spectra as well. We created a simple script to determine values for V and R peaks of Hα line profiles. Values are

presented in Table 7.7 and Table 7.8, for data from Ondřejov Observatory and BeSS Database, respectively.

In Fig. 7.19 we plotted time evolution of V/R ratio of Hα emission line profiles between years 1995 and 2016. Variation of $(V + R)/2$ for Hα emission line profiles can be seen in Fig. 7.21, data are from the same years as in the previous case for EW. In both graphs we plotted V/R and $(V + R)/2$ values for Hα line profiles observed at Ondřejov Observatory (circles) and those adopted from BeSS Database (black points).

We also used Period04 for the period analysis for V/R variation, see Fig. 7.20. From the graph we can say that there is no evident period in the time evolution of data for this variation. The highest peak has the value for signal to noise ratio $S/N = 2.96$. The values of V/R variation fluctuate in range $0.96 - 1.06$. Absence of the period can be due to the fact that there is no one-armed oscillation of the disk present or it is very small and does not influence the V/R variations (one-armed oscillation of the disk is one of the theory that is trying to explain the V/R variation, page 10)

From Fig. 2 in Koubský et al. (2000) we can see V/R and $(V + R)/2$ ratios between years 1976 to 1999 for Be star 60 Cygni. It is clear to see that the $(V+R)/2$ has its peak around 1.75 (at HJD $\approx$ 51000) and then starts decreasing. This peak has smaller value than the one we determined from our graph in this work which is around 2.15 (at HJD $\approx$ 57000). We can see the same behavior in development of EW(Hα) time evolution.

7.10   Discussion

In conclusion it is obvious that EW value is related to the size of the disk and also to the ρ_0 density but this is already known even from the definition of Be stars. As assumed EW(Hα) value is related to the size of the disk. Due to this assumption we can say that the formation of the disk takes longer time than the disk extinction (extinction is much steeper than the formation). We gained the period of one "life" cycle of the disk to be $\sim$ 6050 days. Also the last emission activity of the star is stronger than the previous one.

We found that there is no evident period of changes in V/R variation, it can be due to the fact that there is no one-armed oscillation of the disk present or it is very small and does not influence the V/R variations.

Table 7.7: *Results of spectral analysis of 38 spectra observed in Ondřejov, EW is equivalent width of Hα line profile in Å, RV is radial velocity in absorption core*

name	EW	RV [km/s]	V/R	$(V + R)/2$	HJD - 2450000
md110022	3.633	-18.669	0.999	1.003	2741.586
md120017	3.491	-14.052	1.004	1.005	2742.561

<div align="right">*Continued on next page*</div>

Table 7.7: *Results of spectral analysis of 38 spectra observed in Ondřejov, EW is equivalent width of Hα line profile in Å, RV is radial velocity in absorption core*

name	EW []	RV [km/s]	V/R	(V + R)/2	HJD - 2450000
mg140011	3.464	-6.941	1.000	1.007	2835.402
mg230016	3.534	-14.378	1.003	1.008	2844.423
mi170018	3.817	-22.574	0.997	1.005	2900.333
mk110031	2.941	-7.488	0.992	1.005	2955.386
ml090028	3.988	-10.168	1.004	1.003	2983.323
nd280015	2.12	-8.408	1.012	1.069	3124.434
ng210007	3.856	-0.331	0.998	1.000	3208.403
nk250010	3.852	-19.074	0.997	0.998	3335.310
od020047	2.015	-19.854	0.976	1.024	3463.567
od180011	2.842	-7.305	1.003	1.007	3472.478
oe200032	3.057	-33.350	1.000	1.004	3511.580
oe260004	3.455	-3.607	0.991	1.004	3517.398
oh300033	4.08	-52.93	1.003	1.005	3613.407
oi010018	4.169	-26.703	1.003	1.007	3615.498
oi050016	3.296	-19.888	0.992	1.009	3619.400
oi090022	2.835	-16.326	0.997	1.020	3623.444
oi190030	0.848	-8.957	1.017	1.057	3633.393
oj110026	0.494	-9.979	1.003	1.121	3655.368
oj140024	0.574	-19.384	1.007	1.101	3658.301
oj160010	0.709	-11.209	1.008	1.098	3660.290
oj280017	1.359	-19.976	0.979	1.092	3672.199
oj310009	0.992	-8.134	0.993	1.078	3675.326
ol080018	0.651	-2.928	1.013	1.109	3713.234
pa090021	0.854	-13.739	0.983	1.057	3745.331
pe020017	2.499	-1.068	0.999	1.011	3857.503
qc140015	-0.348	-8.267	0.991	1.174	4174.563
qd040061	-0.159	-15.604	0.979	1.172	4195.631
qf230027	0.485	-9.184	0.986	1.160	4275.536
re070026	-1.165	-3.921	1.014	1.246	4594.509
rj210042	-0.804	-6.276	0.992	1.240	4761.302
sg270024	-4.236	-8.793	0.994	1.427	5040.341

Table 7.7: *Results of spectral analysis of 38 spectra observed in Ondřejov, EW is equivalent width of Hα line profile in Å, RV is radial velocity in absorption core*

name	EW []	RV [km/s]	V/R	(V + R)/2	HJD - 2450000
tc230053	-7.615	-14.657	1.004	1.627	5279.565
td020080	-7.531	-12.725	1.015	1.628	5289.606
te290038	-8.008	-14.758	0.999	1.696	5346.512
tg270022	-7.105	-7.091	0.983	1.633	5405.430
ud210026	-9.432	-16.487	1.005	1.826	5673.429
				Continued from previous page	

Table 7.8: *EW, V/R and (V + R)/2 values for spectra adopted from BeSS Database (2014)*

Observers	HJD - 2400000	EW []	V/R	(V + R)/2
Desnoux	49922.451	-1.199	0.998	1.178
Buil	51327.608	-8.477	1.000	1.622
Buil	52049.643	3.276	0.994	1.014
Buil	52127.509	3.685	0.996	1.008
Buil	52129.488	3.429	0.986	1.010
Buil	52135.387	3.863	0.991	1.009
Buil	52212.244	2.579	0.991	1.012
Buil	52389.622	2.861	0.996	1.016
Buil	52425.502	2.890	0.996	1.016
Buil	52760.682	2.227	0.995	1.022
Buil	53153.618	2.613	0.997	1.011
Thizy, Ribeiro	54384.446	-2.064	0.998	1.270
Ribeiro	54405.479	-1.702	0.985	1.255
Ribeiro	54623.567	-2.086	0.979	1.300
Ribeiro	54666.499	-1.736	0.907	1.352
Terry	55066.402	-7.099	1.000	1.618
Desnoux	55066.506	-5.102	1.000	1.461
Guarro Fló	55067.406	-5.479	0.977	1.456
Mauclaire	55373.587	-9.121	0.984	1.808
			Continued on next page	

Table 7.8: *EW, V/R and (V + R)/2 values for spectra adopted from BeSS Database (2014)*

Observers	HJD - 2400000	EW []	V/R	$(V + R)/2$
Mauclaire	55381.621	-8.384	0.977	1.789
Mauclaire	55382.566	-7.659	0.980	1.724
Terry	55426.406	-7.578	0.972	1.656
Terry	55745.492	-7.957	0.928	1.696
Garrel	55790.545	-9.584	1.000	1.949
Graham	55846.539	-8.316	1.000	1.871
Desnoux	55858.274	-8.427	0.988	1.794
Graham	55876.546	-9.404	0.989	1.864
Garrel	56112.486	-10.138	1.000	1.931
Garrel	56119.402	-9.986	1.000	1.951
Graham	56187.564	-10.130	0.978	1.940
Ubaud	56500.508	-11.060	1.000	2.084
Desnoux	56506.412	-12.188	1.000	2.104
Graham	56579.619	-12.640	0.982	2.186
Desnoux	56874.393	-10.814	0.983	2.140
Graham	56917.596	-10.992	0.992	2.128
Buil	56934.320	-10.512	1.000	2.163
Pujol	56934.332	-10.656	1.000	2.157
Graham	56938.615	-9.932	1.037	2.119
Terry	57218.425	-7.922	1.024	1.947
Graham	57306.519	-8.811	1.015	1.867
Houpert	57514.464	-8.2	1.007	1.932
Terry	57655.399	-6.437	0.983	1.727

Continued from previous page
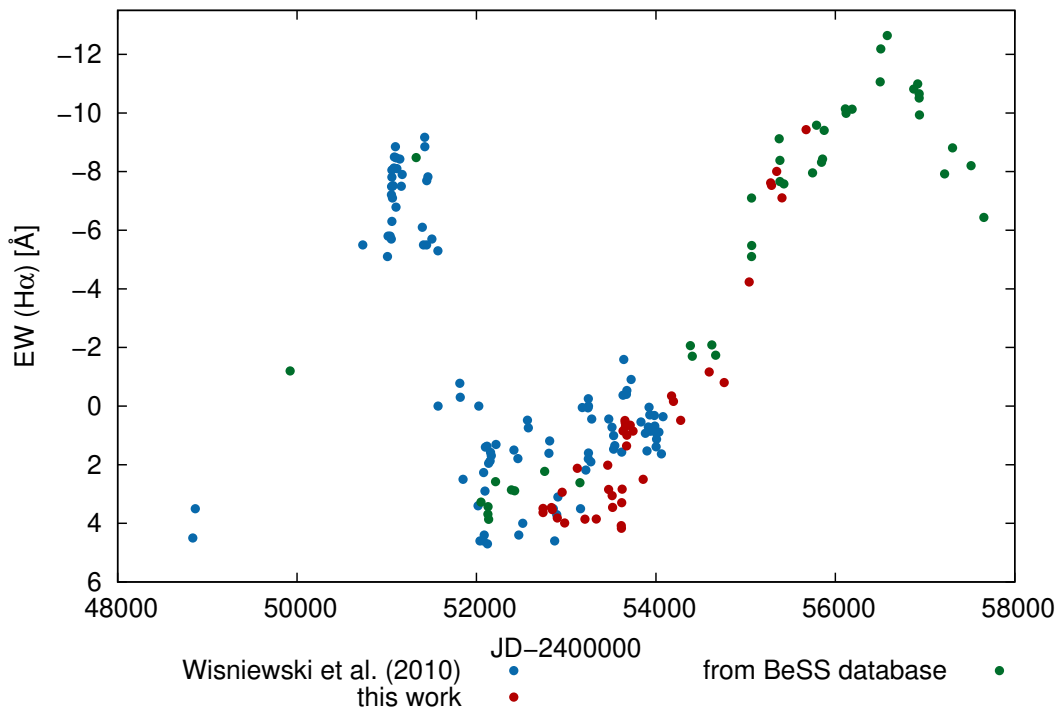
Figure 7.15: *Evolution of a equivalent width of Hα line in Å. Red points mark values found in this work and blue points mark values from Wisniewski et al. (2010). Green points mark the spectra adopted from BeSS database but EW value were determined in this work.*
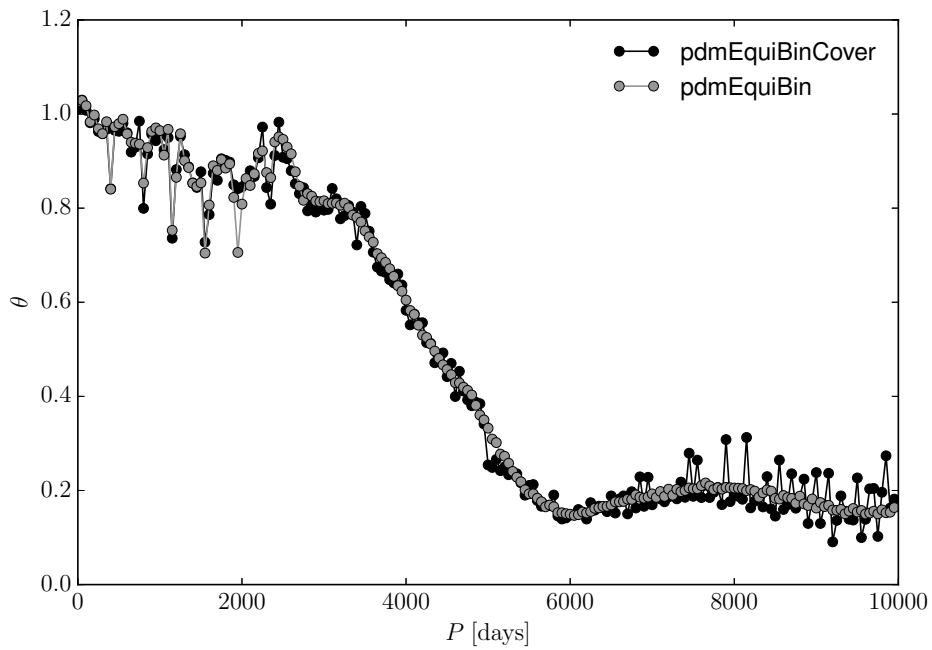
Figure 7.16: *Results of PDM analysis: period for the minimal theta ($\theta = 0.15$) is 6050 days. pdmEquiBin carry out the PDM analysis using equidistant bins and pdmEquiBinCover carry out the PDM analysis using multiple sequences of equidistant bins.*
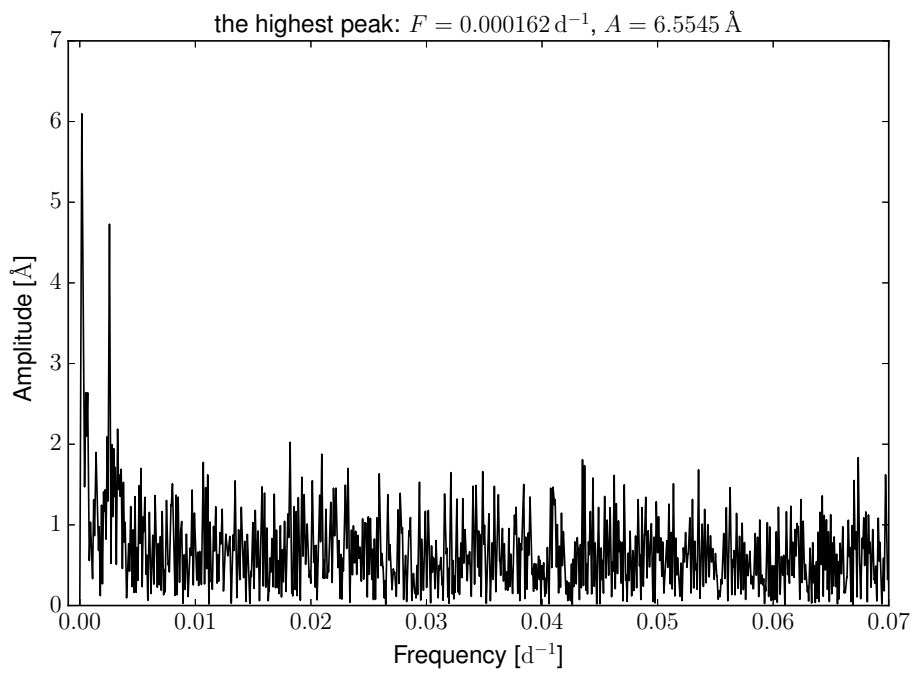
Figure 7.17: *Results of period analysis using Period04, where F is the frequency, A is the amplitude and S/N is signal to noise ratio. Value of found period is $P = 6172.8 \pm 86.4$ days.*
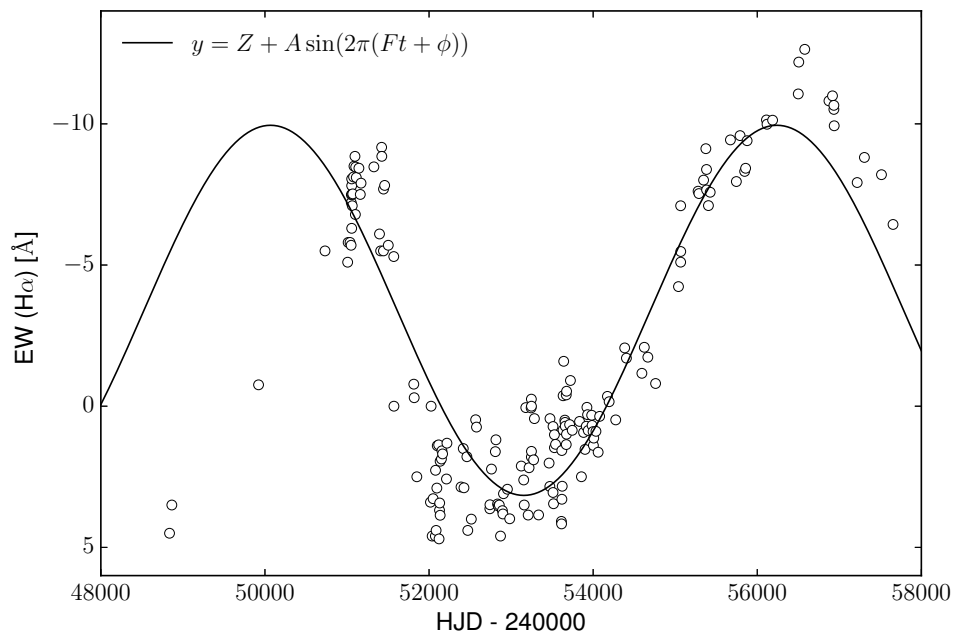
Figure 7.18: *The Least-Squares Fit for data gained by Period04. $Z = -3.39$ as the zero point, $A = 6.56$ as the amplitude, $F = 0.000162\,\mathrm{d}^{-1}$ as the frequency, $\phi = 0.639$ as the phase and t as the time.*
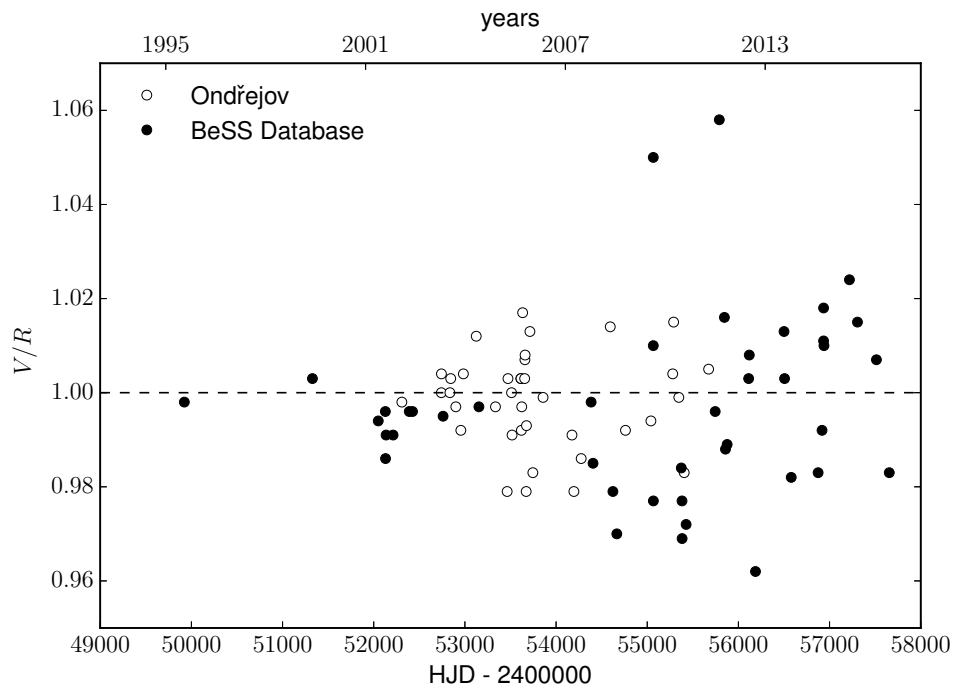
Figure 7.19: *V/R ratio of Hα line profile, dashed line marks normalized intensity with value 1.*
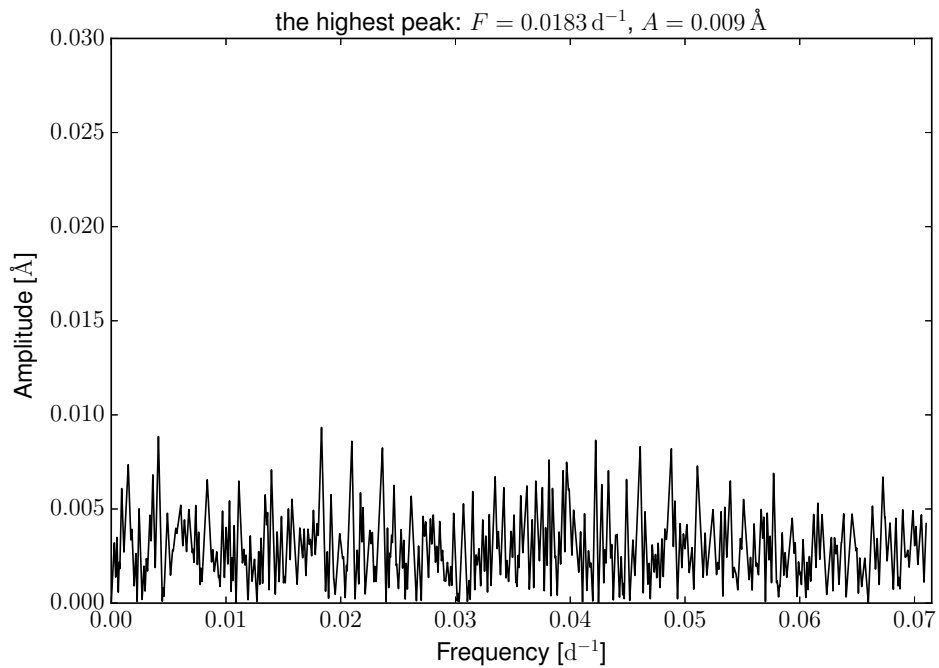
Figure 7.20: *Results of period analysis for V/R variation using Period04, where F is the frequency, A is the amplitude and S/N is signal to noise ratio.*
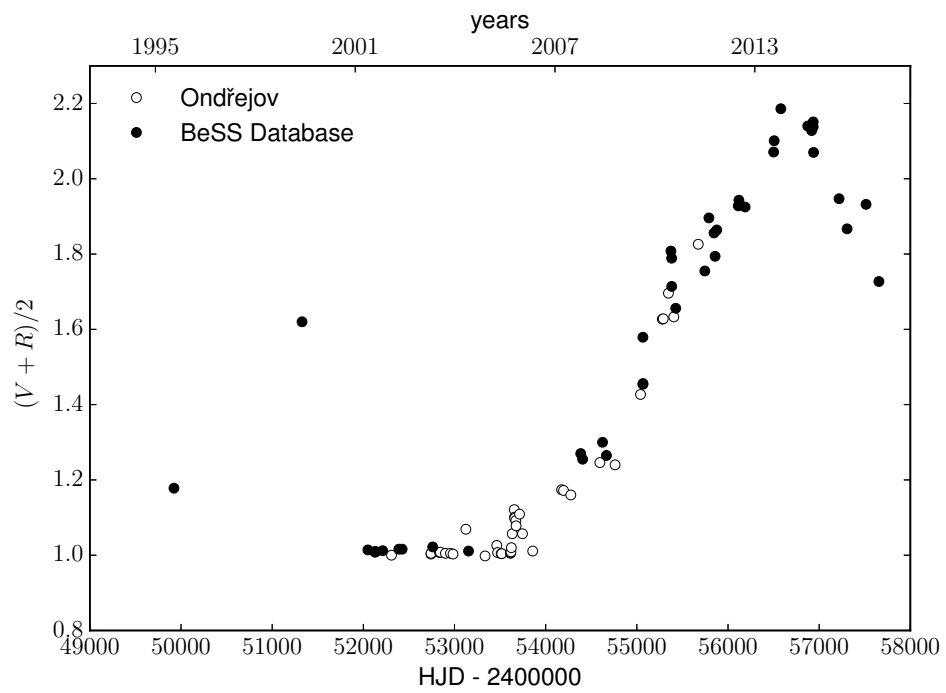
Figure 7.21: $(V + R)/2$ *ratio of Hα line profile.*

Conclusion 8

In this PhD thesis we were focusing on the study of the Be stars. Especially dynamical evolution of properties of their circumstellar disks. The other goal of this work is to find out the characteristics of a disk around the star, this is called inverse problem. An inverse problem is a general framework that is used to convert observed measurements into information about a physical object or system that we are interested in. For the study we used Shellspec code.

We presented here the modification of the Shellspec code which in original version solves simple radiative transfer along the line of sight in moving media. The main reason of the modification was to automize input of the disk's or other object's parameters, it depends on what kind of model the user wants to study. The modified code finds the best fit of the observed spectrum. We provided a simple user guide of how to use the modified version of the Shellspec code (*shellspec17gen1.f90*) and with this we believe everyone will be able to use the code. We also granted the free access to our version of the modified code on webpage. The free version can be found on `http://physics.muni.cz/~klarka/shellspecen`, the link to the original version of the Shellspec code can be found there as well.

We translated original code to Fortran 90 language and made changes which enable application of the genetic algorithm based subroutine PIKAIA. The advantage of the modification is the automatic setting of the free parameters. The user does not have to spend too much time on finding the best value of the free parameter, the modified code finds it by itself. Simply the modified code runs several time and for each run the synthetic spectrum is computed and compared with the observed one (for each run there is different combination of the free parameters) and as a results we get the best fit thus the best values for free parameters.

What we would like to emphasize is that this modified code is not only for studying Be stars it is also a good tool for other studies. That is the original idea of the original Shellspec code to study several different problems. We did not change anything to destroy this philosophy, we believe that we made it just more powerful in finding the free parameters.

We applied modified code to study three stars - TT Hydrae, κ Dra and 60 Cyg. First two cases were stars which we modeled due to the verification of the code. The last one was the Be star for which we were looking for the dynamical evolution of several disk parameters, this star was studied for the first time in respect of the time evolution.

The TT Hya was used to verify that the code works correctly. This was chosen due to the fact that this star was studied by Budaj who is also the author of original Shellspec code. This system is composed of the primary star, the secondary star, the accretion disk and the stream. Values of properties of primary star, secondary star and stream were set up in the same way as in Budaj & Richards (2004), some of the disk properties were left as a free parameters. We found similar results for values of inner and outer radius, density, temperature and microturbulent velocity of the disk as in (Budaj & Richards 2004) which confirmed the correctness of our modified code.

Another model star was κ Dra. This star was selected for its nature. This star is frequently observed Be star for which several disk parameters were known. Thus this example is very nice model case for verification of the modified Shellspec code since this work was focusing on the study of the Be star. We made three models with three different density exponent indexes n. For each model we were able to find values for the disk radius, which are in a good agreement with the estimations by Gies et al. (2007) and Touhami et al. (2013). We also found values for the inclination of the system and the density. We compared estimated quantities with the previous published results about this stars. Our results for the star are in a good agreement with previously published results. Some of the differences between our and other results are assumed to be due to the fact that we used single star model unlike binary model which was applied by others. We also found new parameter for this star which is the opening angle of the disk.

After we confirmed that the code works correctly and finds the best candidate for the free parameters we stepped up to our own modeling. We modeled Be star 60 Cygni. 60 Cyg star and its dynamical evolution of the disk properties were studied for the first time.

We were able to find the parameters of the disk for 38 different Hα profiles plus 5 smoothed Hα profiles. We found that with increasing emission outer radius and density of the the disk is increasing as well. We also found inclination of the star 60 Cyg, $i = 88.9°$ and opening angle value to be $\alpha = 1.8°$. For the Hα line profiles where we do not see any emission activity we found rather chaotic values. This means that for the absorption profiles there is no need to model a disk since there is no disk present.

We tried to find if there is any dependence of the density on the outer radius of the disk. Thus we fitted the data by an power law function. The result can be seen in Fig. 7.13.

We also made spectral analysis of Hα profiles of all the spectra we had in disposal, plus some spectra from BeSS Database, plus results of Wisniewski et al. (2010). We determined equivalent widths of Hα line profiles by SPEFO code, V/R and $(V+R)/2$ variations, we wrote a script to determine V and R values. Values for all three properties can be found in Tab. 7.7 and Tab. 7.8.

We found that this circumstellar disk formed twice in period 1992 - 2016. We can judge of this particularly from the study of the equivalent width where in the graph Fig. 7.15 two maxima are present. It seems that in the second cycle the 60 Cyg shows bigger emission activity. This could be related to the size of the disk which is bigger with bigger emission activity. From the graph we can see that the cycles of the expansion and decretion of the disk is not the same. The second cycle is not finished since there is no further observation of the star (the last observation is from 23$^{\text{rd}}$ September 2016) thus we cannot be sure if the value of EW would continue to increase or decrease.

We noticed the similar behavior of time evolutions of EW values and ρ_0 values. And we found very interesting correlation between EW values and values of ρ_0, Fig. 7.12. We did not find any article which would mention this behavior.

We also studied V/R variation but the star does not show any significant changes or period in changes of this value. We believe that this is the sign that there is no one-armed oscillation of the disk present or it is very small and does not influence the V/R variations. $(V+R)/2$ variation increases linearly when the disk is forming. Unfortunately we did not have too many points for the first cycle in the period 1992 - 2016. Thus we are not able to compare these two forming processes.

In our future work we want to use the code for more Be stars and try to explain the dynamics of the circumstellar disk and maybe find the similar behavior for the Be stars in general. We also want to continue in study of Be star 60 Cygni and model data from BeSS Database as well. We would like to also solve the problem with grid mentioned on page 54 since it would improve the resultant best fit. The other improvement would consist of the vertical dependence of the density which would correspond to the current look to the density which is used in most of the articles published lately. Also temperature distribution is need to be improved. To replace Heaviside function by some more proper function.

Nowadays there is not many codes which are able to find parameters of a system and describe observations so we believe that current and future results will help in understanding of the Be stars.

# *Fits of the observed spectra of 60 Cygni*

In this part of the thesis detailed fits of the observed Hα line profiles are presented. In each graph the synthetic profile (fit) and observed profiles (presented by name of the profile) are plotted. Also for each profile we noted the resulting value for outer radius of the disk. Other resulting values for free parameters can be found in the previous Chapter 7.2 in Tab. 7.6 on page 61.
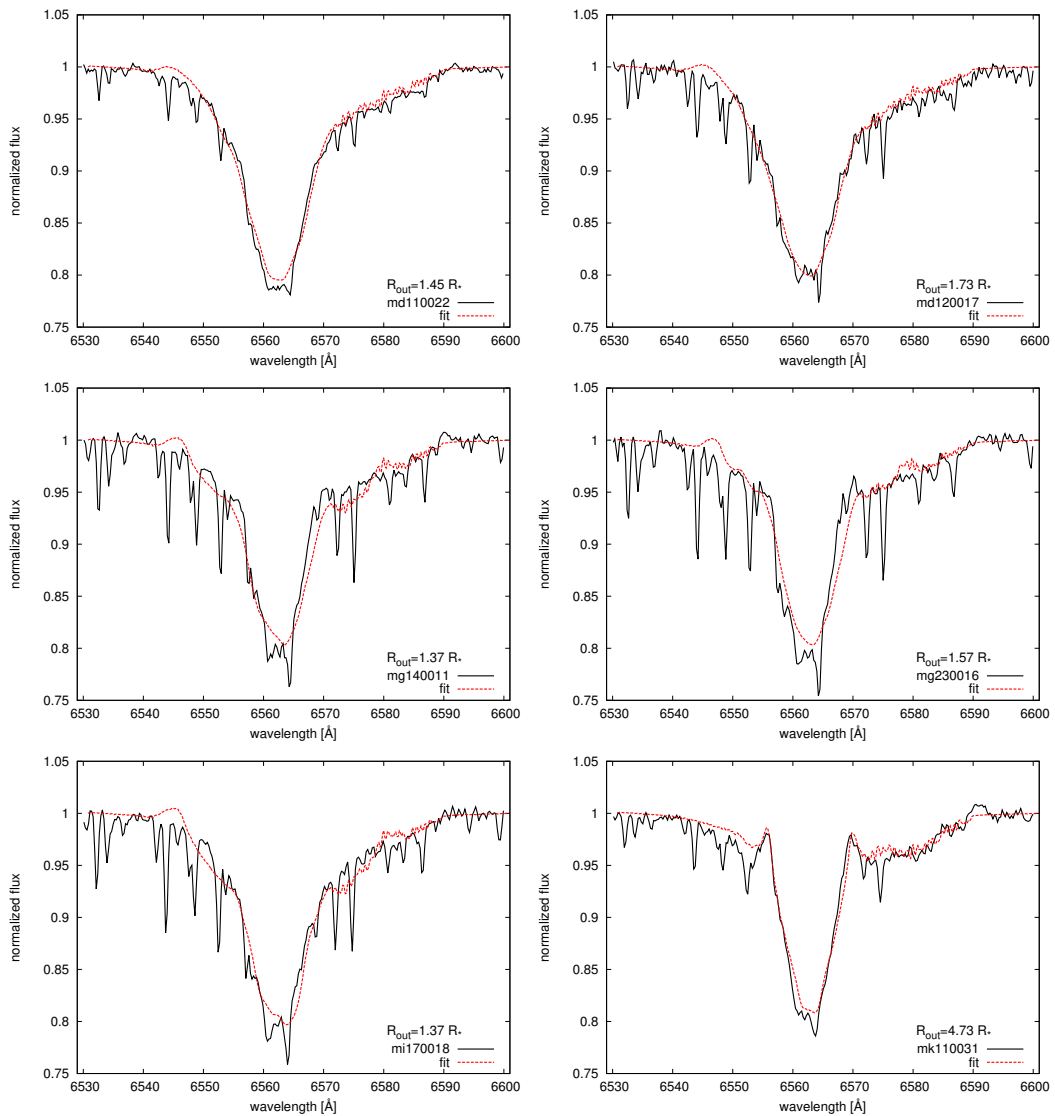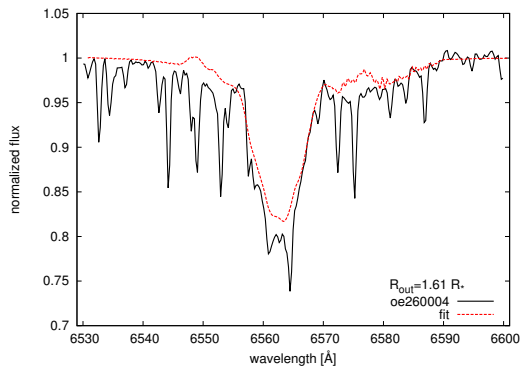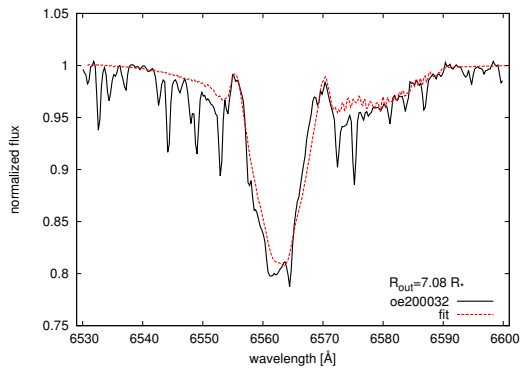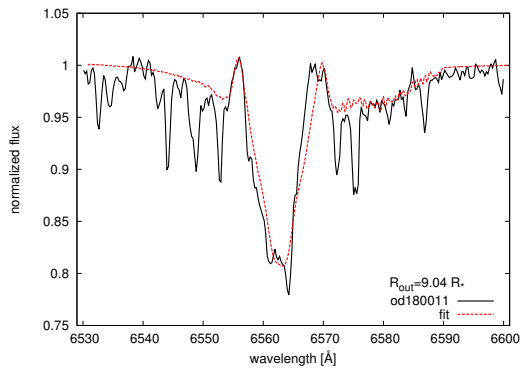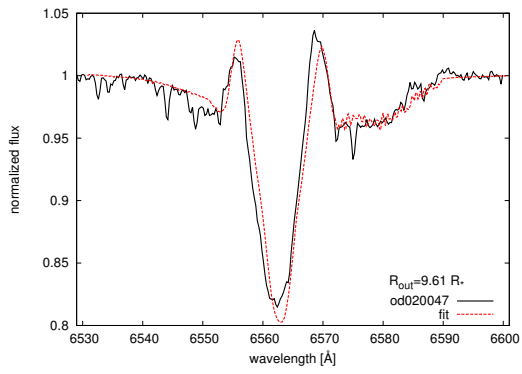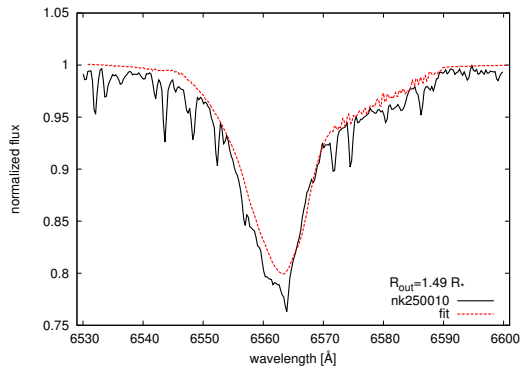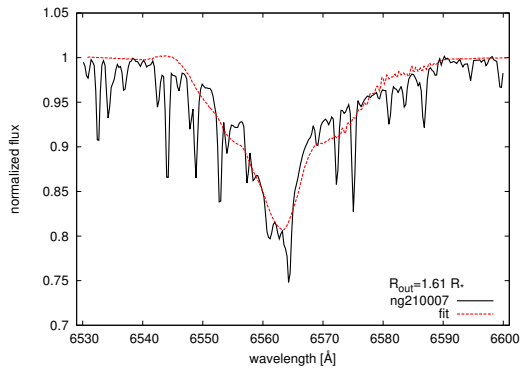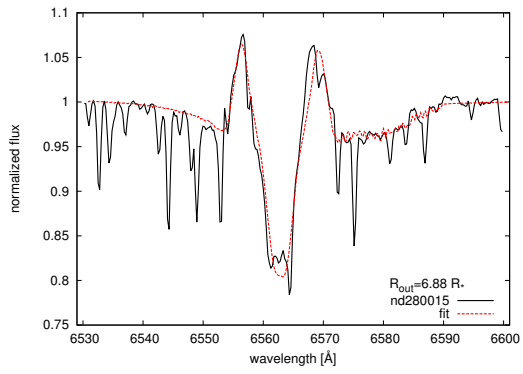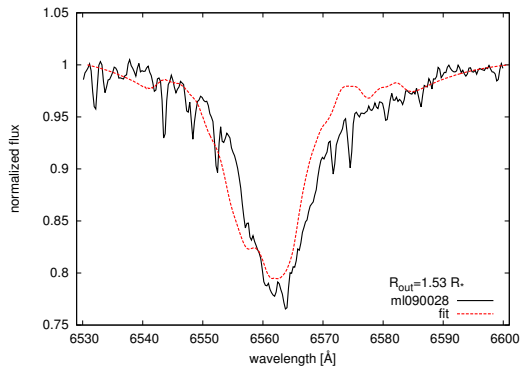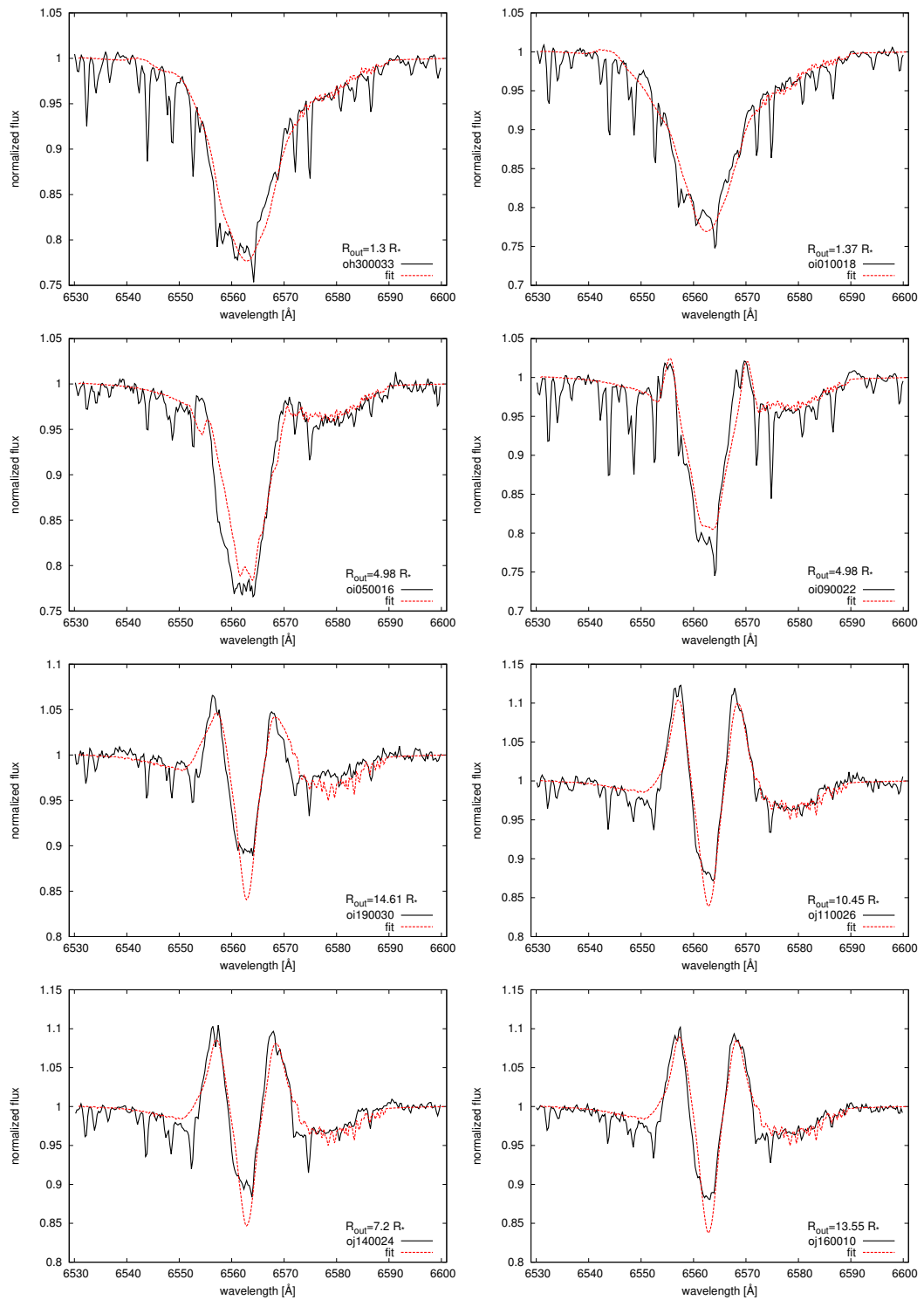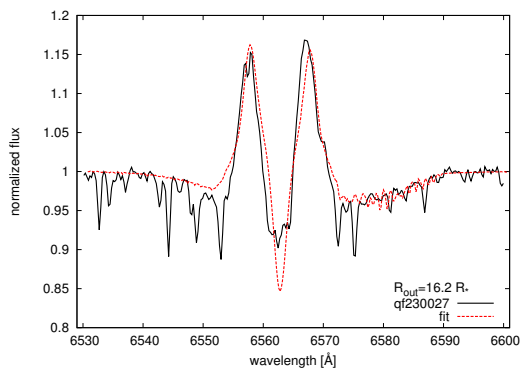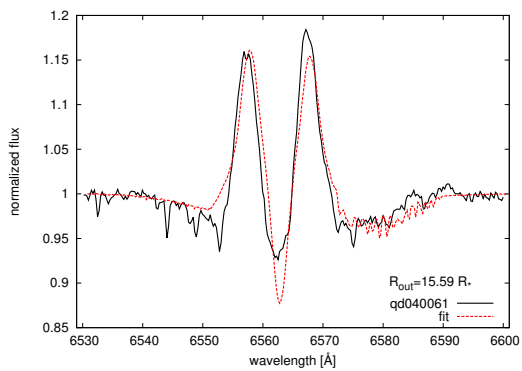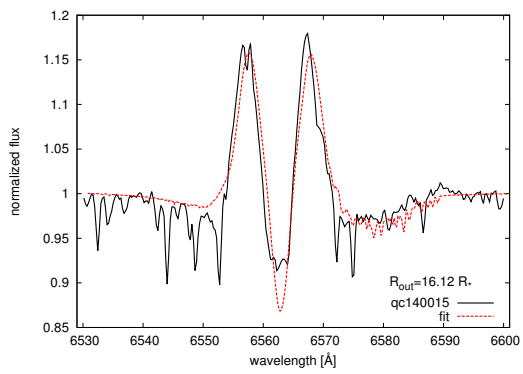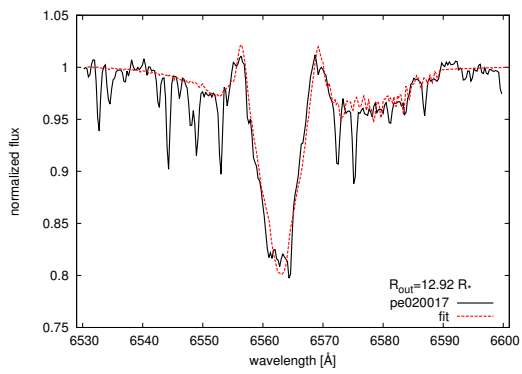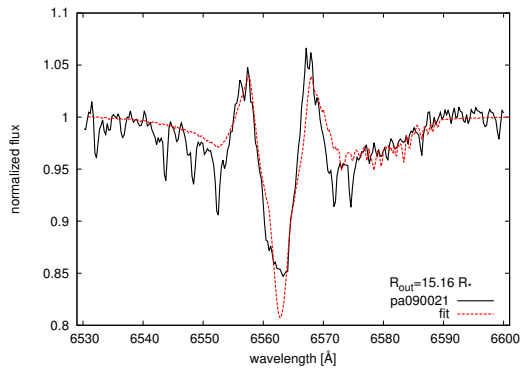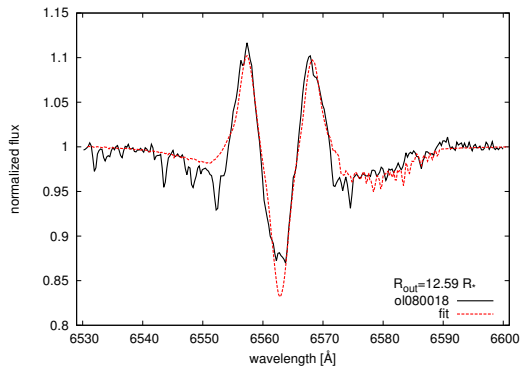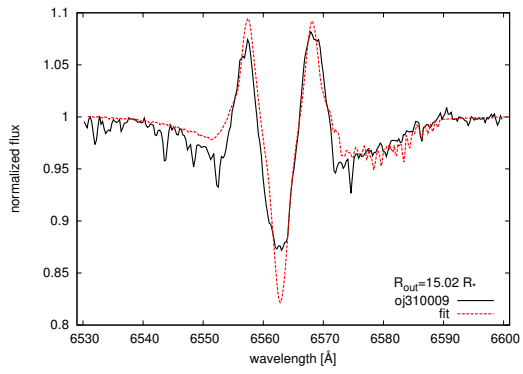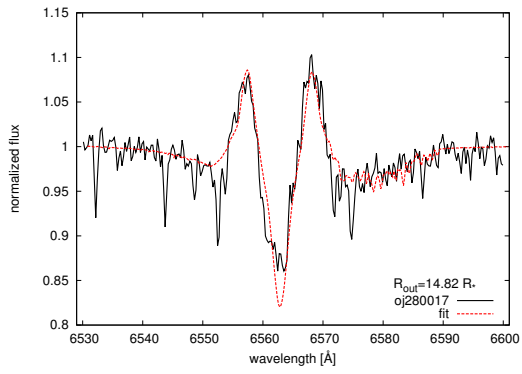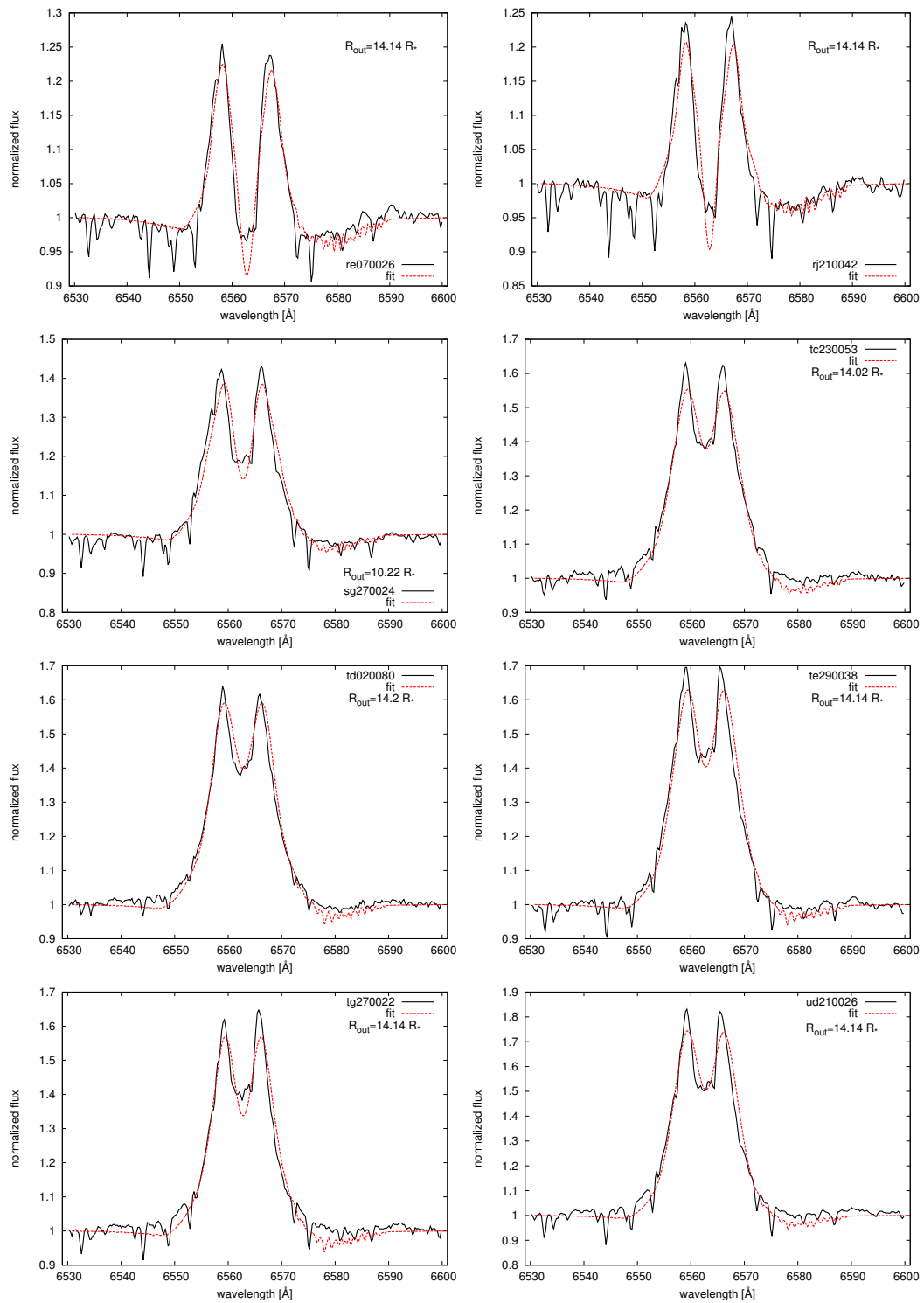
List of Publications B

Article in Journal

1. **Šejnová, K.**, Votruba, V. 2017, Emission activity of the Be star 60 Cygni. In Serbian Astronomical Journal, Vol. 194, p. 51

Conference proceedings

1. **Šejnová, K.**, Votruba, V., & Koubský, P. 2012, Modeling of Be stars. In Astronomical Society of the Pacific Conference Series, Vol. 464, p. 219

2. **Šejnová, K.**, Votruba, V., & Koubský, P. 2012, Modeling of the Be stars. in IAU Symposium, Vol. 282, p. 261-262

3. Votruba, V., **Šejnová, K.**, Koubský, P., Korčáková, D., 2011, Influence of decoupling effect on stellar wind variability, in IAU Symposium, Vol. 272, p. 218-219

Bibliography

Adams, F. C., Lada, C. J., & Shu, F. H. 1987, ApJ, 312, 788

Andrillat, Y. 1983, A&AS, 53, 319

BeSS Database. 2014, `http://basebe.obspm.fr`, accessed: 2014-11-04

Bjorkman, J. E. & Cassinelli, J. P. 1993, ApJ, 409, 429

Bragg, A. E. & Kenyon, S. J. 2002, AJ, 124, 3289

Budaj, J. & Richards, M. T. 2004, Contributions of the Astronomical Observatory Skalnate Pleso, 34, 167

Budaj, J., Richards, M. T., & Miller, B. 2005, ApJ, 623, 411

Carciofi, A. C. & Bjorkman, J. E. 2006, ApJ, 639, 1081

Carciofi, A. C. & Bjorkman, J. E. 2008, ApJ, 684, 1374

Cassinelli, J. P., Brown, J. C., Maheswaran, M., Miller, N. A., & Telfer, D. C. 2002, ApJ, 578, 951

Charbonneau, P. & Knapp, B. 1995, A User's Guide to PIKAIA 1.0, Tech. rep.

Collins, II, G. W. 1987, in IAU Colloq. 92: Physics of Be Stars, ed. A. Slettebak & T. P. Snow, 3–19

Coté, J. & Waters, L. B. F. M. 1987, A&A, 176, 93

Deb, K. 1999, Sadhana, 24, 293

Doubek, J. 2006, Master's thesis, Karlova Univerzita v Praze

Draper, Z. H., Wisniewski, J. P., Bjorkman, K. S., et al. 2011, ApJ, 728, L40

Draper, Z. H., Wisniewski, J. P., Bjorkman, K. S., et al. 2014, ApJ, 786, 120

Etzel, P. B. 1988, AJ, 95, 1204

Gies, D. R., Bagnuolo, Jr., W. G., Baines, E. K., et al. 2007, ApJ, 654, 527

Grundstrom, E. D. & Gies, D. R. 2006, ApJL, 651, L53

Hanuschik, R. W. 1996, A&A, 308, 170

Hirata, R. & Kogure, T. 1984, Bulletin of the Astronomical Society of India, 12, 109

Hoffleit, D. & Jaschek, C. 1982, The Bright Star Catalogue

Huang, S.-S. 1972, ApJ, 171, 549

Hubeny, I. & Lanz, T. 1995, ApJ, 439, 875

Jacobson, L. 2012, Creating a genetic algorithm for beginners

Jaschek, C. & Jaschek, M. 1993, A&AS, 97, 807

Jones, C. E., Tycner, C., Sigut, T. A. A., Benson, J. A., & Hutter, D. J. 2008, ApJ, 687, 598

Kogure, T. & Leung, K.-C., eds. 2007, Astrophysics and Space Science Library, Vol. 342, The Astrophysics of Emission-Line Stars

Koubský, P., Harmanec, P., Hubert, A. M., et al. 2000, A&A, 356, 913

Kříž, S. & Harmanec, P. 1975, Bulletin of the Astronomical Institutes of Czechoslovakia, 26, 65

Lee, U. 2013, Publications of the Astronomical Society of Japan, 65

Lee, U., Osaki, Y., & Saio, H. 1991, MNRAS, 250, 432

Lenz, P. & Breger, M. 2005, Communications in Asteroseismology, 146, 53

Martayan, C., Rivinius, T., Baade, D., Hubert, A.-M., & Zorec, J. 2011, in IAU Symposium, Vol. 272, IAU Symposium, ed. C. Neiner, G. Wade, G. Meynet, & G. Peters, 242–253

McGill, M. A., Sigut, T. A. A., & Jones, C. E. 2011, ApJ, 743, 111

McGill, M. A., Sigut, T. A. A., & Jones, C. E. 2013, ApJs, 204, 2

Meilland, A., Millour, F., Kanaan, S., et al. 2012, A&A, 538, A110

Metcalf, M., Reid, J., & Cohen, M. 2004, Fortran 95/2003 Explained

Metcalfe, T. S. & Charbonneau, P. 2003, Journal of Computational Physics, 185, 176

Mihalas, D. 1978, Stellar atmospheres /2nd edition/

Millar, C. E. & Marlborough, J. M. 1998, ApJ, 494, 715

Miller, B., Budaj, J., Richards, M., Koubský, P., & Peters, G. J. 2007, ApJ, 656, 1075

Mokiem, M. R., de Koter, A., Puls, J., et al. 2005, A&A, 441, 711

Okazaki, A. T. 1991, PASJ, 43, 75

Okazaki, A. T. 2001, PASJ, 53, 119

Owocki, S. & Ud-Doula, A. 2003, in Astronomical Society of the Pacific Conference Series, Vol. 305, Magnetic Fields in O, B and A Stars: Origin and Connection to Pulsation, Rotation and Mass Loss, ed. L. A. Balona, H. F. Henrichs, & R. Medupe, 350

Park, S. K. & Miller, K. W. 1988, Commun. ACM, 31, 1192

Porter, J. M. 1996, MNRAS, 280, L31

Porter, J. M. 1999, A&A, 348, 512

Porter, J. M. & Rivinius, T. 2003, Publications of the Astronomical Society of the Pacific, 115, 1153

Pringle, J. E. 1981, ARA&A, 19, 137

Quirrenbach, A., Bjorkman, K. S., Bjorkman, J. E., et al. 1997, ApJ, 479, 477

Rivinius, T., Baade, D., Stefl, S., et al. 1998, A&A, 333, 125

Rivinius, T., Baade, D., Štefl, S., & Maintz, M. 2001, A&A, 379, 257

Rivinius, T., Carciofi, A. C., & Martayan, C. 2013, ArXiv e-prints

Rutten, R. J. 2003, Radiative Transfer in Stellar Atmospheres

Saad, S. M., Kubát, J., Koubský, P., et al. 2004, AAP, 419, 607

Secchi, A. 1866, Astronomische Nachrichten, 68, 63

Shakura, N. I. & Sunyaev, R. A. 1973, A&A, 24, 337

Sigut, T. A. A. & Jones, C. E. 2007, ApJ, 668, 481

Silaj, J., Jones, C. E., Tycner, C., Sigut, T. A. A., & Smith, A. D. 2010, ApJS, 187, 228

Skoda, P. 1996, in Astronomical Society of the Pacific Conference Series, Vol. 101, Astronomical Data Analysis Software and Systems V, ed. G. H. Jacoby & J. Barnes, 187

Stellingwerf, R. F. 1978, ApJ, 224, 953

Struve, O. 1931, The Astrophysical Journal, 73, 94

Touhami, Y., Gies, D. R., Schaefer, G. H., et al. 2013, ApJ, 768, 128

Šejnová, K., Votruba, V., & Koubský, P. 2012a, in Astronomical Society of the Pacific Conference Series, Vol. 464, Astronomical Society of the Pacific Conference Series, ed. A. C. Carciofi & T. Rivinius, 219

Šejnová, K., Votruba, V., & Koubský, P. 2012b, in IAU Symposium, Vol. 282, IAU Symposium, ed. M. T. Richards & I. Hubeny, 261–262

Šejnová, K. 2010, Master's thesis, Masarykova Univerzita v Brně

Walker, M. F. 1953, The Astrophysical Journal, 118, 481

Waters, L. B. F. M. 1986, A&A, 162, 121

Waters, L. B. F. M., Coté, J., & Lamers, H. J. G. L. M. 1987, A&A, 185, 206

Williams, W., Kelley, C., & many others. 2013, Gnuplot 4.6.4: an interactive plotting program, `http://gnuplot.sourceforge.net/`

Wisniewski, J. P., Draper, Z. H., Bjorkman, K. S., et al. 2010, ApJ, 709, 1306

Wood, H. E. 1926, Circular of the Union Observatory Johannesburg, 69, 368